

Attention is drawn to the fact that the copyright of this thesis rests with its author.

This copy of the thesis has been supplied on condition that anyone who consults it is understood to recognise that its copyright rests with its author and that no quotation from the thesis and no information derived from it may be published without the author's prior written consent.

D12776/75  
Henshall, S.A.E.  
pp231

ABSTRACT

Studies of Molecular Motions in Selected  
Polymer Systems

An abstract of a thesis submitted to the  
University of Stirling  
for the degree of  
Doctor of Philosophy

S.A.E. Henshall

Department of Chemistry  
Autumn 1974

## ABSTRACT

Torsional Braid Analysis, TBA, of various polysaccharide derivatives and of members of the poly(di-n-alkylitaconate) series, complemented by a limited number of Differential Scanning Calorimeter thermograms, has enabled the molecular motions associated with several secondary glass transitions to be tentatively identified. A damping peak observed at less than  $-190^{\circ}$  to  $-166^{\circ}\text{C}$  in TBA thermograms for polymers with side groups containing n-alkyl moieties as large as the n-propyl group has been attributed to the onset of rotational motion of this alkyl group alone. TBA of higher poly(di-n-alkylitaconates) also revealed a large secondary transition between  $-70^{\circ}$  and  $-45^{\circ}\text{C}$ ; from the relationship between their temperatures these two transitions were identified with the glass and melting transitions of the n-alkyl side-chains and it was suggested that the  $\beta$ -transition for the entire polymer also contributes to the high damping associated with the latter process. Two of the secondary transitions that are visible in TBA thermograms for various polysaccharide derivatives may be associated with absorbed water: the damping maximum occurring between  $15^{\circ}$  and  $33^{\circ}\text{C}$  has been attributed to the rupture of hydrogen bonds, the increased mobility of bonded water molecules possibly being responsible for the damping variation at about  $-14^{\circ}\text{C}$ . It was suggested that motion of the oxycarbonyl portion of ester groups and/or of the C6 oxymethylene group may be initiated at approximately  $-55^{\circ}\text{C}$ . It was concluded that chair-chair conformational interchange of main-chain glucose

rings becomes energetically feasible between  $-90^{\circ}$  and  $-140^{\circ}\text{C}$ , the temperature of this secondary transition being particularly dependent on the structure of substituent groups. The glass transition temperature was also determined for each available sample, the variety in their structures enabling the relationship between these two parameters to be discussed.

Studies of Molecular Motions in Selected  
Polymer Systems

A thesis submitted to the  
University of Stirling  
for the degree of  
Doctor of Philosophy

S.A.E. Henshall

Department of Chemistry  
Autumn 1974

To my husband  
and to my parents;  
without their encouragement  
this thesis would not have  
been written.

#### ACKNOWLEDGEMENTS

I am grateful to J. Velickovic and W. Burchard who generously provided many samples and also to M. R. Cottrell of Perkin-Elmer Ltd. for the use of the Differential Scanning Calorimeter Model DSC-2 and their facilities.

I wish to thank members of the Shared Technical Services and the Chemistry Department for all their help; particular thanks go to W. McCormack of the Glass-Blowing Workshop, W. Stirling for his help with electrical problems, B. Povey of the Engineering Workshop and to A. Paterson and S. G. Castle for tirelessly supplying me with liquid and gaseous nitrogen. This thesis was beautifully typed by Mrs. J. Weber.

I am indebted to J.M.G. Cowie for guiding me through this stage of my research training.

## CONTENTS

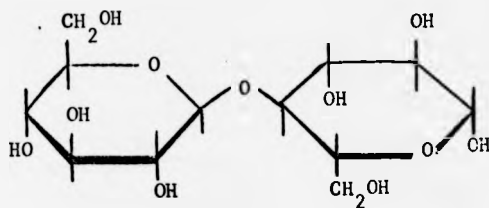
	Page
Chapter 1 INTRODUCTION	1
Chapter 2 EXPERIMENTAL	19
<u>A: Materials</u>	22
(i) Samples previously prepared by other workers.	22
(ii) Esterification of branched $\alpha$ -(1 $\rightarrow$ 4)-linked glucans.	23
<u>B: Methods</u>	30
(i) Density Gradient Technique.	30
(ii) Torsional Braid Analysis.	30
(iii) Differential Scanning Calorimetry.	39
(iv) The significance of the Transition Temperature Data.	43
Chapter 3 RESULTS	
<u>A: TBA Data of Several Poly(di-n-alkylitaconates) and of Poly(methyl methacrylate)</u>	56
(i) The glass transition region.	56
(ii) The secondary transition regions.	74
<u>B: TBA Data of Several Polysaccharide Derivatives</u>	85
(i) The glass transition region.	85
(ii) The secondary transition regions.	101
<u>C: Differential Scanning Calorimeter Data</u>	126
(i) Thermogram features of several poly(di-n-alkylitaconates) and of poly(methyl methacrylate).	134
(ii) Thermogram features of several polysaccharide derivatives.	150
Chapter 4 DISCUSSION	181
(i) The glass transition temperatures of polysaccharide derivatives.	183
(ii) The glass and sub-glass transition temperatures of poly(di-n-alkylitaconates) and of poly(methyl methacrylate).	188
(iii) The sub-glass transition temperatures of polysaccharide derivatives.	198
REFERENCES	203

CHAPTER 1

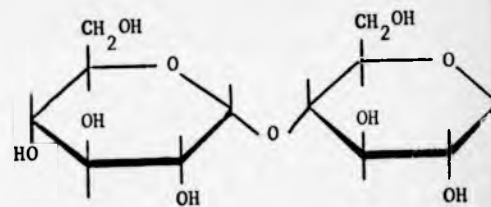
INTRODUCTION

DIAGRAM 1

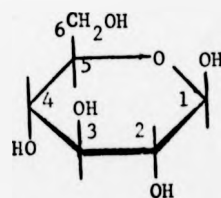
Haworth Formulae for :



Cellobiose



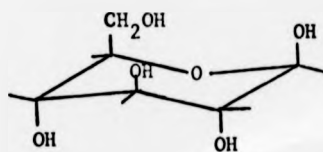
Maltose



β-D-Glucose

Chair Conformations for :

1C



β-D-Glucose

C1

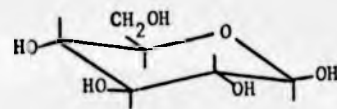
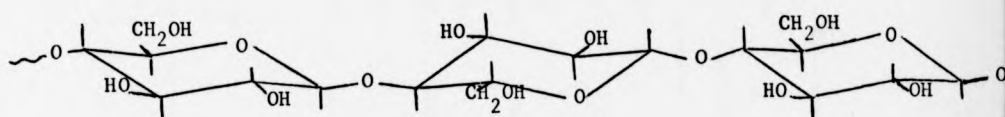
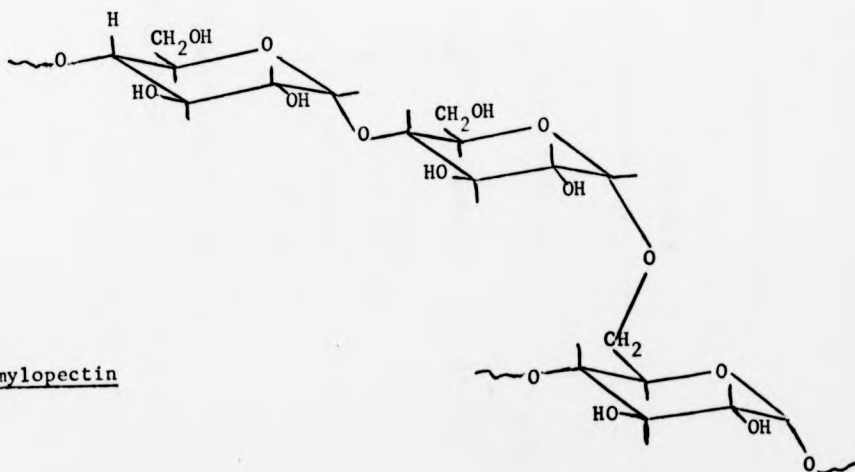


DIAGRAM 2

Chair Conformations for :



Cellulose



Amylopectin

TABLE 1(i)

Sample Structures

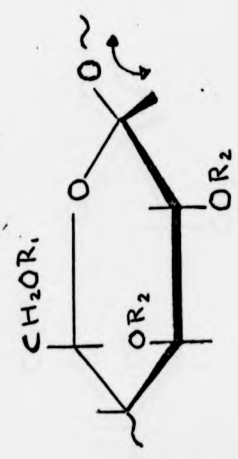
<u>Generalized Monomer Unit</u>	<u>Name of Sample Parent Polysaccharide</u>	<u>Name(s) of -OR<sub>1</sub>, -OR<sub>2</sub></u>	<u>Chemical Structure of Substituent Groups -OR<sub>1</sub>, -OR<sub>2</sub></u>
	amylose	triacetate	$\left. \begin{array}{l} -OR_1, \\ -OR_2 \end{array} \right\} = CH_3 - C \begin{array}{l} \diagup O \\ \diagdown O \end{array}$
	amylopectin	tripropionate	$\left. \begin{array}{l} -OR_1, \\ -OR_2 \end{array} \right\} = CH_3 - CH_2 - C \begin{array}{l} \diagup O \\ \diagdown O \end{array}$
	amylopectin β-L-D	tributyrate	$\left. \begin{array}{l} -OR_1, \\ -OR_2 \end{array} \right\} = CH_3 - (CH_2)_2 - C \begin{array}{l} \diagup O \\ \diagdown O \end{array}$
	glycogen	trivalerate	$\left. \begin{array}{l} -OR_1, \\ -OR_2 \end{array} \right\} = CH_3 - (CH_2)_3 - C \begin{array}{l} \diagup O \\ \diagdown O \end{array}$
	glycogen β-L-D	tri-isobutyrate	$\left. \begin{array}{l} -OR_1, \\ -OR_2 \end{array} \right\} = \begin{array}{c} CH_3 \\ \diagdown \\ CH - C \begin{array}{l} \diagup O \\ \diagdown O \end{array} \\ \diagup \\ CH_3 \end{array}$

TABLE 1(i)

Sample Structures

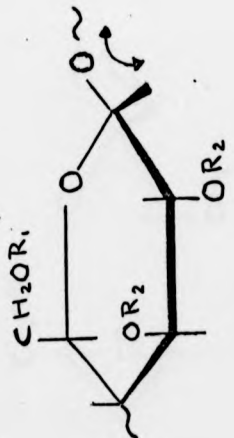
Generalized Monomer Unit	Parent Polysaccharide	Name of Sample	Name(s) of $-OR_1, -OR_2$	Chemical Structure of Substituent Groups $-OR_1, -OR_2$
	amylose		triacetate	$\left. \begin{array}{l} -OR_1, \\ -OR_2 \end{array} \right\} = CH_3 - C \begin{array}{l} \text{O} \\ \parallel \\ \text{O} \end{array} -$
	amylopectin		triacetate	$\left. \begin{array}{l} -OR_1, \\ -OR_2 \end{array} \right\} = CH_3 - CH_2 - C \begin{array}{l} \text{O} \\ \parallel \\ \text{O} \end{array} -$
	amylopectin $\beta$ -L-D		tripropionate	$\left. \begin{array}{l} -OR_1, \\ -OR_2 \end{array} \right\} = CH_3 - (CH_2)_2 - C \begin{array}{l} \text{O} \\ \parallel \\ \text{O} \end{array} -$
	glycogen		tributyrate	$\left. \begin{array}{l} -OR_1, \\ -OR_2 \end{array} \right\} = CH_3 - (CH_2)_2 - C \begin{array}{l} \text{O} \\ \parallel \\ \text{O} \end{array} -$
	glycogen $\beta$ -L-D		trivalerate	$\left. \begin{array}{l} -OR_1, \\ -OR_2 \end{array} \right\} = CH_3 - (CH_2)_3 - C \begin{array}{l} \text{O} \\ \parallel \\ \text{O} \end{array} -$
	glycogen		tri-isobutyrate	$\left. \begin{array}{l} -OR_1, \\ -OR_2 \end{array} \right\} = \begin{array}{c} CH_3 \\ \diagup \\ CH - C \begin{array}{l} \text{O} \\ \parallel \\ \text{O} \end{array} - \\ \diagdown \\ CH_3 \end{array}$

TABLE I(i) (continued)

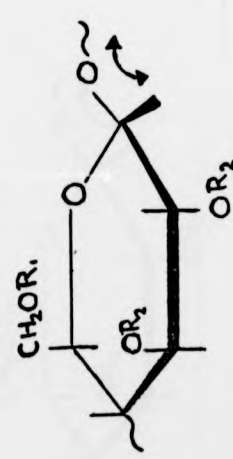
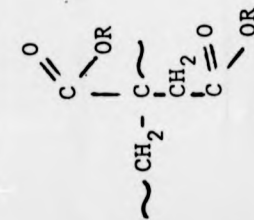
<u>Generalized Monomer Unit</u>	<u>Name of Sample Parent Polysaccharide</u>	<u>Name(s) of -OR<sub>1</sub>, -OR<sub>2</sub></u>	<u>Chemical Structure of Substituent Groups -OR<sub>1</sub>, -OR<sub>2</sub></u>
	<p>amylose glycogen amylose-grafted-glycogen cellulose</p>	<p>tricarbanilate</p>	<p>-OR<sub>1</sub>, -OR<sub>2</sub> =</p> 
cellulose		triacetate	<p>-OR<sub>1</sub>, -OR<sub>2</sub> = <math>\text{CH}_3 - \text{C} \begin{matrix} \text{O} \\ \parallel \\ \text{O} \end{matrix} - \text{O} -</math></p>

TABLE 1(ii)  
Sample Structures

<u>Generalized Monomer Unit</u>	<u>Name(s) of Substituent Groups</u>	<u>Name of Sample Parent Polysaccharide</u>	<u>Chemical Structure of Substituent Groups -OR<sub>1</sub>, -OR<sub>2</sub></u>
	tri-0-tosyl	amylose	$-OR_1, -OR_2 = \text{CH}_3 - \text{C}_6\text{H}_4 - \text{S}(=\text{O})_2 - \text{O}-$
	2,3-di-0-acetyl, 6-0-trityl	amylose	$-OR_1 = \text{C}_6\text{H}_5 - \text{C}(=\text{O}) - \text{O}-$ $-OR_2 = \text{CH}_3 - \text{C}(=\text{O}) - \text{O}-$
	6-0-trityl	amylose	$-OR_1 = \text{C}_6\text{H}_5 - \text{C}(=\text{O}) - \text{O}-$ $-OR_2 = -\text{OH}$

TABLE 1(iii)  
Sample Structures

<u>Generalized Monomer Unit</u>	<u>Name of Polymer</u>	<u>Structure of Alkyl Groups -R<sub>1</sub>, -R<sub>2</sub></u>
$\begin{array}{c} \sim \text{CH}_2 - \text{C} \begin{array}{l}   \\ \text{R}_1 \end{array} \\   \\ \text{O} = \text{C} - \text{OR}_2 \end{array}$	poly(methyl methacrylate)	-R <sub>1</sub> , -R <sub>2</sub> = -CH <sub>3</sub>



Poly(di-n-alkylitaconate) polymers, of which samples were provided, -R representing the n-alkyl group in the general formula:  
with the exception of poly(di-n-pentylitaconate), all series members between poly(di-methylitaconate), with R = CH<sub>3</sub>, to poly(di-n-dodecylitaconate), with R = C<sub>12</sub>H<sub>25</sub>, inclusive.

TABLE 2

Literature Values of Tg's, Evaluated with Low Frequency Techniques, for Polymers Structurally Identical to Samples to be Studied in this Work

<u>Sample</u>	<u>Tg(°C)</u>	<u>Details of Technique</u>	<u>Reference</u>
amylose triacetate	167	Differential Scanning Calorimetry;	
amylose tripropionate	133	scan rate of 5 or 10 degrees per	(20)
amylose tributyrate	92	minute	
amylose trivalerate	57		
<hr/>			
	179	Differential Thermal Analysis; scan rate	(28)
		of 20 degrees per minute	
<hr/>			
cellulose triacetate	190	Torsional Braid Analysis at about 0.1 Hz;	(29)
		heated at 2 degrees per minute	
<hr/>			
	155	Dilatometrically obtained Specific Volume-Temperature	(30)
		data	
<hr/>			
Conventional poly-(methyl methacrylate)	105	Generally accepted value	(32)

Polymers are composed of exceptionally long molecules and therefore at intermediate temperatures and frequencies, in addition to varying with temperature, their physical properties are time-dependent; polymers are therefore said to be viscoelastic. Tobolsky (1) describes the viscoelastic behaviour of linear, amorphous polymers, of high molecular weight, in terms of five characteristic regions in the variation with temperature of the 10-second, tensile-stress relaxation modulus. The explanation of the involved molecular motions are based on Tobolsky's ideas (1), together with those of Billmeyer (2), Meares (3) and Treloar (4).

When studied at very low temperatures (or high frequencies) the polymer behaves like a glass; a glassy polymer is stiff, hard, brittle and frequently transparent. Transparency is a characteristic of randomly arranged molecules. The magnitude of stress required to produce unit deformation is known as the modulus of a material, providing a measure of its stiffness or dimensional stability. Intermolecular forces predominate in the glassy state, resulting in a very high value for the tensile-stress relaxation modulus; as a result, in time intervals of less than 10 seconds, there is effectively no diffusional motion of the chain segments and polymer behaviour tends towards that of an ideal elastic solid (5), the application of stress resulting in instantaneous bond stretching and bond angle deformation according to Hooke's Law.

At higher temperatures, the polymer feels leathery and the 10-second modulus decreases by a factor of about a

thousand within a narrow temperature range. In this transition region, the unique viscoelastic behaviour of polymers predominates, polymer deformation under stress being both reversible and very time-dependent. Short-range diffusional motion of chain segments takes place within about 10 seconds, the majority of polymer molecules being distorted from their equilibrium conformations in the direction of the applied stress. Due to the viscous resistance of the surrounding medium, the highly elastic response of the polymer is delayed, although appreciable during 10 seconds, and relative molecular movement results in the dissipation of a large amount of energy, maximum energy loss, or damping, occurring at about the median temperature of the transition range, where the modulus is decreasing most rapidly with increase in temperature and many segments become mobile within the 10-second interval.

At temperatures immediately above the transition region the modulus varies little with temperature and polymers exhibit rubber-like elasticity: with respect to the 10-second time scale they are capable of very large extensions, which are instantaneously completely reversible. Hooke's Law describes the effectively time-independent elastic behaviour of rubbers and glasses which therefore dissipate little potential energy into heat on deformation. Rapid short-range diffusional motion of the chain segments, involving rotation about covalent bonds, results in internal rearrangement of molecular conformations and is manifest as flexibility of the polymer, but breakdown of the restraining molecular entanglements is still relatively slow.

In the adjacent viscoelastic region, the rubbery polymer feels tacky, because under stress long-range chain

entanglements are breaking down in times of the order of 10 seconds, enabling whole molecules to flow into unstressed situations where they become entangled again. At higher temperatures, the polymer is a viscous liquid, stresses or strains maintained for longer than 10 seconds resulting in effectively irreversible bulk deformation. Elastic recovery is negligible because co-operative diffusional movement of many chain segments can take place in less than 10 seconds, unimpeded by temporary crosslinks which unravel at a similar rate. Damping is high in the fifth region, energy being required to enable molecules to flow past one another.

On raising the temperature of a polymer through the second region, its properties change from those of a rigid glass to those of a flexible rubber, the temperature interval therefore being known as the glass transition region. Boyer (6) defines "the glass transition as being associated with a coordinated segmental motion of the grouping  $-(\text{CH}_2-\text{CHR})_n-$  about the polymer chain axis, with  $n$  having a value in the range 10 to 20." Conventionally, the glass transition temperature,  $T_g$ , is identified with the temperature at which the specific volume-temperature plot of an amorphous polymer exhibits an abrupt change in slope; because a true change in state or structure is not involved, there is no discontinuity in the volume of a polymer at its  $T_g$ . Similarly, the temperature-dependence of physical properties such as heat content and refractive index alters quite sharply at  $T_g$ , although the change in mechanical properties extends over a wide temperature range. An arbitrary modulus value must therefore be chosen in

order to identify  $T_g$  from modulus-temperature data in the transition region. "Tobolsky and his school specified the reference state as  $0.33 \times 10^8$  dynes per  $\text{cm}^2$  after 10 seconds of stress relaxation, the resulting temperature being very near the dilatometrically or calorimetrically determined value of  $T_g$ ." (1)

$T_g$  is a parameter of primary importance in determining the behaviour of a polymer under its conditions of application; however, despite extensive study of the variation of  $T_g$  with chemical structure "much of the knowledge is empirical due primarily to the difficulty of separating intramolecular and intermolecular effects." (7) Although prediction of  $T_g$  from detailed considerations of molecular structure is still not possible, some general trends are apparent, as reported by Boyer (8), Nielsen (9) and many other authors. The polymer with the simplest structure is polyethylene; structurally different polymers containing substituents which lower the over-all energy requirements of microbrownian segmental motion reduce  $T_g$  and conversely the presence of groups which decrease molecular flexibility increases  $T_g$  relative to that of polyethylene. The introduction into the main chain of moieties such as oxygen or sulphur lowers  $T_g$  by increasing the flexibility of the polymer molecules.  $T_g$  is elevated for macromolecules including side groups which restrict rotation about the backbone chain by sterically hindering main chain motion and/or side group motion relative to the main chain, or which are themselves bulky and inflexible. A reduction in intramolecular stiffness results from the replacement of a bulky rigid side group with a more flexible isomer;  $T_g$  is also

order to identify  $T_g$  from modulus-temperature data in the transition region. "Tobolsky and his school specified the reference state as  $0.33 \times 10^8$  dynes per  $\text{cm}^2$  after 10 seconds of stress relaxation, the resulting temperature being very near the dilatometrically or calorimetrically determined value of  $T_g$ ." (1)

$T_g$  is a parameter of primary importance in determining the behaviour of a polymer under its conditions of application; however, despite extensive study of the variation of  $T_g$  with chemical structure "much of the knowledge is empirical due primarily to the difficulty of separating intramolecular and intermolecular effects." (7) Although prediction of  $T_g$  from detailed considerations of molecular structure is still not possible, some general trends are apparent, as reported by Boyer (8), Nielsen (9) and many other authors. The polymer with the simplest structure is polyethylene; structurally different polymers containing substituents which lower the over-all energy requirements of microbrownian segmental motion reduce  $T_g$  and conversely the presence of groups which decrease molecular flexibility increases  $T_g$  relative to that of polyethylene. The introduction into the main chain of moieties such as oxygen or sulphur lowers  $T_g$  by increasing the flexibility of the polymer molecules.  $T_g$  is elevated for macromolecules including side groups which restrict rotation about the backbone chain by sterically hindering main chain motion and/or side group motion relative to the main chain, or which are themselves bulky and inflexible. A reduction in intramolecular stiffness results from the replacement of a bulky rigid side group with a more flexible isomer;  $T_g$  is also

decreased with increase in the length of pliant pendant groups which experience weak intermolecular interactions, the decrease in intramolecular flexibility due to enlargement of such side groups as n-alkyl chains apparently being of secondary importance. Increased polarity of polymer molecules, due to atoms which do not reduce intramolecular stiffness, raises Tg by enhancing intermolecular attraction, thereby restricting main chain mobility. Some polymers with symmetrically substituted monomer units,  $-\text{CH}_2-\text{CR}_2-$ , are known to have lower Tg's than those composed of  $-\text{CH}_2-\text{CHR}-$  groups.

Tg is essentially independent of molecular weight for high polymers: for samples composed of relatively short molecules Tg decreases concomitantly with their average molecular weight; in addition, because the extent of molecular entanglement, and therefore hindrance to flow, depends on the length of the polymer chains, very low molecular weight samples do not exhibit rubber-like elasticity above Tg. Polymers with perfectly regular chains are capable of crystallization, but due to the length of macromolecules and the resulting strength of the intermolecular forces, a proportion of the polymer always remains randomly disordered. In semi-crystalline polymers, molecular mobility in the persistent amorphous regions is restricted by the ordered phase, the glass transition being manifest at higher temperatures by property changes of diminishes magnitude.

Below its glass transition temperature the polymer is likely to be brittle, being unable to withstand large stresses or strains because the large scale segmental motion responsible for rubber-like elasticity is no longer energetically feasible. However the brittleness of a polymeric glass is less extreme than that of inorganic glasses because local molecular motions

persist to temperatures lower than  $T_g$ . Many polymers in the glassy state exhibit discontinuities in temperature-dependent properties at temperatures where motion, often restricted, of a significant number of short chain segments or side groups becomes possible (9). These less obvious secondary glass transitions can modify mechanical behaviour and are therefore of considerable technological importance (1): for example, Boyer (10) has shown that a substantial low-temperature secondary transition can impart toughness to a glassy polymer. Multiple glass transitions may be the manifestations of a variety of molecular motions (11), the size of the moving group increasing concomitantly with its onset temperature (10). Eby (12) deduced that 2 to 5 monomer units are involved in secondary glass transitions and 16 to 29 monomers in the main glass transition. Boyer (8) reports that Schmieder and Wolf were the first to find "that most polymers exhibit a small number of discrete but relatively broad dynamic mechanical energy loss peaks when examined over a wide temperature range by a low frequency method." It is recognised that the lower the transition temperature at 1 Hz, and therefore the more localized the associated motion, the greater is the transition temperature elevation with increase in frequency of the measuring technique. This effect is a result of the differing activation energies of mechanisms controlling the modes of molecular motion in solid polymers, the lower activation energies being associated with the damping peaks at lower temperatures: Heijboer (13) states that "the activation energy for the glass transition is of the order of magnitude of 100 kcals per mole, whereas for the secondary processes the activation energy is of the order of 10 kcals per mole."

Consequently, the lower the frequency of a dynamic test, the greater the resolution of the damping data; as an additional advantage, the results of low frequency methods can be easily correlated with transition temperatures evaluated by the effectively static dilatometric and thermal techniques (14). It was therefore decided to attempt to determine  $T_g$  and secondary transition temperatures, sub- $T_g$ 's, of selected polymer systems with a low frequency dynamic mechanical technique, complemented by measurements of their coefficients of expansion and specific heats. It was hoped that a study of the temperature-dependence of damping, heat capacity and specific volume of new polymer series would provide greater understanding about the "relationship between variations in macroscopic physical properties and mobilities of certain atomic groups in the polymers" (15). Likewise, Klarman, Galanti and Sperling (16) studied "six homologs of the cellulose triester series" because such "polymer systems, which exhibit multiple transitions offer special research advantages in that possibly each transition may be attributed to specific chemical groups."

The polysaccharides to be studied are polycondensation products of D-glucose monosaccharide units, glycosidically linked with the elimination of water; these polymers are known as glucans. The Haworth formula for  $\beta$ -D-glucose is shown at the centre of Diagram 1 and includes numbering of the carbon atoms, C1 to C6, hydrogen atoms bonded to carbon atoms in the pyranose, or six-membered, ring being omitted for clarity. Cellulose is the most abundant naturally-occurring organic compound; its linear molecules consist of up to five thousand  $\beta$ -D-glucopyranose units, with a  $\beta$ -glycoside linkage between C1 and C4 of adjacent

rings. Its essentially rigid molecules, containing a regularly alternating arrangement of D-glucose rings, may be regarded as a series of cellobiose units (17); cellobiose, illustrated at the top of Diagram 1, is a disaccharide formed by the condensation of two  $\beta$ -D-glucopyranose monomers, the second ring being inverted in order to minimize non-bonded interactions.

Starch is a widely distributed plant reserve carbohydrate, the essentially linear, water-soluble component being known as amylose. Like cellulose, amylose contains as many as five thousand D-glucopyranose units: unlike cellulose, the monosaccharides are joined by  $\alpha$ -(1 + 4) glucoside linkages to form flexible, extended molecules, which are able to exist in helical conformations. The polycondensation of maltose, also shown in Diagram 1, would yield amylose. About four-fifths of starch carbohydrate is insoluble in water, this fraction being composed of the polyglucan called amylopectin. The highly-branched amylopectin structure contains up to one million pyranose rings; 20 to 25  $\alpha$ -D-glucose units are linked  $\alpha$ -(1 + 4) to form chains, structurally similar to those in amylose, which branch via  $\alpha$ -(1 + 6) bonds. The amylopectin molecule contains no definite principal chain and is therefore spherical in shape and multiply-branched, manifest macroscopically by its fibrous nature. Glycogen is a granular, water-soluble reserve polysaccharide found in several animal species. Glycogen molecules have an apparent molecular weight of many million, being more highly branched than the structurally-similar amylopectin molecules;  $\alpha$ -(1 + 6) links at the multiple branch points connect chains of 12 to 18  $\alpha$ -D-(1 + 4)-linked glucose monomers (18).

The enzyme  $\beta$ -amylase hydrolyses linear  $\alpha$ -D-(1  $\rightarrow$  4)-linked glucans to maltose. The degradation of amylopectin and glycogen is never complete, the enzyme proceeding from the non-reducing end of a pendant  $\alpha$ -(1  $\rightarrow$  4)-linked D-glucose chain until it is stopped by an  $\alpha$ -(1  $\rightarrow$  6) branch point; the product is called the  $\beta$ -amylase limit dextrin, abbreviated to  $\beta$ -L-D.  $\beta$ -amylase degrades the shorter  $\alpha$ -(1  $\rightarrow$  4)-linked chains of glycogen to maltose in 45 per cent yield, the  $\beta$ -amylolysis limit for amylopectin being about 55 per cent (19).

The oxygen atom in pyranose monosaccharide rings has little effect on their molecular geometry and it has been confirmed that conformational knowledge based on observations of the differing forms of the cyclohexane ring may be applied to the cyclic monosaccharides. In general, pyranose monosaccharides such as D-glucose tend to exist in two interchangeable chair conformations, designated C1 and 1C, which are represented in Diagram 1; in preferred conformations, large substituents, such as the group attached to C5, extend outwards in equatorial positions (19). Diagram 2 illustrates portions of cellulose and amylopectin molecules with the D-glucose monomer units in chair conformations (18).

The structure of the samples to be studied are given in Table 1. Cowie et al provided a series of characterized amylose triesters from the acetate to the n-valerate inclusive; a Perkin-Elmer Differential Scanning Calorimeter, Model DSC-1, was used in the measurement of their Tg's, given in Table 2 (20). Branched polysaccharides were to be acylated, as their Tg's would be relevant to evaluation of the various theories of the glass transition. A sample of poly(methyl methacrylate),

free-radically prepared and therefore with sixty to eighty per cent in the syndiotactic form, was also made available by Cowie, together with tri-O-tosyl amylose; 2,3-di-O-acetyl, 6-O-trityl amylose; 6-O-trityl amylose and cellulose triacetate samples.

Burchard, of the Institute of Macromolecular Chemistry in Freiburg, provided carbanilate derivatives of polysaccharides, formed by their reaction with phenyl isocyanate. Studies have been made of the hydrodynamic properties of cellulose and amylose tricarbanilates (21) and of amylose-grafted-glycogen tricarbanilates (22). The solid state structures of cellulose and amylose tricarbanilate molecules have been investigated by electron-microscopy (23). Cowie has made several attempts to measure Tg's of carbanilate derivatives: satisfactory interpretation of their Differential Thermal Analysis, DTA, records proved impossible; the density-gradient technique provided specific volume-temperature data which revealed secondary transitions but which always ceased at temperatures below Tg due to sample dissolution (24).

The general formula of poly(di-n-alkylitaconate) polymers is shown at the foot of Table 1. Velickovic developed the synthesis of this relatively new series of polymers and generously provided many samples, Velickovic et al have investigated the solution properties of poly(di-n-alkylitaconates) (25,26,27), but no other solid state study is known to date.

Cowie and Ranson (28) used a Du Pont 900 DSC instrument to measure Tg's of several cellulose acetate samples, the average of their values for the two samples with the highest degree of substitution being given in Table 2. Gillham (29) determined the Tg of a cellulose triacetate sample containing

only 0.15 per cent of unsubstituted hydroxyl; the DTA thermogram, obtained at about five degrees per minute, contained an endothermic shift centred on  $191^{\circ}\text{C}$ , effectively coincident with the maximum in mechanical damping recorded on his Torsional Braid Analyzer. Cellulose triacetate, CTA, and poly-(methyl methacrylate) are the only samples to be studied whose sub-Tg's have been evaluated by low frequency techniques. Correlated torsional pendulum data enabled Russel and Van Kerpel (30) to attribute the discontinuity in the CTA coefficient of expansion at  $155^{\circ}\text{C}$  to Tg. Their dilatometric data also revealed transitions at  $40^{\circ}\text{C}$  and  $120^{\circ}\text{C}$ , in general agreement with the specific volume studies of Mandelkern and Flory and of Nakamura, summarized in reference 30. Russel and Van Kerpel detected a small dynamic mechanical loss peak at  $-48^{\circ}\text{C}$ , possibly associated with mobility of the acetate group (30). Sharples and Swinton (31) also detected three second-order transitions in their CTA dilatometric data at  $46^{\circ}\text{C}$ ,  $112^{\circ}\text{C}$  and  $157^{\circ}\text{C}$ .

McCrum, Read and Williams (32) have reviewed the considerable quantity of data on conventional poly(methyl methacrylate), which is prepared by free-radical initiation at elevated temperatures and is known to be predominantly syndiotactic. With a measuring frequency of 1 Hz, Heijboer (33) observed a secondary dynamic mechanical loss peak at  $10^{\circ}\text{C}$ , which has been reported by many other authors and which is generally attributed to a hindered rotation of the ester side chain. In addition, dynamic mechanical measurements at 1 Hz revealed a small loss peak at  $-173^{\circ}\text{C}$ , assigned to rotation of  $\alpha$ -methyl groups, and another in the vicinity of  $-100^{\circ}\text{C}$  which

is known to be caused by water in the sample (32).

Tg and sub-Tg data for cellulose acetates with various degrees of substitution and for longer-chain cellulose esters, and transition temperatures of members of the poly(alkyl-alkacrylate) series, structurally similar to poly(di-n-alkyl-itaconate) polymers, are well reported in the literature and will be presented in the final chapter, as relevant to the interpretation of results obtained for the samples described above.

CHAPTER 2

EXPERIMENTAL

TABLE 3(i)

Abbreviated Names and Characteristics of Poly(di-n-alkyl-itaconates) and of Poly(methyl methacrylate)

<u>Name of Sample</u>	<u>Abbreviated Name</u>	<u>Symbol</u>	<u>Approximate Mw</u>
Poly(di-methylitaconate)	PDM1	80/25	74,000*
	PDM1	37/100	451,000*
Poly(di-ethylitaconate)	PDE1		200,000
Poly(di-propylitaconate)	PDP1		489,000
Poly(di-n-butylitaconate)	PDB1	70/100	95,000
	PDB1	35/25	1,881,000
Poly(di-n-hexylitaconate)	PDH1	55/100	277,000
	PDH1	45/100	684,000
Poly(di-n-heptylitaconate)	PDHp1	70/50	434,000
	PDHp1	60/50	395,000
	PDHp1	50/50	763,000
Poly(di-n-octylitaconate)	PD01		400,000
Poly(di-n-nonylitaconate)	PDN1		300,000
Poly(di-n-decylitaconate)	PDD1	60/32	107,700
	PDD1	40/42	800,000
	PDD1	40/32	212,000
Poly(di-n-undecylitaconate)	PDU1		1,840,000
Poly(di-n-dodecylitaconate)	PDD01		200,000
Poly(methyl methacrylate)	PMMA		

\* Note: These values are number-average molecular weights

TABLE 3(ii)

Abbreviated Names and Characteristics of Polysaccharide Derivatives

<u>Name of Sample</u>	<u>Abbreviated Name</u>	<u>Sample Characteristics</u>	
		<u>Approximate D.S.</u>	<u>M<sub>n</sub></u>
amylose triacetate	ATA	3.0	62,000
amylose tripopionate	ATP	3.0	68,000
amylose tributyrate	ATB	3.0	106,000
amylose trivalerate	ATV	2.8	145,000
cellulose triacetate	CTA	3.0	
amylose carbanilate	AC(2.5)	2.5	
amylose tricarbanilate	ATC	3.0	
cellulose tricarbanilate	CTC(15.1x10 <sup>3</sup> )	3.0	<u>M<sub>w</sub></u> 15,100
glycogen tricarbanilate	GTC(5.0x10 <sup>6</sup> )		5.0x10 <sup>6</sup>
grafted glycogen tricarbanilate	GTC(gr 8.3x10 <sup>6</sup> )		8.3x10 <sup>6</sup>
6-0-trityl amylose	ATr(1.0)		
2,3-di-0-acetyl,6-0-trityl amylose	ATr(1.0), A(2.0)		
tri-0-tosyl amylose	ATT		{sulphur content approx. 12 per cent
glycogen tri-iso-butyrate	GTiso-B		
glycogen triacetate	GTA		
glycogen β-amylase limit dextrin tripropionate	GTP(β-L-D)		
amylopectin tributyrate	ApTB		
amylopectin β-amylase limit dextrin trivalerate	ApTV(β-L-D)		

TABLE 3(ii)

Abbreviated Names and Characteristics of Polysaccharide Derivatives

<u>Name of Sample</u>	<u>Abbreviated Name</u>	<u>Sample Characteristics</u>	
		<u>Approximate D.S.</u>	<u>M<sub>n</sub></u>
amylose triacetate	ATA	3.0	62,000
amylose tripopionate	ATP	3.0	68,000
amylose tributyrate	ATB	3.0	106,000
amylose trivalerate	ATV	2.8	145,000
cellulose triacetate	CTA	3.0	
<hr/>			
amylose carbanilate	AC(2.5)	2.5	
amylose tricarbaniolate	ATC	3.0	
<hr/>			
cellulose tricarbaniolate	CTC(15.1x10 <sup>3</sup> )	3.0	<u>M<sub>w</sub></u> 15,100
glycogen tricarbaniolate	GTC(5.0x10 <sup>6</sup> )		5.0x10 <sup>6</sup>
grafted glycogen tricarbaniolate	GTC(gr 8.3x10 <sup>6</sup> )		8.3x10 <sup>6</sup>
<hr/>			
6-0-trityl amylose	ATr(1.0)		
2,3-di-0-acetyl,6-0-trityl amylose	ATr(1.0), A(2.0)		
tri-0-tosyl amylose	ATT		{sulphur content approx. 12 per cent
<hr/>			
glycogen tri-iso-butyrate	GTiso-B		
glycogen triacetate	GTA		
glycogen β-amylase limit dextrin tripropionate	GTP(β-L-D)		
amylopectin tributyrate	ApTB		
amylopectin β-amylase limit dextrin trivalerate	ApTV(β-L-D)		

Section A: Materials(i) Samples previously prepared by other workers

As mentioned in the previous chapter, many polymer samples were provided by my supervisor, J.M.G. Cowie, and his colleagues; characteristics of these samples and abbreviations for their names, which will be subsequently used, are given in Table 3. Velickovic prepared the poly(di-n-alkylitaconates) by bulk free-radical polymerization, their symbols being derived from their conditions of synthesis: for example, PDMI 80/25 was produced at 80°C with 0.25 weight per cent of initiator. Weight-average molecular weights,  $\bar{M}_w$ 's, for all samples except PDMI were evaluated by Velickovic from limiting viscosity numbers and from light scattering data (34). Osmotic pressure measurements with a Melabs Recording Membrane Osmometer on PDMI 80/25 and PDMI 37/100 solutions in nitromethane yielded number-average molecular weights,  $\bar{M}_n$ 's, of 74,000 and 451,000 respectively. PDOI, PDNI, PDUI and PDDoI were supplied as n-heptane solutions and PDDI 60/32, PDDI 40/42 and PDE1 samples were dissolved in benzene; with the exception of PDDI, these samples were heated in the pistol oven, attached to the internal vacuum system of the University, for about six hours at 55°C to 70°C. PDHI 55/100 had been transferred from a broken container by dissolution in chloroform; neither PDHI 55/100 nor the two PDDI samples were heated during solvent evaporation. It is feasible that these poly(di-n-alkylitaconates) contain residual solvent.

The  $\beta$ -amylolysis limit for the amylose triesters is 75 per cent on average (24);  $\bar{M}_n$  and the degree of substitution, D.S., of each unfractionated sample is given in Table 3(ii) (20).

The ATC sample is unfractionated, but it is thought that CTC ( $410 \times 10^3$ ) is the only CTC sample that is not composed of molecules with a narrow molecular weight distribution (24). In addition to GTC, three tricarbanilate derivatives of the star-shaped molecules, formed by grafting long amylose chains onto the glycogen kernel (22), were provided, being GTC (gr  $8.3 \times 10^6$ ), GTC(gr  $25 \times 10^6$ ) and GTC(gr  $100 \times 10^6$ ). Fully substituted ATT contains 14 per cent sulphur; it is evident from Table 3 that the sample used in this work has a D.S. below 3.0.

(ii) Esterification of branched  $\alpha$ -(1  $\rightarrow$  4)-linked glucans

The abbreviated names of each type of these polysaccharide esters complete Table 3. Glycogen was obtained from B.D.H. Biochemicals. The amylopectin used in the preparation of acyl derivatives was supplied by J.M.G. Cowie and had been extracted from potatoes by the method of Greenwood et al (35). A further amylopectin sample was supplied by W. Banks of Edinburgh University and was degraded by  $\beta$ -amylase to give the  $\beta$ -amylase limit dextrin; W. Banks also carried out the  $\beta$ -amylolysis of glycogen.

Due to the extreme susceptibility of starch to degradation (36), the preparation, purification and drying of these esters was carried out at ambient temperatures (36,37).

Potter and Hassid's method (37) for the acetylation of the two components of starch at room temperature involved prior dispersion in formamide, enabling mild reaction conditions to be effective. Branched  $\alpha$ -(1  $\rightarrow$  4) glucans were acylated by reaction with the relevant anhydrides in the presence of pyridine, n-alkyl anhydrides being used in all preparations except that of glycogen

The ATC sample is unfractionated, but it is thought that CTC ( $410 \times 10^3$ ) is the only CTC sample that is not composed of molecules with a narrow molecular weight distribution (24). In addition to GTC, three tricarbanilate derivatives of the star-shaped molecules, formed by grafting long amylose chains onto the glycogen kernel (22), were provided, being GTC (gr  $8.3 \times 10^6$ ), GTC(gr  $25 \times 10^6$ ) and GTC(gr  $100 \times 10^6$ ). Fully substituted ATT contains 14 per cent sulphur; it is evident from Table 3 that the sample used in this work has a D.S. below 3.0.

(ii) Esterification of branched  $\alpha$ -(1  $\rightarrow$  4)-linked glucans

The abbreviated names of each type of these polysaccharide esters complete Table 3. Glycogen was obtained from B.D.H. Biochemicals. The amylopectin used in the preparation of acyl derivatives was supplied by J.M.G. Cowie and had been extracted from potatoes by the method of Greenwood et al (35). A further amylopectin sample was supplied by W. Banks of Edinburgh University and was degraded by  $\beta$ -amylase to give the  $\beta$ -amylase limit dextrin; W. Banks also carried out the  $\beta$ -amylolysis of glycogen.

Due to the extreme susceptibility of starch to degradation (36), the preparation, purification and drying of these esters was carried out at ambient temperatures (36,37).

Potter and Hassid's method (37) for the acetylation of the two components of starch at room temperature involved prior dispersion in formamide, enabling mild reaction conditions to be effective. Branched  $\alpha$ -(1  $\rightarrow$  4) glucans were acylated by reaction with the relevant anhydrides in the presence of pyridine, n-alkyl anhydrides being used in all preparations except that of glycogen

isobutyrate; reagent proportions for the two-stage procedure of Potter and Hassid were based on those used by Cowie in the acetylation of amylopectin (35): "amylopectin (250 mg) was dispersed by stirring in formamide (6 ml) and pyridine (10 ml) was added slowly with continuous stirring, followed by acetic anhydride (8 ml) in small portions over a period of 1 hour." After continual magnetic stirring at ambient temperatures and subsequent precipitation and isolation, the procedure was repeated by dissolving the partially acetylated product in pyridine (10 ml) and acylating at room temperature with the same anhydride (8 ml) as before. Between 0.6 and 1.0g of the parent polysaccharide was magnetically stirred in pyridine dried with molecular sieve and, in general, the total reaction time increased with the molecular weight of the esterifying anhydride (20,36); glycogen appeared to require a longer reaction time than the analogous amylopectin derivative. Amylopectin spent a total of 5 days in an acetylating reaction mixture, whereas the valeration of glycogen and its  $\beta$ -limit dextrin took 17.5 days. Final reaction mixtures were usually deep gold and/or brown in colour, only the glycogen esters being in solution; insoluble particles were observed in two glycogen ( $\beta$ -L-D) reaction mixtures and due to the difficulty in dispersing amylopectin ( $\beta$ -L-D) gelatinous lumps generally persisted in the latter systems.

After the final esterification, there were at least three precipitations into methanol, with continuous magnetic stirring during slow sample addition, reprecipitations being most frequently from chloroform; although acetone and dioxan have been used as solvents, chloroform proved the most efficient

dispersive agent of the insoluble amylopectin esters. Volumes of drum solvent and precipitant were of the order of 50 ml and 1ℓ respectively. A large volume of solvent was generally required to disperse or dissolve the ester, being subsequently reduced in order to achieve the optimum concentration for sample precipitation in a manageable form; further solvent was frequently required to minimize mechanical losses by rinsing the involved glass surfaces, resulting in a second addition to the precipitant. Unswollen material was rarely removed, filtration of the polymer 'solutions' being particularly impracticable for amylopectin and amylopectin ( $\beta$ -L-D) derivatives. Each purification was optimized by stirring the system for several hours and particle enlargement was often enhanced with repeated stirring after allowing the precipitate to settle; volume reduction sometimes encouraged precipitation. Methanol frequently precipitated the ester at room temperature, but occasionally coagulation of a very fine suspension was initiated by cooling with cardice-acetone; sometimes the precipitate only appeared with subsequent warming of a cold methanol system. The supernatant was frequently siphoned off, leaving between 50 and 100 ml to evaporate from the precipitate; when the sample was suspended in the supernatant it was collected on a grade 4 sintered-glass filter and subsequently eluted with solvent. It was generally easier to handle too dilute a polymer "solution" and to separate the precipitate by filtration. In practice both methods were used, often in conjunction, their inherent limitations with respect to purification efficiency being recognised.

Cowie et al (20) precipitated reaction mixtures for the acylation of amylose into ice water or into petrol ether at  $-25^{\circ}$  to  $-30^{\circ}\text{C}$ ; the colder non-solvent was used for systems containing the largest anhydride molecules because the lower its  $T_g$ , the more gummy the product, this tendency being increased by the presence of low molecular-weight reagents. Difficulty was experienced in the purification of the intractable samples which resulted from precipitation into cold water and/or petrol ether and Ann Macconnachie (38) recommended methanol as a good precipitant for this reaction mixture provided that it was cooled with a cardice-acetone bath and that the methanol rinses were cold. In fact, methanol was found to be so uniquely efficient at preferentially dissolving the low molecular-weight reagents that cooling was rarely necessary and a white precipitate was obtained at room temperature; in comparison, the purification of these esters achieved by freeze drying their benzene solutions or dispersions was negligible and this method was therefore latterly ignored.

Samples were usually dried for several days in the pistol oven at ambient temperatures; the heater was not generally used because its thermostat was unreliable and thermal degradation of the esters was to be avoided. GTB and GTB( $\beta$ -L-D) were the only samples to be dried for a few days in the pistol oven, with its heater at a low setting. The pistol oven was attached to a rotary pump or more frequently to the internal vacuum line of the University, it being known that the latter system rarely achieved very low pressures and that therefore drying in the pistol oven at room temperature cannot have been very efficient. Samples were stored in stoppered sample bottles over silica-gel in a dessicator.

Infra-red, I.R., absorption spectra of all the esterification products were obtained in order to provide an approximate estimate of their degree of substitution together with general confirmation of sample identity and that substantial degradation had not occurred. Sample masses were insufficient for chemical analyses. All I.R. samples had spent at least four days in the pistol oven, evacuated, for all except the valerate esters, by the rotary pump for some of this time. Because amylopectin esters were difficult to dissolve in chloroform, their swollen dispersions were cast directly onto sodium chloride plates and gave reasonable spectra despite visible evidence of undissolved particles. I.R. spectra of films of glycogen esters, soluble in chloroform, were similarly obtained. The rate of evaporation of spectroscopic chloroform, silica-gel dried, from the plates was originally enhanced with the use of an air-blower and latterly with an anglepoise lamp (39), which resulted in spectra with smaller hydroxyl peaks, presumably as cooling caused by evaporation and the resulting condensation of water was thereby minimised; latterly, surfaces contaminated with water were polished from the sodium chloride plates (40). The spectra were obtained, at a medium scan speed, over the 4000 to 250 wavenumbers range, relevant absorption peaks being:

- (a) in the vicinity of 3500 wavenumbers and assigned to the stretching vibrations of unbonded hydroxyl groups and of weak inter- and intramolecularly hydrogen-bonded hydroxyl groups.
- (b) in the 2950 wavenumber region and associated with the C-H stretching mode of primary and secondary alkane groups.
- (c) at about 1750 wavenumbers and attributed to the stretching vibration of the ester carbonyl group (41).

Because of variables in the analysed samples and as the Perkin-Elmer 457 spectrophotometer does not actually record the absorbance, peak areas could not be meaningfully compared (40); however, the optimized procedure enabled qualitative comparison of I.R. spectra of similar samples, obtained on the same day in order to minimise the effects of variables such as atmospheric humidity. Inspection of the magnitude of hydroxyl peaks in spectra containing carbonyl and alkane absorptions of similar magnitude to those of the analogous, characterized amylose ester revealed that sometimes recent esterifications had resulted in noticeably smaller hydroxyl peaks, as demonstrated by the majority of the valerate ester spectra, ATV uniquely having a degree of substitution of only 2.8 (see Table 3). Thus, the I.R. spectra indicated when further esterification was required, as with GTV and GTB and that finally all esters were effectively fully substituted. The spectra also revealed the existence of hydroxyl groups in all samples, emphasizing that water from the laboratory atmosphere was probably present in the I.R. samples.

T<sub>g</sub> is known to vary with molecular weight of small polymer molecules. It is thought that molecules of any polymer with  $\bar{M}_n$  greater than 100,000 and, more specifically, of the amylose esters whose  $\bar{M}_n$  values are given in Table 3 are "sufficiently large to ensure a minimum dependence of T<sub>g</sub> on  $\bar{M}_n$ ." (24,20). Amylopectin and amylopectin (β-L-D) esters are generally insoluble; knowing that the product of deliberate acid hydrolysis of amylopectin had a molecular weight of 500,000 (24), it was assumed that their molecular weights would be

sufficiently high to ensure Tg-constancy, provided that molecular weight data for glycogen esters, prepared under similar, mild, reaction conditions, did not suggest that considerable degradation had occurred. Light scattering data, obtained with the help of Ann Maconnachie, provided very approximate  $\bar{M}_w$  estimates for GTB ( $\beta$ -L-D), one of the two samples dried at above-ambient temperatures, and GTV of 3.5 and 7.0 million respectively. It is therefore assumed that Tg's for the branched esters are molecular-weight-independent.

## Section B: Methods

### (i) Density Gradient Technique

Over a year was spent acquiring apparatus for and experience in the density gradient technique, with reference to many papers and articles, including those by Bauer and Lewin (42), Beevers (43), Oster and Yamamoto (44) and Ranson (45). In addition to pycnometers, density gradient tubes and jacketed cylinders (for the determination of glass float densities from their velocities in homogeneous solutions of known density), pyrex floats containing nickel wire, eventually obtained through the persistence of R. Dey, were manufactured in the glass-blowing workshop according to the method of Gordon and Macnab (46). Unfortunately, further refinement of the technique, necessary for the determination of sub-Tg's, was discontinued due to shortage of time; it is hoped that this work will be continued by a successor as the author believes that this conceptually simple, and therefore reliable, technique justifies further development.

### (ii) Torsional Braid Analysis

Torsional Braid Analysis, TBA, a modification of the conventional Torsional Pendulum technique, was initiated and developed by Gillham (47). As its name implies, the technique of TBA involves the use of an inert multifilament glass braid to support smaller sample quantities; free torsional oscillations of the composite are periodically initiated and its subsequent low frequency, oscillatory deformation is recorded. A Torsional Braid Analyzer Model 100-B1, based on Gillham's apparatus and manufactured by the Chemical Instruments Corporation, CIC, of New York, was used in this work. The reader is referred to

Gillham's comprehensive review (47) for a description of the instrument; in the commercial instrument a glass disc coated with a film gradient acts as the linear optical transducer, enabling the oscillatory movement to be recorded. An external programmer is required in order to provide a constant elevation rate of above-ambient temperatures, the Hewlett-Packard Model 240 Temperature Programmer also being supplied by the CIC together with a 10Mv Heathkit chart recorder. After considerable adjustment to the controls of the temperature programmer, designed for use with G.L.C. ovens, it was realized that cycling of the temperature could not be eliminated. Voltage transformers were required to enable these instruments to be powered by electricity from the National Grid. The Torsional Braid Analyzer facility enabling automatic correction for the un-thermostatted reference junction temperature was by-passed on the realization that a constant ambient temperature of 25°C had been implicitly assumed for the operating environment. During the majority of runs, a continuous non-potentiometric record was obtained of the emf generated by the central iron-constantan thermocouple junction on the inner surface of the sample chamber wall; a portable 27,000 chart recorder, manufactured by Bryans Ltd., was used, the chart being calibrated at the beginning and end of each sub- and above-ambient temperature scan with the output of a millivolt generator on battery supply. Modification of an additional iron-constantan thermocouple, provided by the CIC, and the immersion of its junction in a thermos flask filled with ice and water, enabled the effective reference junction of the central thermocouple, monitoring the sample chamber temperature, to be maintained at 0°C. The signal from the thermocouple in the vicinity of the

Gillham's comprehensive review (47) for a description of the instrument; in the commercial instrument a glass disc coated with a film gradient acts as the linear optical transducer, enabling the oscillatory movement to be recorded. An external programmer is required in order to provide a constant elevation rate of above-ambient temperatures, the Hewlett-Packard Model 240 Temperature Programmer also being supplied by the CIC together with a 10Mv Heathkit chart recorder. After considerable adjustment to the controls of the temperature programmer, designed for use with G.L.C. ovens, it was realized that cycling of the temperature could not be eliminated. Voltage transformers were required to enable these instruments to be powered by electricity from the National Grid. The Torsional Braid Analyzer facility enabling automatic correction for the un-thermostatted reference junction temperature was by-passed on the realization that a constant ambient temperature of 25°C had been implicitly assumed for the operating environment. During the majority of runs, a continuous non-potentiometric record was obtained of the emf generated by the central iron-constantan thermocouple junction on the inner surface of the sample chamber wall; a portable 27,000 chart recorder, manufactured by Bryans Ltd., was used, the chart being calibrated at the beginning and end of each sub- and above-ambient temperature scan with the output of a millivolt generator on battery supply. Modification of an additional iron-constantan thermocouple, provided by the CIC, and the immersion of its junction in a thermos flask filled with ice and water, enabled the effective reference junction of the central thermocouple, monitoring the sample chamber temperature, to be maintained at 0°C. The signal from the thermocouple in the vicinity of the

lower end of the sample composite controlled the temperature programmer. Although the Heathkit recorder functioned satisfactorily after substitution of a gear wheel suitable for a mains frequency of 50 Hz, a second Bryans recorder was generally used to optimize the synchronisation of the oscillation chart with the associated temperature record.

The glass braids supplied by the CIC are eight inches long and made from eight strands, loosely combined with 3.8 turns per inch (48); these substrates are illustrated on page 85 of reference 47. Glass braids were impregnated by immersion, for at least 12 hours, in solutions or inhomogeneous dispersions containing between 1 and 22 per cent (weight/volume) of polymer sample. Samples of CTC, PMMA and PDMI to PDBI inclusive dissolved in acetone, the higher poly(di-n-alkylitaconates) being soluble in chloroform. Chloroform was also used in the preparation of acylated polysaccharide composites; glycogen and amylose esters gave solutions, whereas amylopectin derivatives merely dispersed in this solvent. ATr(1.0), ATT, ATC, AC(2.5), GTC and grafted GTC samples were dissolved in 1,4-dioxan. On removal from the impregnating medium, bulk solvent removal was effected by suspending each braid in the laboratory atmosphere for several hours, tension usually being provided by a boss-head, weighing approximately 70g. After carefully removing any sample from the tags at the ends of the braids, composite specimens were dried for at least two days at room temperature in the pistol oven, the internal vacuum system producing a minimum pressure of 1 mm.

The method of coupling an impregnated braid to the extension rods is illustrated in Figure 2A of reference 47.

In most of this work, four pieces, 1 to 2mm thick, of thin silicon tubing were subsequently placed at the ends of the coupling pins to prevent uncoupling during long TBA experiments. The lower part of Figure 2C in reference 47 contains an illustration of the linear-with-angle optical transmission disc, which displays the serrated teeth designed to couple magnetically with those at the foot of the lower extension rod. Reference 49 contains a detailed description of the magnetic stabilizer, used to break this magnetic coupling at the end of a run, the optical transducer disc, constituting the inertial mass of the suspended assembly, and the method of oscillation activation, involving rotation of the upper part of the assembly through about 30 degrees. Because of extension rod fragility, all operations which could move or shake the instrument were carried out before carefully loading the sample assembly into the Analyzer. In order to prevent sunlight from being reflected into the phototube, folders were always placed around the instrumentation chamber. Oxygen-free nitrogen, O.F.N., flowed, via a column of molecular sieve, through the sample chamber at a rate controlled by a needle valve and monitored by a MeTaRaTe flow meter. The CIC recommended 20ml per minute as the flow rate of environmental gas; at above-ambient temperatures the float height was maintained at about 10 cm, corresponding to the recommended flow rate at room temperature, the analogous height at  $-180^{\circ}\text{C}$ , of about 6.5cm, being generally adopted during analysis at sub-ambient temperatures.

The CIC Torsional Braid Analyzer may be operated between  $-190^{\circ}$  and  $500^{\circ}\text{C}$ . The bed of silica-gel, fluidized by gaseous nitrogen coolant or by air, that constitutes the heat transfer medium of Gillham's instrument (47) is not included

in the Model 100-B1, although Gillham believes that this heat transfer medium is responsible for minimising the temperature spread along the sample to  $\pm 1$  degree (49), even at temperatures below  $0^{\circ}\text{C}$ . The recommended cooling procedure for the Model 100-B1 involves the flow of liquid nitrogen refrigerant from a pressurized cylinder through the two concentric stainless steel jackets that surround the cylindrical sample chamber. The controls of the resistance heater, coiled round the sample chamber, enable voltage to be applied to the lower section alone, in order to minimise the temperature differential along the sample that is a "characteristic of the Model 100-B1" (50). Despite use of the Compensating Heater facility, the recommended method of cooling the instrument produced a very large temperature difference between the iron-constantan thermocouple junctions spanning the vertical location of the braid within the chamber. At very low temperatures, frosting of the lower half of the TBA casing was observed and it was concluded that excessive accumulation of liquid nitrogen at the bottom of the cooling jacket was responsible, the liquefied coolant being unable to exit at the recommended flow rate. In an attempt to minimise the temperature differential across the sample, gaseous O.F.N. was adopted as the coolant, the magnitude of the resulting temperature decrease being controlled by the rate of O.F.N. flow through two large copper spirals immersed in liquid nitrogen (51) within 4.5 litre dewar vessels. A very fast flow rate, of the approximate order of 50 litres per minute, being required for cooling to  $-190^{\circ}\text{C}$ , a glass Venturi flow meter, containing silicon fluid, was designed and made by I. J. McEwen, enabling the high rates of flow to be reproduced. Since the beginning of 1973 a

general procedure was routinely carried out during sub-ambient runs, the following Heater Power settings of the manually-controlled Compensating Heater, supplied by an internal power source, being adopted at the specified temperatures recorded by the central Iron-constantan thermocouple junction:

- (a) as soon as  $-192^{\circ}\text{C}$  was attained, the control was set at 4.
- (b) on warming to approximately  $-120^{\circ}\text{C}$ , the "Heater Power Set" was increased to 4.5.
- (c) at about  $-30^{\circ}\text{C}$ , the Compensating Heater Power was turned OFF.

After maintaining a temperature of  $-192^{\circ}\text{C}$  for about half an hour, to optimize thermal equilibration of the sample with the chamber walls, the coolant flow rate was reduced and warming began. The average rate of temperature increase was estimated periodically, rarely exceeding one degree per minute, and on falling below a half a degree per minute the flow rate was reduced. Above  $-20^{\circ}\text{C}$ , the warming rate was increased by a flow of uncooled O.F.N. through the cooling jacket. For analysis at above-ambient temperatures, a programmed heating rate of one degree per minute was generally used. To enable the heater to be powered by an external programmer the Rear Heater Selector Switch should be changed from INT to EXT, and the Heater Control Switch from COMP to MAIN. During "dry" runs, samples were dissolved in solvents that had been dried with molecular sieve and, after drying in the pistol oven, the composites were exposed to the laboratory atmosphere for a minimal length of time before being loaded into the Analyzer, supplied by environmental O.F.N. which had experienced further drying by passage through two traps full of liquid nitrogen.

Gillham's review (47) outlines the method of reduction of raw TBA data and its theoretical basis. Because of damping within the sample, arising from the gradual conversion of the initial potential energy of deformation into heat, the amplitude of the free oscillations decreases with time; the greater the mechanical damping, the more rapidly the oscillations die out. The duration, in seconds, of one complete oscillation is known as the period,  $P$ , which is the reciprocal of the oscillatory frequency, in cycles per second (Hz). The number of oscillations,  $n$ , that have been recorded between two fixed, but arbitrary, amplitude values,  $A_i$  and  $A_i + n$ , is counted and their average period is evaluated from knowledge of the associated time interval. The two derived characteristic parameters are  $(1/n)$  and  $(1/P^2)$ : the mechanical damping index,  $(1/n)$ , is directly related to the logarithmic decrement,  $\Delta = (1/n)\ln(A_i/A_i + n)$  of the free resonance vibrations;  $(1/P^2)$ , known as the relative rigidity, is a measure of the storage modulus,  $G'$ , provided that damping is low and that the sample dimensions remain constant. The relative shear modulus is evaluated because estimation of the absolute shear modulus  $G'$  would require accurate knowledge of sample dimensions. It should be noted that  $(1/P^2)$  is directly proportional to  $(\text{frequency})^2$ .  $G'$  is defined as the ratio of the stress in phase with the strain to the strain and is directly proportional to the maximum potential energy stored on cyclic deformation. The mechanical loss or damping is given by the ratio  $G''/G'$ , which is "proportional to the ratio of energy dissipated per cycle to the maximum potential energy stored during a cycle" (9). For small values of the loss tangent,  $G''/G'$ :

$$\Delta = \pi(G''/G')$$

(13)

By convention  $(1/n)$  and  $(1/P^2)$  are plotted on a logarithmic (to the base 10) scale, the corresponding temperatures being spaced linearly along the abscissa. The vertical spacing of the  $(1/n)$  data in the original graphs implied the magnitude of the variation related to a unit change in  $n$  and the  $(1/P^2)$  variation resulting from an evaluation error of  $\pm 0.5\text{mm}$  in the length of the associated oscillation record had been estimated; knowledge of these factors enabled the significance of changes in the relative parameters of damping and relative rigidity within a given thermogram to be assessed. For some composites, the alternating direction of the initiating pulse produced a consistent discrepancy between TBA parameters associated with odd and even numbered oscillations, the resulting data being referred to for brevity as "anisotropic".

Because  $G'$  and  $\Delta$  are known to vary with tensile load, the relationships

$$G' \propto (1/P^2)$$

and

$$\Delta = (1/n) \ln(A_i/A_{i+n})$$

are only applicable in the absence of tension (9). It has been assumed that in TBA, the use of a braid with a high tensile modulus ensures that this condition is satisfied. The linear relation between stress and strain, their proportionality constant uniquely defining the modulus, is only observed at small sample deformations. Assuming the composite to be 0.03 inches in diameter (49), the maximum torsional strain for the initial displacement of 30 degrees has been calculated as about 0.001 inches

per inch. Gillham has described several other noteworthy features of TBA: "Although most of the changes in the mechanical behaviour of composite specimens used in TBA can be attributable to the polymer, changes which are the consequence of the composite nature of the specimen are to be anticipated and form the basis of current investigations. Complications can arise from fracture of the polymer, from adhesive failure and from polymer-substrate and polymer-water interactions." The definition of relative rigidity "implicitly assumes that the contribution of dimensional changes to the value of the relative rigidity parameter is dominated by changes in the modulus of the polymer" (47). The validity of this assumption was demonstrated by a calculation of the reduction in relative rigidity arising from substantial weight loss and a resultant radial shrinkage of 25 per cent; it was shown that  $(1/P^2)$ , proportional to  $r^4$ , would decrease by a factor of about 3, considerably less than the change which occurs at  $T_g$ . In this work, samples were heated to just above  $T_g$ , the resulting degradation usually being minimal.

Liquid nitrogen flowed through a coolant jacket during the very earliest sub-ambient experiments and the ensuing temperature differentials between the top and bottom iron-constantan thermocouple junctions were determined. Three thermocouple junctions are located at the inner surface of the Model 100-B1 sample chamber wall, at heights equivalent to those of the mid-point and ends of the sample braid when suspended at the centre of the chamber, which has an internal diameter of 0.7 inches. After the cooling procedure involving gaseous O.F.N. had been optimized, an attempt was made to

evaluate the temperature differentials within the sample chamber and to minimize the actual temperature spread across the sample with the use of the Compensating Heater. An improved estimate of this temperature differential was obtained by lowering a Chromel-Alumel thermocouple junction to the appropriate positions within the chamber. In addition, measurement of the temperature at a height approximating to that of the mid-point of the braid enabled the difference between measured and actual temperatures to be estimated. The final sub-section in this Chapter contains details of the general trends that were observed by a necessarily, rather crude experimental procedure.

(iii) Differential Scanning Calorimetry

The amount of heat required to raise the temperature of a polymer shows a substantial increase when temperature is increasing through its glass transition region. Because a Differential Scanning Calorimeter, DSC, measures the differential energy required to heat both the sample and reference at the same rate of temperature change, the sample temperature always equalling that of the empty sample pan constituting the reference, this increase in heat capacity of a polymer sample will result in an endothermic shift of the baseline. Temperature is indicated along the abscissa of a DSC chart, while endothermic heat flow rate to a sample is recorded on the positive side of the baseline position along the ordinate. In descriptions of DSC thermograms, gradient changes which result in the final higher-temperature gradient being more endothermic will be referred to for brevity as "endothermic gradient increases" or "endothermic gradient changes". A DSC detects the increased energy absorption of

degrees of freedom newly available to the rubbery polymer and hence the temperature,  $T_g$ , of the associated transition; it is therefore theoretically possible that the beginning of smaller molecular motions at secondary transition temperatures could be detected by a sufficiently sensitive DSC. The Differential Scanning Calorimetry technique was developed by the Perkin-Elmer Corporation (52) who have recently introduced the advanced Model DSC-2, with an optimized performance: for example, high levels of sensitivity and baseline stability have been achieved over a wider temperature range. Perkin-Elmer Ltd. generously permitted their Demonstration Model DSC-2 to be used for a week, at Beaconsfield, and many samples were scanned under the supervision of their Micro-Analytical Product Specialist, M. R. Cottrell.

Small quantities of samples to be studied in the DSC had been left for at least four days, at ambient temperatures, in the pistol oven, which was attached to the internal vacuum system of the University or to a rotary pump. In general, particle size had been reduced with the use of a mortar and pestle, but otherwise most samples were in their original form: it should be noted that ATB and ATV samples had been heated to about  $50^{\circ}\text{C}$  and that CTC samples consisted, at least partially, of residues from solutions used to impregnate TBA braids after subsequent evaporation of the "Pronalys" acetone solvent; the cream, orange and salmon-orange colours of CTC ( $59.7 \times 10^3$ ), CTC ( $15.1 \times 10^3$ ) and CTC ( $3.1 \times 10^3$ ) residues being noteworthy. Prior to analysis, samples were encapsulated in standard aluminium pans, with the aid of a crimping press. As the glass

transition is more obvious with faster scan rates, samples were practically always heated at forty degrees per minute, the associated chart speed being forty mm per minute. For the majority of samples, weighing about 13mg, recorder and instrument ranges were generally 10mV and 5 millicalories per second full-scale deflection, fsd, respectively: instrument ranges of 10 or 2 millicalories per second fsd were used when sample masses differed considerably from 13mg.

Samples were studied over the temperature range of  $100^{\circ}$  to  $623^{\circ}\text{K}$ , approximately equivalent to  $-175^{\circ}$  to  $350^{\circ}\text{C}$ , with the use of two temperature-programming procedures. From  $-175^{\circ}$  to  $150^{\circ}\text{C}$ , the sub-ambient accessory was used to enable the heat sink surrounding the sample and reference holders to be maintained at the temperature of liquid nitrogen. The general procedure at the beginning of sub-ambient first and re-runs (i.e. those involving the sub-ambient accessory) involved cooling the sample, with the programmed rate set at 320 degrees per minute, from ambient temperatures or up to  $150^{\circ}$  respectively until temperature control was achieved at  $-163^{\circ}\text{C}$ ; after adjusting the Lower Temperature Limit Control to  $-183^{\circ}\text{C}$ , the sample was left for about 5 minutes before programmed heating was initiated. The phrase "temperature control" implies that the temperature indicated by the programmer equals that of the holders, themselves in thermal equilibrium. Helium flowed past the sample and reference holders in the analyzer head at about 20ml per minute in order to optimize baseline stability at sub-ambient temperatures. Sub-ambient cooling with liquid nitrogen necessitated the use of a clear plastic dry-box, which was

transition is more obvious with faster scan rates, samples were practically always heated at forty degrees per minute, the associated chart speed being forty mm per minute. For the majority of samples, weighing about 13mg, recorder and instrument ranges were generally 10mV and 5 millicalories per second full-scale deflection, fsd, respectively: instrument ranges of 10 or 2 millicalories per second fsd were used when sample masses differed considerably from 13mg.

Samples were studied over the temperature range of  $100^{\circ}$  to  $623^{\circ}\text{K}$ , approximately equivalent to  $-175^{\circ}$  to  $350^{\circ}\text{C}$ , with the use of two temperature-programming procedures. From  $-175^{\circ}$  to  $150^{\circ}\text{C}$ , the sub-ambient accessory was used to enable the heat sink surrounding the sample and reference holders to be maintained at the temperature of liquid nitrogen. The general procedure at the beginning of sub-ambient first and re-runs (i.e. those involving the sub-ambient accessory) involved cooling the sample, with the programmed rate set at 320 degrees per minute, from ambient temperatures or up to  $150^{\circ}$  respectively until temperature control was achieved at  $-163^{\circ}\text{C}$ ; after adjusting the Lower Temperature Limit Control to  $-183^{\circ}\text{C}$ , the sample was left for about 5 minutes before programmed heating was initiated. The phrase "temperature control" implies that the temperature indicated by the programmer equals that of the holders, themselves in thermal equilibrium. Helium flowed past the sample and reference holders in the analyzer head at about 20ml per minute in order to optimize baseline stability at sub-ambient temperatures. Sub-ambient cooling with liquid nitrogen necessitated the use of a clear plastic dry-box, which was

mounted on the analyzer deck in order to minimize the condensation of water in the vicinity of the holders during sample change-over.

Perkin-Elmer staff had observed that constancy of sample holder environment, including the temperature of the surrounding heat sink, over the entire temperature range enhanced baseline reproducibility; therefore, for normal above-ambient operation, a circulating water system is provided to maintain the heat sink at a temperature just above ambient. M. R. Cottrell had assembled a refrigerated methanol-water bath which cooled the holder environment to an effective "ambient" temperature of about  $-25^{\circ}\text{C}$ , enabling "above-ambient" runs to include the  $0^{\circ}\text{C}$  region of interest; a commercial freon unit is now available for this purpose, but was not used in this work. When temperature control was indicated at  $22^{\circ}\text{C}$ , the holder temperature at which samples were changed, after actually cooling at a rate generally slower than the programmed rate of 320 degrees per minute, the Lower Temperature Limit was re-set to  $-33^{\circ}\text{C}$ ; a five minute interval elapsed before programmed heating began. The availability of a two-pen recorder enabled sample weight loss to be recorded simultaneously to above-ambient DSC thermograms for several samples. Thermobalance sample masses varied between 1.5 and 2.5mg, their decreasing weight being monitored with increase in temperature above  $25^{\circ}\text{C}$ .

The reader is referred to Perkin-Elmer literature for further details of the capabilities and the operational procedure of the Model DSC-2, which is recommended by the author. The reliability of all transition temperatures is analysed in the following sub-section, which includes estimates of temperature

errors in DSC data.

(iv) The Significance of the Transition Temperature Data

Knowledge of the orders of magnitude of experimental errors in temperature evaluation and of other pertinent variables, such as the temperature differentials within the Torsional Braid Analyzer sample chamber and the rate-dependence of these transitions, is necessary for correlation of DSC and TBA results, mutually and with those of other workers using a variety of techniques. The actual reproducibility of DSC and TBA transition data will be indicated, although not always explicitly, in the following Chapter.

(a) DSC temperature errors

1. It is estimated that the finite line width of both the recorder pen and the event marker (indicating temperature in 1 degree units and 1mm intervals along the chart abscissa) in addition to the operator error in temperatures, estimated by laying a ruler across the chart, result in a maximum random error of  $\pm 1$  degree.
2. The thermograms of re-runs were frequently superimposed on those of first runs; operator error in failing to obtain exact temperature coincidence of the chart with the temperature programmer may have produced a systematic error in such re-run data, the apparent temperature being erroneously low by as much as 1 degree.
3. M. R. Cottrell checked the temperature calibration of the DSC-2, using the general run conditions described in the previous sub-section, and evaluated the discrepancy between theoretical and measured phase transition temperatures as given below.

<u>Phase Transition</u>	<u>Measured (°C)</u>	<u>Theory (°C)</u>	<u>Correction: <math>\Delta T</math> (theory- measured degrees)</u>
Cyclopentane Form I to Form II	-153.0	-151.2	+1.8
Cyclopentane Form II to Form III	-134.9	-135.1	-0.2
Cyclohexane Form I to Form II	-85.2	-87.1	-1.9
Cyclohexane Form II to Melt	9.6	6.5	-3.1

A graph of  $\Delta T$  vs. Measured Temperature shows a smooth curve, tending asymptotically towards an ordinate value of -3.0 degrees at about 0°C; in the absence of further calibration data it is visually estimated that at above-ambient temperatures, apparent transition temperatures are erroneously high by about 3.5 to 4.0 degrees. The appropriate corrections to sub-ambient transition temperatures may be interpolated from the calibration data given in the Table.

(b) TBA temperature errors

1. For each run, errors in temperature evaluation were cumulated from estimates of rounding errors and from those implied by the lack of reproducibility of recorded calibrating millivoltages and discrepancies in the length of the temperature and reduced oscillation records. The general run procedure had been optimized and instrument malfunction, frequently causing large increases in temperature errors, had for the most part been minimised by the beginning of 1973 and during subsequent experiments the estimated error at sub-ambient temperatures averaged approximately  $\pm 2.5$  degrees, the analogous above-ambient average being slightly smaller.

<u>Phase Transition</u>	<u>Measured (°C)</u>	<u>Theory (°C)</u>	<u>Correction: <math>\Delta T</math> (theory- measured degrees)</u>
Cyclopentane Form I to Form II	-153.0	-151.2	+1.8
Cyclopentane Form II to Form III	-134.9	-135.1	-0.2
Cyclohexane Form I to Form II	-85.2	-87.1	-1.9
Cyclohexane Form II to Melt	9.6	6.5	-3.1

A graph of  $\Delta T$  vs. Measured Temperature shows a smooth curve, tending asymptotically towards an ordinate value of -3.0 degrees at about 0°C; in the absence of further calibration data it is visually estimated that at above-ambient temperatures, apparent transition temperatures are erroneously high by about 3.5 to 4.0 degrees. The appropriate corrections to sub-ambient transition temperatures may be interpolated from the calibration data given in the Table.

(b) TBA temperature errors

1. For each run, errors in temperature evaluation were cumulated from estimates of rounding errors and from those implied by the lack of reproducibility of recorded calibrating millivoltages and discrepancies in the length of the temperature and reduced oscillation records. The general run procedure had been optimized and instrument malfunction, frequently causing large increases in temperature errors, had for the most part been minimised by the beginning of 1973 and during subsequent experiments the estimated error at sub-ambient temperatures averaged approximately  $\pm 2.5$  degrees, the analogous above-ambient average being slightly smaller.

2. The horizontal temperature gradient within the sample chamber,  $\Delta T$  (centre - wall), was estimated at a height corresponding to the middle of the braid, the temperature of the wall normally being recorded with the sample composite suspended at the centre of the chamber cross-section. Between ambient temperatures and 180°C, results indicate that the centre of the chamber was cooler than the walls by  $1 \pm 1$  degree, the apparent transition temperatures being on average too high by about 1 degree.

As the Chromel-Alumel thermocouple was not calibrated at temperatures above 200°C, the trend apparent above 180°C may be erroneous: the negative  $\Delta T$  apparently decreased to 0 degrees at 180°C and subsequently increased with temperature, implying that at 220°C the centre of the chamber may have been warmer by less than 1 degree.

Above 100°C, temperature cycling, with a timelag between cycles at the centre of the chamber and at the wall of up to a quarter of a minute, was observed; the data implies that cycling of the power input to the heaters in the wall was responsible. It is thought that this effect contributed to the breadth of observed transition regions and to the variation in their temperature location.

Below 0°C, the temperature differential across the chamber appeared to be independent of Compensating Heating and of slight changes in the rate of flow of atmospheric O.F.N. Because it is reasonable to expect a smooth increase in the actual  $\Delta T$  (centre - wall) with decreasing temperature, the  $\Delta T$  values tabulated below were obtained by arbitrarily modifying the trend visually derived from the multiple graph in order to

allow for systematic errors in the calibration formula of the Chromel-Alumel thermocouple (as indicated by a  $\Delta T$  (calculated - actual) plot) and to obtain a smoother trend below  $-70^{\circ}\text{C}$  by  $\Delta T$  alterations of up to 1.5 degrees.

Wall temp. ( $^{\circ}\text{C}$ )	0	-10	-20	-30	-40	-50	-60	-70	-80	-90
$\Delta T$ (centre-wall), degrees	0	0.5	1	1	1.5	2.5	3.5	4	4.5	5
Wall temp. ( $^{\circ}\text{C}$ )	-100	-110	-120	-130	-140	-150	-160	-170	-180	-190
$\Delta T$ (centre-wall), degrees	7	7.5	7.5	8	8	8	8.5	9.5	10	10

Above  $-70^{\circ}\text{C}$ ,  $\Delta T$  is quoted to  $\pm 2$  degrees; below  $-70^{\circ}\text{C}$ , the unreliability of the data is recognised, being caused by the inadequacy of the Chromel-Alumel thermocouple calibration. The positive  $\Delta T$  values indicate that wall temperatures gave erroneously low apparent transition temperatures.

3. It is thought that a vertical temperature gradient along the sample,  $\Delta T$  (top - bottom), increased the apparent breadth of transition regions, the wall temperature corresponding to the centre of the sample being the recorded temperature.

Above  $0^{\circ}\text{C}$ , a negative differential was generally observed, with values fluctuating by as much as 1.5 degrees about approximately  $-1$  degree. The temperature at the top of the braid was determined before that at the bottom, the involved time interval being on average one third of a minute; thus, with an over-all heating rate of one degree per minute, it is thought that negative  $\Delta T$  values were over-estimated by one third of a degree. The corrected observation is that the top of the braid was on average cooler than the bottom by

about  $0.66 \pm 1.5$  degrees.

Below  $0^{\circ}\text{C}$ , the use of the Compensating Heater, in the vicinity of the lower part of the sample, was found to affect  $\Delta T$  behaviour.  $\Delta T$  was generally larger in the absence of Compensating Heating, the approximate trend indicated by the multiple graph being tabulated below.

Central Wall Temperature ( $^{\circ}\text{C}$ )	-180	-100	-60	-20	-10	0
$\Delta T$ (Top-Bottom), degrees	6	8	8	3.5	0	-2

The rate of decrease of  $\Delta T$  increased concomitantly with temperature between  $-60^{\circ}$  and  $-10^{\circ}\text{C}$ . These  $\Delta T$  values have not been corrected, although:

- (a) due to the prior determination of the temperature at the top of the braid, the positive  $\Delta T$  values could have been underestimated by as much as 0.5 degree.
- (b)  $\Delta T$  data is scattered about indicated values by up to  $\pm 2$  degrees.
- (c) the  $\Delta T$  (calculated - actual) value for the Chromel-Alumel thermocouple changes, at approximately  $-90^{\circ}\text{C}$ , from approximately 2.5 to -3.0 degrees. Therefore, although both temperatures were determined with this thermocouple,  $\Delta T$  data spanning  $-90^{\circ}\text{C}$  may have been distorted.

When the Compensating Heater was used in the standardized manner,  $\Delta T$  fluctuated by as much as  $\pm 3.0$  degrees about 2.5 degrees, at temperatures above  $-160^{\circ}\text{C}$ . At lower temperatures,  $\Delta T$  values, also uncorrected for under-estimation, increased with decreasing temperature. Data obtained with

Compensating Heating indicated that the faster the rate of warming, the smaller the temperature differential.

4. The portion of the recorded oscillatory decay that is used in the evaluation of damping and relative rigidity occurred during a finite time and therefore temperature interval: when automatic pulsing took place every 2.5 minutes, the involved temperature increment is estimated as about 0.5 degrees; for oscillations initiated at 5 minute intervals, the most probable associated temperature change was of the order of 1.5 degrees.

(c) Rate-dependence of T<sub>g</sub>

1. TBA is a dynamic mechanical technique with the measuring frequency usually less than 1.0 Hz. "The temperature of maximum damping generally is 5° to 15°C higher than the conventional glass transition temperature, if the dynamic measurements are made at about 0.10 to 1.0 Hz". (9)

2. Samples were generally heated at one degree per minute during TBA and at forty degrees per minute in the DSC. With increase in the heating rate from one to forty degrees per minute, the dimethyl siloxane T<sub>g</sub>, measured in a Du Pont DSC Module, was elevated by 5 degrees. (24)

It is obvious that these two effects may be cancelled, at least partially, on comparison of TBA and DSC results reported in the next Chapter.

CHAPTER 3

RESULTS

The first two sections contain the results of Torsional Braid Analysis (TBA) of several poly(di-n-alkylitaconate) polymers and polysaccharide derivatives. Figures 1 to 7 inclusive contain tracings of a selection of typical thermograms, their overall dimensions having been photographically reduced by a factor of two. A large number of thermograms were obtained and due to the non-reproducible nature of their damping and relative rigidity variations, this results presentation may seem unusual. The thermograms were studied intensively, features of interest were identified and the relevant information then assembled from all available thermograms; this iterative procedure was repeated several times until suitable transition regions, which in general contained significant transitions, had been defined. It should be implicitly understood that the transitions to be subsequently described were originally identified as maxima or shoulders in the mechanical damping index,  $(1/n)$ , and that transition temperatures have been evaluated from the damping data. Analysis of relative rigidity behaviour assumed secondary importance, because effective modulus variations were found to be even less consistent and significant patterns were therefore more difficult to identify and correlate than those of the damping data. Relative rigidity data have been used to provide supplementary evidence on the relative magnitude of a damping transition within a given thermogram, or to clarify the identification of a transition.

All the temperatures quoted in the TBA results tables, in degrees Celsius ( $^{\circ}\text{C}$ ), are those of the central thermocouple junction in the sample chamber wall, which have not been corrected for any of the temperature differentials within the chamber that were described at the end of the previous chapter.

FIGURE 1

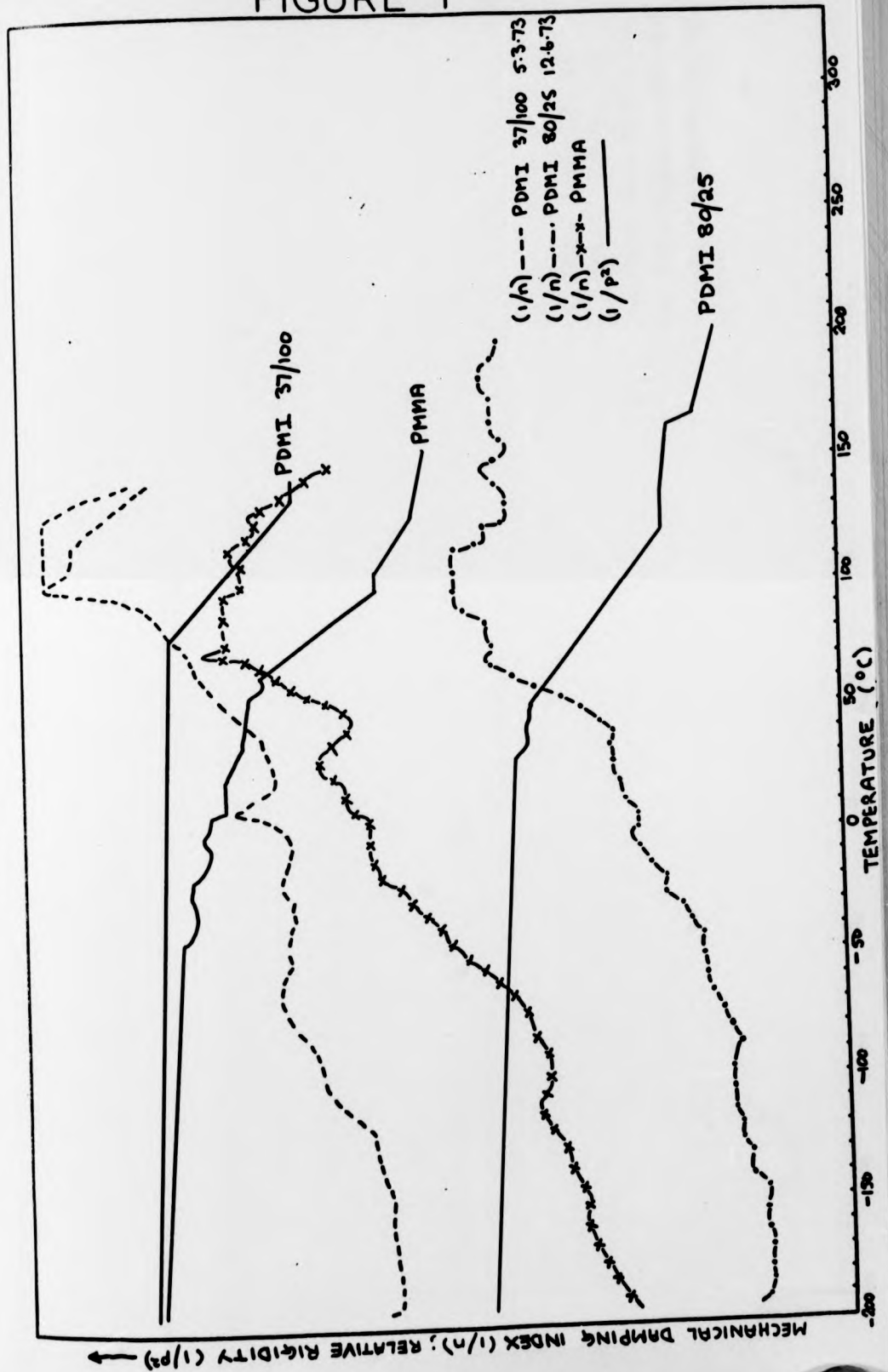


FIGURE 2

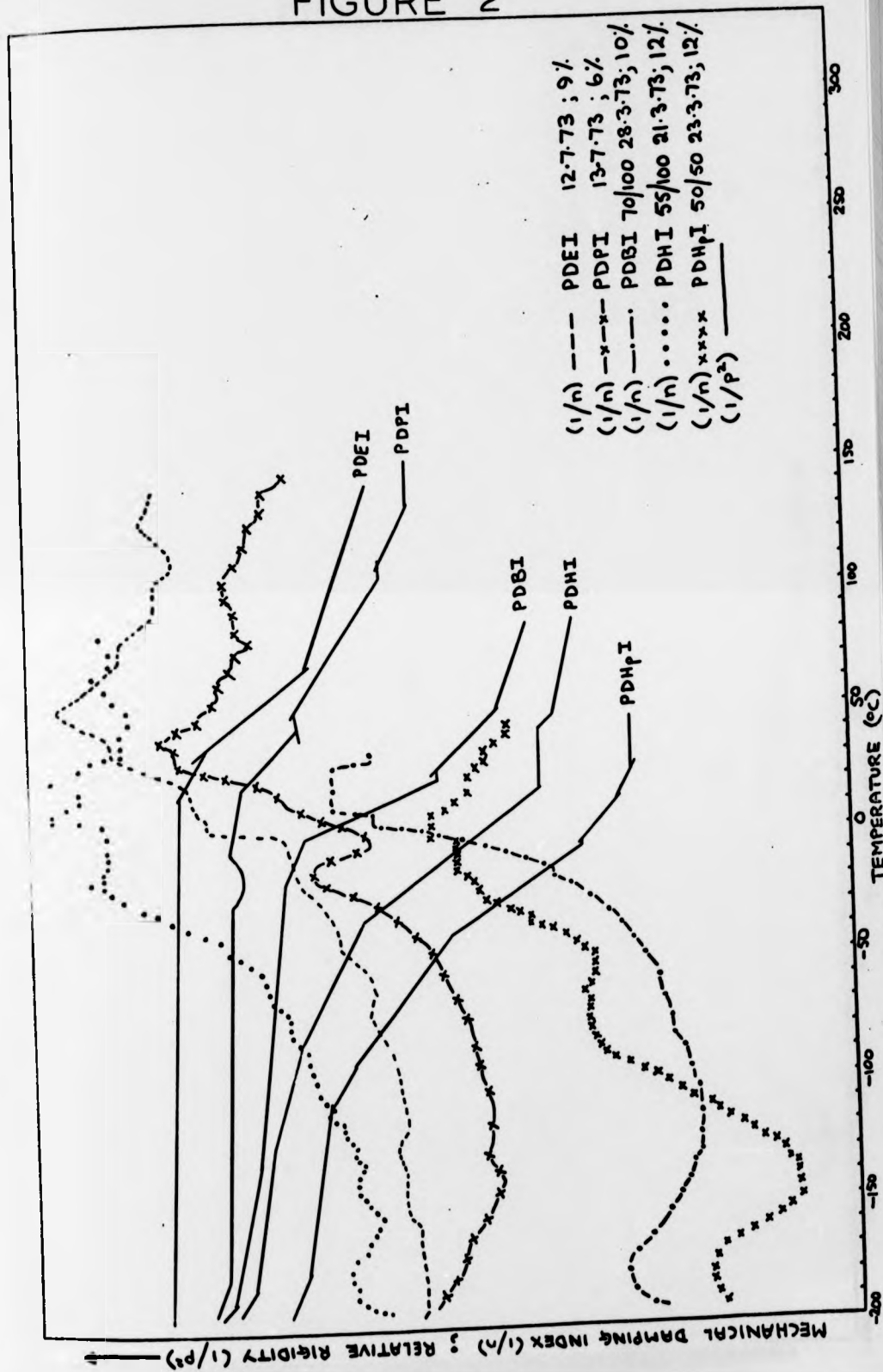


FIGURE 3

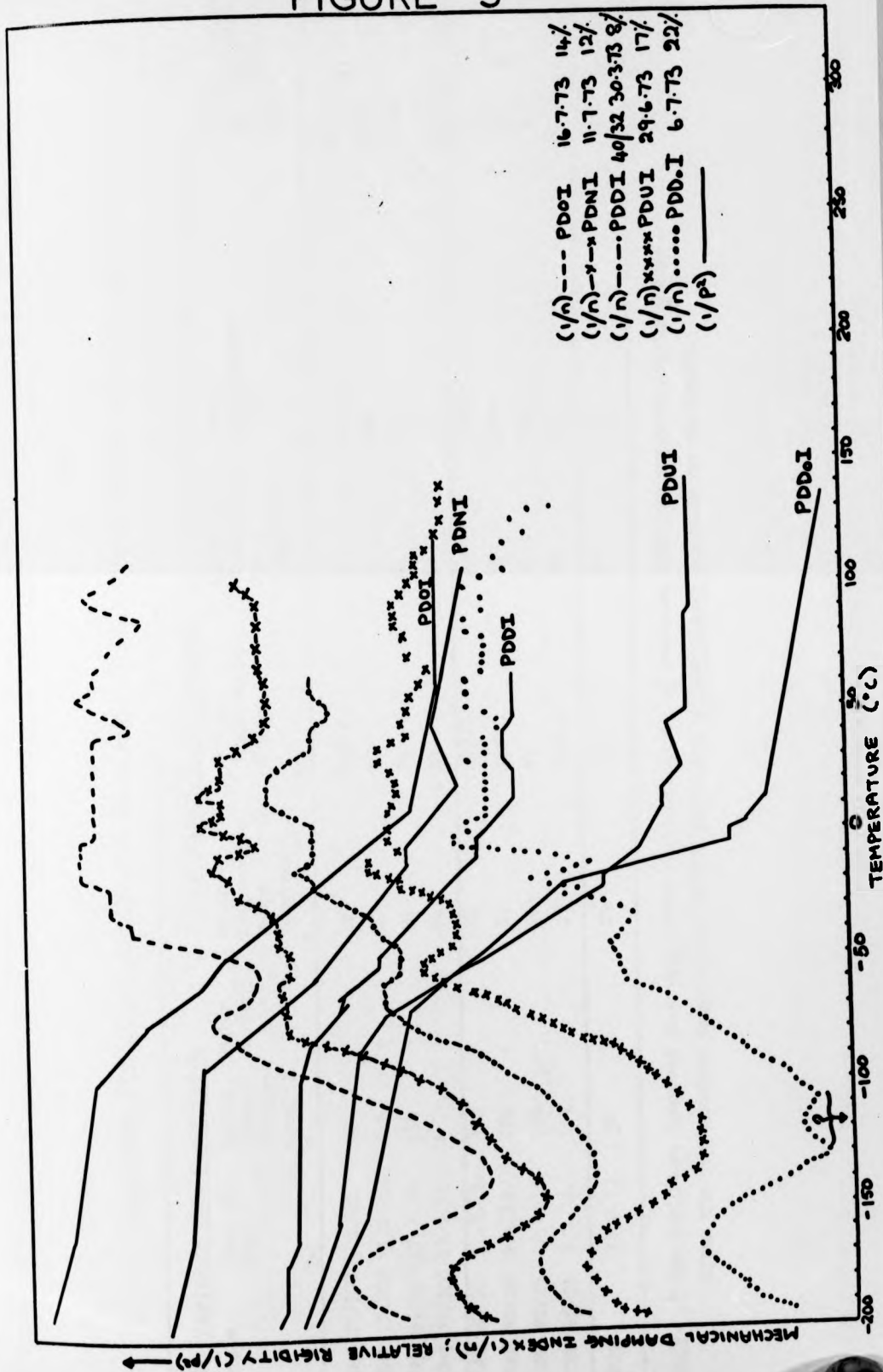


TABLE 4

The Glass Transition Region for Poly(di-methylitaconate) and Poly(methyl methacrylate)

Sample	Date of Run	(1) Variable Run Conditions		(2) Maximum (1/n) Values		(3) Steepest Linear (1/P <sup>2</sup> ) Decrease		(4) Median Frequency of Oscillations with Maximum (1/n) (Hz)
		Approx. Concentration (gcm <sup>-3</sup> )	Water Content	Width of Temperature Range (degrees)	Median Temperature (°C)	Width of Temperature Range (degrees)	Median Temperature (°C)	
a	b	c	d	a	b	a	b	
PDMI 37/100	5.3.73.	7%		19	110.5	42	108	0.13
PDMI 37/100	26.3.73.	12%	+	30	101	42	104	0.19
PDMI 37/100	17.7.73.	11%	-	32	79	54	74	0.22
PDMI 37/100	17.8.73.	*		24	51	34	53	0.31
PDMI 80/25	11.3.73.	7%		33	113.5	23	104.5	0.13
PDMI 80/25	9.4.73.	12%	+	31	105.5	28	104	0.17
PDMI 80/25	12.6.73.	13%	-	58	95	70	86	0.15
PDMI 80/25	5.7.73.	12%		27	110.5	70	95	0.15
PMMA	15.8.73.	7%		24	86	34	81	0.25

Note. \* The braid was immersed in a very concentrated solution of residues from two previous impregnations. After the run (maximum temperature 220°C) there were yellow glassy deposits on the braid.

TABLE 5  
 The Median Temperature for Maximum (l/n) Values, for all Poly(di-n-alkylitaconate) Polymers except PDMI

Sample	PDEI	PDPI	PDBI	PDHI	PDHpI	PDOI	PDNI	PDDI	PDUI	PDDoI
Mean of Median Maximum $\delta_{(l/n)}$ Values (°C)	50	38	20	14	12	-6.5	14	15.5	-11	-1
Number of Runs Spanning Maximum (l/n)	2		2	2	3			2		
Total Divergence of their Median Values (degrees)	7		2	12	18			10		
Approximate Mean Frequency for Maximum Damped Oscillations (Hz)	0.19	0.20	0.20	0.13	0.13	0.12	0.13	0.11	0.13	0.13

TABLE 6  
Approximate Median Temperatures of the Steepest Relative Rigidity Gradient

Sample	PDEI	PDPI	PDBI	PDHI	PDHpI
Median Temperature (°C)	50	32	11 to 14 → $\overline{M}_w$	-7.5 to -1.5 → $\overline{M}_w$	-34 to -22
Temperature Difference (degrees) between					23.5
(1) Mean Median Temperatures	18	19.5	17		
(2) Highest Median Temperatures	18	18	15.5		20.5

Note "→  $\overline{M}_w$ " indicates the direction of increasing weight-average molecular weight.

TABLE 7

Damping Behaviour at Temperatures Higher than T<sub>g</sub>

Sample	Column (1) Upper Temperature of Persistent High Damping (°C)	Column (2) Temperature Range or Onset Temperature of Further High Damping (°C)
(PDMI)		170)
PDEI		120 to 140
PDPI		85 to 115
PDBI	$\bar{M}_w$ 35/25 (95) ↑ 70/100 (85)	
PDHI	$\bar{M}_w$ 45/100 ↑ 55/100	- 50
PDHpI	$\bar{M}_w$ 50/50 ↑ 70/50 40 60/50 (50)	
PDOI	120	50 to 85? 95 to 110?
PDNI		(65) or 100
PDDI	$\bar{M}_w$ 40/42 (65) ↑ 40/32 60/32 90	
PDUI	50	70 to 100
PDDoI	110	50 to 65? 80 to 100?

Note. "→"  $\bar{M}_w$  indicates the direction of increasing weight-average molecular weight.

Section A: TBA Data of Several Poly(di-n-alkylitaconates) and of Poly(methyl methacrylate).

(i) The glass transition region

The effective glass transition region for PDMI has been identified from the temperature location of the largest damping,  $(1/n)$ , peak and the steepest linear decrease in relative rigidity  $(1/P^2)$ . See Figure 1 for a sketch of two PDMI thermograms. As the thermograms obtained from a total of eight runs differed greatly, their results for the glass transition temperature,  $T_g$ , are detailed in Table 4. Column (1) indicates variables in run conditions which may have contributed to this distribution, approximate concentration ( $\text{g cm}^{-3}$ ) of the impregnating solution being given in (1)c and variation in water content from the average in (1)d. The sample composites were not prepared under dry-box conditions. Some runs, with a "+" in (1)d, were stopped at about room temperature and with the removal of a cool braid into the laboratory atmosphere, it is possible that water condensed onto the surface of the composite; the "-" sign describes runs where there had been attempts to decrease the water content of the solvent, used in the impregnating solution, and of the atmospheric OEN. (Details are given in the previous chapter). Column (2)a contains the width of the temperature range of the two largest  $(1/n)$  values considered to be  $T_g$  associated; the median temperature of this range is given in (2)b. Similarly column (3) defines the temperature location of the steepest linear decrease in  $(1/P^2)$ . Column (4)

contains the approximate median frequency, in hertz (Hz), of the oscillations with maximum damping; frequency decreases with increasing temperature, as indicated in the  $(1/P^2)$  versus temperature traces in Figure 1. The structure of the repeating units in PDMI and PMMA are very similar (see Table 1). The only thermogram obtained for PMMA has therefore been included in Figure 1 and details of the glass transition region, identified as for PDMI, have been given at the bottom of Table 4. For PDMI 80/25, Table 4 indicates that the median temperatures for the  $(1/n)$  maxima and the largest  $(1/P^2)$  decreases are approximately:-  
 $105 + 10^\circ\text{C}$  and  $95 + 10^\circ\text{C}$  respectively, 0.15 Hz

being a typical frequency magnitude for the maximum damped oscillations. Table 4 indicates that PMMA has a lower  $T_g$  than PDMI 80/25, the oscillations in this region having a higher frequency. A feature of interest is the coincidence, within  $5^\circ\text{C}$ , of the  $(1/n)$  and  $(1/P^2)$  median temperatures for each PDMI 37/100 run and for the PMMA run, not in general apparent for PDMI 80/25. PDMI 37/100 thermograms indicate a larger variation in frequency and median temperature than those of the lower molecular weight sample, PDMI 80/25. Although a contributory factor may have been plasticization by a yellow impurity, it is interesting that the PDMI 37/100 composite with the greatest concentration and the highest oscillation frequency, should have experienced highest damping at the same temperature as the PDEI composite. For each PDMI sample, the temperature location of the largest damping peak and the largest decrease in relative

rigidity is effectively that of the glass transition region. However the lack of reproducibility of these temperature locations indicates that, on the molecular level, the effective glass transition for PDMI is not a simple amorphous glass to rubber transition.

Figures 2 and 3 are multiple tracings of thermograms for all the other available members of the poly(di-n-alkylitaconate) series. If there is more than one thermogram and/or more than one sample for a member of the series, the thermogram of the sample with the highest molecular weight and with the least scatter in the data has usually been selected. PDMI thermograms are visually simple, but a lack of correlation between the two median temperatures is apparent in the PDMI 80/25 data. Interpretation of the thermograms of PDEI, PDPI and PDBI is similarly straight forward, but the relative location of the steepest decrease in  $(1/P^2)$  and the largest peak in  $(1/n)$  varies with series member. With increase in length of the alkyl group, members of the poly(di-n-alkylitaconate) series give increasingly complex thermograms. Interpretation of the relative rigidity versus temperature,  $(1/P^2)$  vs. T, graph, in terms of linear gradients, reveals that the temperature location of the steepest gradient does not necessarily correspond to the temperatures at which maximum damping is observed. Thus, in general, the glass transition region for the poly(di-n-alkylitaconates), unlike that of simple amorphous polymers, cannot be identified from the approximately coincident temperature location of the steepest  $(1/P^2)$  decrease and the highest  $(1/n)$  values.

For members of the series for which the alkyl group contains six or more carbon atoms [the lack of a poly(di-n-pentylitaconate) sample is unfortunate], the region of highest damping appears to be caused by the onset of at least two molecular motions. A transition region, A, has therefore been identified for PDHI and higher members of the series; it has been characterized by the following three features:-

(1). Transition region A has an approximately constant temperature location on the low temperature side of the maximum damping region, associated high damping usually being visible from about  $-25^{\circ}\text{C}$ .

(2)a. The magnitude of damping associated with transition A varies relative to the maximum damping values with series member; for A,  $(1/n) \leq \text{maximum } (1/n)$ .

(2)b. Hence A is not always visible for a given series member, visibility varying from run to run. Frequently the high damping region cannot be easily interpreted in terms of two processes, as if the onset of the two molecular motions has coalesced under certain run conditions.

(2)c. A variation in the relative damping magnitude with sample molecular weight has been observed for PDDI.

(3). The temperature location of the steepest  $(1/P^2)$  decrease differs with series member and sample molecular weight, in some cases spanning transition region A. Consideration of the variations in relative rigidity gradients has aided identification of A for individual series members.

Assuming that the glass transition occurs within the high damping region, these characteristic features of A imply that for some of the higher series members these two transitions are intimately related on the molecular level and may not therefore be truly separate entities. However, for the group of esters from PDHI to PDDoI definition of transition A helps to rationalize trends and variations in complex damping and relative rigidity behaviour.

Details of thermograms not represented in Figures 2 and 3 and which contributed to the above definition of transition region A are now provided. Identification of the onset temperature of this transition is approximate and it varies between  $-20$  and  $-35^{\circ}\text{C}$ , PDHpI 70/50 and PDDI 60/32 having the lowest apparent locations for transition A.

Feature (2)a is obvious from inspection of the thermogram tracings. A shoulder is clearly defined in region A for PDHI and PDDI, whereas the damping data for PDDoI merely hints at one. PDUI is the only series member to indicate maximum damping values in this region. An unusual example of feature (2)b is provided by PDHI 45/100. Of two thermograms obtained for this sample, one shows a well defined shoulder in region A, as indicated by PDHI 55/100 in Figure 2, and the other indicates a smooth symmetrical damping maximum centred on  $+9^{\circ}\text{C}$ . In the thermograms of PDHpI, PDDoI and PDNI, the magnitude of the damping in transition region A is very slightly less than that of the maximum damped oscillations; it is therefore difficult to identify A and the relative rigidity data described below

is particularly useful. Identification of A from the PDOI damping data is particularly difficult; the highly damped oscillations occur at slightly lower temperatures than usual, define a narrow shoulder from  $-30^{\circ}\text{C}$  and effectively persist, with scatter, until the upper temperature limit of the run. The significance of the shoulder cannot therefore be determined from peak-symmetry considerations.

Figure 3 shows the damping versus temperature,  $(1/n)$  vs.  $T$ , graph for PDDI 40/32, the PDDI sample of intermediate molecular weight. In general, for the higher poly(di-n-alkylitaconates) transition B (to be more fully discussed later) has been identified within the temperature region  $-110^{\circ}$  to  $-30^{\circ}\text{C}$ . Transition B is apparent as a small  $(1/n)$  maximum within  $-80^{\circ}$  and  $-45^{\circ}\text{C}$  for PDDI 40/32. The higher molecular weight sample, PDDI 40/42, indicates a damping shoulder, not a peak, for B, the difference in associated damping between transitions B and A being at least as large as that for PDDI 40/32. However, the thermogram for PDDI 60/32, of lowest molecular weight and onset temperature for A, indicates a maximum for transition B, of equal damping magnitude as the shoulder in region A. The damping data therefore implies that with decrease in sample molecular weight, transition B relative to transition A, becomes increasingly important. A concurrent damping magnitude increase for B and decrease for A with decrease in molecular weight may be responsible for the differences in their relative magnitude.

Significant variations in experimental conditions are, possible benzene contamination for PDDI 60/32 and PDDI 40/42 and the impregnation of the PDDI 60/32 braid with a solution of approximately twice the concentration used in the preparation of the other PDDI composites.

Feature (3) is a statement about the complexity of these  $(1/P^2)$  thermograms. The steepest gradient of decreasing  $(1/P^2)$  with temperature is associated with transition A for PDHI, PDHpI and PDDoI. For PDHI, the median temperature of this gradient is more than  $10^\circ\text{C}$  higher than the temperature at the onset of high damping associated with A: for PDHpI the two temperatures are approximately coincident. The decrease in  $(1/P^2)$  from  $-20^\circ$  to  $-2^\circ\text{C}$  is extremely well defined for PDDoI; this location of the steepest gradient is the most significant evidence for a transition in region A, the damping data being scattered and merely hinting at a small shoulder. Inspection of both  $(1/n)$  and  $(1/P^2)$  behaviour also enables a more satisfactory interpretation of sample behaviour in thermograms where  $(1/n)$  in region A is approximately equivalent to the maximum  $(1/n)$  values. A continuous decrease in  $(1/P^2)$  occurs from approximately  $-50^\circ$  to  $+10^\circ\text{C}$  for PDOI, defining the temperature region for A and the glass transition and implying that they may be effectively coalescent. However, the existence of constant  $(1/P^2)$  data from approximately  $-10^\circ$  to  $0^\circ\text{C}$  confirms the definition of two high damping regions for PDNI. In general thermograms for the group of esters from PDOI to PDUI inclusive, show that the steepest  $(1/P^2)$  gradient is associated with

transition B and that, for all but PDUI, a large decrease in  $(1/P^2)$  also occurs in the region of A and continues until  $10^\circ$  or  $20^\circ\text{C}$ . A large proportion of the  $(1/P^2)$  decrease occurs in the temperature region of transition B for PDUI, whereas for PDDoI approximately half the change in effective modulus occurs during the very steep decrease specified above.

The relative rigidity behaviour of PDDI is particularly interesting; it supports the damping trend of increase in importance of transition B, relative to A, with decrease in sample molecular weight. For the highest molecular weight sample, PDDI 40/42, data show a point of inflection from  $-50^\circ$  to  $-40^\circ\text{C}$ , which defines two  $(1/P^2)$  gradients of equal magnitude, the smaller net decrease being associated with region B. Similarly the PDDI 60/32 behaviour is less complex than that illustrated in Figure 3: the largest net decrease and steepest  $(1/P^2)$  gradient is associated with transition B, a more gradual decrease spanning region A. The complex  $(1/P^2)$  vs. T behaviour illustrated for PDDI 40/32, can thus be understood as being intermediate between that of the other two samples with extreme molecular weight values.

Prior to identification of transition A it had been realized that, due to the lack of coincidence of the temperatures for which  $(1/n)$  was a maximum and the  $(1/P^2)$  decrease steepest, identification of the glass transition region could not, in general, be straightforward for the poly(di-n-alkylitaconates). For esters with six or more carbon atoms in the n-alkyl group, the steepest decrease in  $(1/P^2)$  occurs in transition regions A or B. In defining

transition A, it has also become apparent that satisfactory identification of the glass transition region may not even be possible from the damping data. Median temperatures of maximum damped oscillations are given in Table 5, and details of the derivation of these temperatures are given in the paragraph below. The last row of Table 5 contains very approximate estimates of the mean frequency of the maximum damped oscillations whose median temperatures are given in the second row. Although higher concentrations of impregnating solution were in general used for higher series members, no correlation of frequency with concentration is apparent. For example, the concentration of the two PDDI samples varied by a factor greater than two, but their frequencies were very similar.

As for PDMI, the simple damping peaks of PDEI and PDPI have allowed evaluation of the median temperatures from the two largest  $(1/n)$  values. The 7 degree discrepancy in this temperature for the two PDEI runs, is due to scatter in one set of data, which resulted in poor definition of the peak. High damping is persistent over a broader temperature range in the PDBI thermogram. It is only possible to define the median temperature of the maximum  $(1/n)$  values for the lower molecular weight sample. For the higher molecular weight sample (by a factor of ten), the median temperature of the two largest  $(1/n)$  values indicates a median temperature increase with molecular weight of 20 degrees: a single maximum damped oscillation occurs at  $21^{\circ}\text{C}$ , only 2 degrees higher than the median temperature of the other sample. For PDBI the steepest  $(1/P^2)$  decrease is assumed to be associated with the glass

transition, and this median temperature is only increased by 3 degrees with increase in sample molecular weight. The median temperature of the maximum damped oscillations of PDBI have therefore been quoted in Table 5. For PDHI the damping maximum can be easily defined in terms of the two largest  $(1/n)$  values. However, with molecular weight increase there is an unusual depression in this median temperature; it is thought that lack of damping evidence for transition A in the PDHI 45/100 thermograms may be responsible. For higher series members the median temperatures of the maximum  $(1/n)$  values have been quoted. Median temperatures for PDHpI 50/50, 70/50 and 60/50 were 4, 9 and  $22^{\circ}\text{C}$  respectively, implying an inverse molecular weight versus temperature relationship. The occurrence of maximum damping for both odd and even numbered oscillations consecutively was the only method of identifying the relevant temperature range for PDOI, PDNI, PDDI 60/32, PDUI and PDDoI. From  $-20^{\circ}\text{C}$   $(1/n)$  data of odd numbered oscillations for PDDI 40/32 has been ignored due to their distortion by flexural vibrations and from Figure 3 it is apparent that identification of the resulting peak is slightly more convincing than for other esters with long alkyl chains. The run had been ended at  $20^{\circ}\text{C}$  for PDDI 40/42, but more complete data for the other two PDDI samples indicated elevation of the median maximum  $(1/n)$  temperature with molecular weight increase. Maximum damping occurs in transition region A for PDUI. For PDDoI the two consecutive maximum damped oscillations, with median temperature of  $-1^{\circ}\text{C}$ , define the onset of persistent high damping and the end of the very large  $(1/P^2)$  decrease.

From Table 5 and the supplementary information given above, it is obvious that both PDUI and PDDoI display unique damping behaviour. Ignoring low estimates, possibly due to molecular weight depression or the absence of transition A, a median temperature of about 20°C is particularly significant for PDBI, PDHI and PDDI. Maximum damping occurs at lower average temperatures for PDHpI and PDNI; PDOI defines a minimum in this variation of median temperature with n-alkyl chain length. For PDOI, PDUI and PDDoI the above identification of high damping with transition A and the glass transition may prove to be inappropriate.

It has been recognised that despite the same molecular causes, the magnitude of changes in the macroscopic variables of  $(1/P^2)$  and  $(1/n)$  within the same temperature regions do not necessarily correspond. Nevertheless, analysis of  $(1/P^2)$  behaviour should provide additional clues to behaviour on the molecular level. The  $(1/P^2)$  vs. T tracings in Figures 2 and 3 are vertically spaced for clarity and thus visually apparent trends can be misleading. This spacing precludes the existence of a scale on the vertical axis; when considering the relative magnitude of changes in  $(1/P^2)$  and  $(1/n)$  within a thermogram, the use of a  $\log_{10}$  scale on the abscissa should be remembered.

Table 6 contains approximate median temperatures of the steepest relative rigidity decrease and should be studied with reference to the overall  $(1/P^2)$  behaviour, as shown in Figure 2. The magnitude and temperature range of the steepest decrease for PDPI is unusually small. For two PDHpI samples of identical molecular weight, median temperatures

differed by 4 degrees, providing an estimate of the reproducibility of this interpretation of the  $(1/P^2)$  data. The variation in median temperature with molecular weight, indicated for PDBI and PDHI, may not be significant. When visible for PDHI, transition A is also spanned by the steepest  $(1/P^2)$  gradient, a finite decrease also occurring over transition region B for PDHI and PDHpI. For PDHpI, the median temperature correlates more closely with the onset temperature of high damping associated with A than with sample molecular weight. The median temperatures for the steepest  $(1/P^2)$  gradients illustrated in Figure 3 have not been quoted, as for all polymers represented there, except PDDoI, this gradient is associated with transition B. With the exception of PDUI all poly(di-n-alkylitaconates) with six or more carbon atoms in the alkyl group require at least two straight lines to interpolate their  $(1/P^2)$  data over the temperature region during which a large change in magnitude occurs. To identify, very approximately, the relative temperature location of the large change in effective modulus, the median temperature of the range defined by gradients involving a large  $(1/P^2)$  decrease was evaluated for these esters. The results indicated that the large  $(1/P^2)$  decrease for PDHpI occurs at lower temperatures than for PDHI, in agreement with the steepest gradient trend. However, for PDHpI and the esters represented in Figure 3, the evaluated temperature varied randomly between  $-30^\circ$  and  $-55^\circ\text{C}$ , with 10 degree discrepancies among individual series members indicative of the lack of reproducibility of this estimate. It was therefore concluded that due to the

differed by 4 degrees, providing an estimate of the reproducibility of this interpretation of the  $(1/P^2)$  data. The variation in median temperature with molecular weight, indicated for PDBI and PDHI, may not be significant. When visible for PDHI, transition A is also spanned by the steepest  $(1/P^2)$  gradient, a finite decrease also occurring over transition region B for PDHI and PDHpI. For PDHpI, the median temperature correlates more closely with the onset temperature of high damping associated with A than with sample molecular weight. The median temperatures for the steepest  $(1/P^2)$  gradients illustrated in Figure 3 have not been quoted, as for all polymers represented there, except PDDoI, this gradient is associated with transition B. With the exception of PDUI all poly(di-n-alkylitaconates) with six or more carbon atoms in the alkyl group require at least two straight lines to interpolate their  $(1/P^2)$  data over the temperature region during which a large change in magnitude occurs. To identify, very approximately, the relative temperature location of the large change in effective modulus, the median temperature of the range defined by gradients involving a large  $(1/P^2)$  decrease was evaluated for these esters. The results indicated that the large  $(1/P^2)$  decrease for PDHpI occurs at lower temperatures than for PDHI, in agreement with the steepest gradient trend. However, for PDHpI and the esters represented in Figure 3, the evaluated temperature varied randomly between  $-30^\circ$  and  $-55^\circ\text{C}$ , with 10 degree discrepancies among individual series members indicative of the lack of reproducibility of this estimate. It was therefore concluded that due to the

complexity of the  $(1/P^2)$  behaviour for PDHPi and higher series members, no significant trends could be discerned in the temperature location of the major  $(1/P^2)$  decrease.

In general, steep gradients in  $(1/P^2)$  involving a large decrease cease in the vicinity of maximum  $(1/n)$  temperatures, as defined above and summarized in Tables 4 and 5. This generalization that only relatively small and usually gradual changes in  $(1/P^2)$  occur at higher temperatures, supports identification of the median temperatures of maximum damping with  $T_g$  and is relevant to thermograms of the higher series members, where  $T_g$  is poorly defined by  $(1/n)$  data; it is therefore fortunate that the relative magnitude of any decrease in  $(1/P^2)$ , above the median temperatures given in Table 5, is barely significant for these esters. The PDNI thermogram, traced in Figure 3, shows unusual behaviour,  $(1/P^2)$  increasing with temperature to a small peak at about  $45^\circ\text{C}$ . Above the glass transition region, finite, more gradual  $(1/P^2)$  decreases are apparent for esters represented in Figure 2. The decrease in  $(1/P^2)$  from  $40^\circ$  to  $130^\circ\text{C}$  for PDPI is exceptionally large, being of equal magnitude to the change between  $10^\circ$  and  $40^\circ\text{C}$ . This fact is not easily confirmed by inspection of Figure 2 due to the lack of a scale on the abscissa; the increased spacing of smaller  $(1/P^2)$  values which results from the use of a logarithmic scale should be remembered.

Damping behaviour is varied above  $T_g$  and significant features are now described. The PDMI 37/100 thermogram shown in Figure 1 has consistently high damping from  $100^\circ$  to  $120^\circ\text{C}$ , with scattered, anisotropic data indicating relatively high

( $1/n$ ) values until about  $140^{\circ}\text{C}$ . In the other PDMI 37/100 thermograms which indicate lower  $T_g$  values (see Table 4), a small damping peak or shoulder is evident within  $100^{\circ}$  and  $140^{\circ}\text{C}$ . The lower the location of the largest ( $1/n$ ) peak, the more obvious is this subsequent damping variation. No significant changes in ( $1/P^2$ ) are associated with this feature. For PDMI 37/100 the agreement between median temperatures for the ( $1/n$ ) maximum and the steepest ( $1/P^2$ ) gradient has already been noted. From Table 4, the difference in ( $1/n$ ) and ( $1/P^2$ ) behaviour associated with the glass transition region for the two samples of PDMI is apparent and it is therefore not surprising that the damping behaviour described above is not obvious in the thermograms for the sample of lower molecular weight. It is interesting to note from Figure 1, that PMMA shows an additional high damping process which, like that of PDMI 37/100, occurs in the vicinity of the maximum ( $1/n$ ) peak. Unlike the PDMI 37/100 situation, a small but significant decrease in ( $1/P^2$ ), between  $109^{\circ}$  and  $126^{\circ}\text{C}$ , is associated with these highly damped oscillations. From approximately  $170^{\circ}\text{C}$ , PDMI 37/100 thermograms show an increase in ( $1/n$ ) with temperature. In two of the PDMI 80/25 thermograms, increased damping is visible by  $170^{\circ}\text{C}$ , the 9.4.73 data defining a broad damping peak from  $170^{\circ}$  to  $205^{\circ}\text{C}$ . In the PDMI 80/25 thermogram traced in Figure 1, the existence of high damping in this temperature region is apparent, 12.6.73 data also showing a steep but barely significant decrease in ( $1/P^2$ ) from  $160^{\circ}$  to  $180^{\circ}\text{C}$ . The increasingly damped oscillations of 5.7.73 show a larger decrease in ( $1/P^2$ ) from  $150^{\circ}$  to  $170^{\circ}\text{C}$ . However the thermogram obtained on 11.3.73, with a braid composite of

considerably lower sample concentration, shows constant  $(1/n)$  from  $145^{\circ}$  to  $185^{\circ}\text{C}$  after which damping decreases with increasing temperature. The PDMI thermograms suggest that a transition occurs in the vicinity of  $170^{\circ}\text{C}$ , but that the dynamic mechanical evidence of this transition changes in shape and temperature location with molecular weight, sample concentration and other run conditions.

Table 7 summarizes high damping behaviour at temperatures above  $T_g$ , identified at present with the median temperatures given in Table 5. For samples where relatively high damping persists above the glass transition region, the end of the run often occurs before a  $(1/n)$  decrease. For these samples, the upper temperature limit of the run is given in brackets in column (1); when the upper temperature of persistently high damping is observed, it is given there without brackets. In some thermograms separate high damping regions have been identified; column (2) contains the onset temperature of the defining  $(1/n)$  increase, or the temperature range over which high damping occurs. A dash in column (2) indicates the lack of temperature data in the region of interest. It appears that persistently large  $(1/n)$  values extend to higher temperatures for samples with an even number of carbon atoms, greater than two, in the  $n$ -alkyl chain: contrary to this generalization, the  $(1/n)$  peak of PDHI is unusually well defined. From PDMI to PDHI a depression in the onset temperature of additional high damping is apparent.

TABLE 8  
 Summary Table of Secondary Transitions of the Poly(di-n-alkylitaconate) Polymers  
 and of PMMA

Sample	(1) $0^{\circ}\text{C} < T < 40^{\circ}\text{C}$			(2) $-30^{\circ}\text{C} < T < +5^{\circ}\text{C}$			(3) $-160^{\circ}\text{C} < T < -30^{\circ}\text{C}$			(4) Run Onset Temperature $< T < -160^{\circ}\text{C}$		
	a (degs.)	b (degs.)	c ( $^{\circ}\text{C}$ )	a	b (degs.)	c ( $^{\circ}\text{C}$ )	a	b (degs.)	c ( $^{\circ}\text{C}$ )	a	b (degs.)	c ( $^{\circ}\text{C}$ )
PMMA	$\bar{m}$ 13	$\bar{s}$ 31		$\bar{s}$ 25	-4		m 15		-109			
$\bar{M}_w$ 37/100 (m) PDMI $\uparrow$ 80/25 (m/s) 16	12.5	17		-	$\sim$ -15		(m/s) 25		-66			
	27			(m) 12	-10		(s) 19		-106			
PDEI	(m/s) 18	12		(s) 11	-14		(s) 12		-54			
PDPI				$\bar{m}$ 14	-16.5 (m)		m 29		-141			
							34		-113	$\bar{m}$	-	$\bar{s}$ -190
$\bar{M}_w$ 35/25 PDBI $\uparrow$ 70/100				(s) 10	-10							
				(s) 2	-17		s 14		-80	$\bar{m}$	10	-181.5

Table continued:

TABLE 8 (continued)

Sample	Onset Temperature of High Damping Associated with A (°C)	Transition B			Run Onset		
		a	b	c	a	b	c
PDHI $\overline{M}_w$ ↑ 45/100 55/100	-20	(s/m)	21	-70	(m)	13	-183
PDHpI $\overline{M}_w$ ↑ 50/50 70/50 60/50	-25 to -35	(s/m)	26	-67	m	14	-184
PDOI	-30	m	7	-70.5	m	12	-177
PDNI	-20	(s)	37	-57	m	19	-181
PDDI $\overline{M}_w$ ↑ 40/42 40/32 60/32	-20 -40	(m)	20	-60.5	(m)	15	-174
PDuI	-20	m	15	-49	m	10	-170
PDDoI	-25	m	20	-45.5	m	15	-166

/Key...

TABLE 8 (continued)

Key: "  $\xrightarrow{\quad}$   $\overline{M}_w$ " indicates the direction of increasing weight-average molecular weight.

In column a, the letter "m" or "s" indicates that the most frequent (l/n) outline is a maximum or shoulder respectively, brackets indicating poor transition reproducibility, i.e. (l/n) evidence varies in temperature and/or magnitude with  $\overline{M}_w$  and/or run and/or initial oscillation direction. This letter is underlined if the associated (l/n) change is substantial. Columns b and c contain the width of the temperature range and the median temperature respectively. For each series member, these parameters were estimated from the temperatures of the two largest (l/n) values associated with the transition in every available thermogram, average values for the parameters being quoted above.

(ii) The secondary transition regions

In Figures 1, 2 and 3 poly(di-n-alkylitaconate) thermograms have been sketched over their entire temperature range in order to show the changes in  $(1/n)$  and  $(1/P^2)$  which may indicate the existence of secondary processes below the glass transition region. Temperature regions which frequently contain similar  $(1/n)$  and  $(1/P^2)$  features have been recognised, and the approximate temperature limits of these regions have been used to characterize the implied transitions. Table 8 summarizes these poly(di-n-alkylitaconate) transitions in order to facilitate comparison with secondary transition evidence of the polysaccharide esters. From run to run, the temperature, shape and magnitude of a  $(1/n)$  feature frequently differs, and therefore reduction of the data has necessarily involved subjective judgment; dynamic mechanical data of greater quantity and quality may well indicate different transition regions. The following paragraph supplements the contents of Table 8, providing details relevant to the interpretation of the molecular processes which may be occurring within the identified transition regions. Some small  $(1/n)$  fluctuations of dubious significance have been omitted from the summary table, but will also be described below.

Transition B has been identified within region (3) and occurs within  $-110^\circ$  and  $-30^\circ\text{C}$  for poly(di-n-alkylitaconates) with six or more carbon atoms in the n-alkyl chain. A large change in  $(1/P^2)$  is associated with this transition,  $(1/P^2)$  decreasing linearly for 30 to 70 degrees with increase in temperature from within the range  $-100^\circ$  to  $-70^\circ\text{C}$ . The capital

letter notation has been adopted due to the similarity of two characteristics to those of transition A: a large  $(1/P^2)$  reduction is also associated with the latter transition, which has only been identified for PDHI and higher series members. As shown by the underlining in column a, transition B causes relatively high damping, but the existence of brackets in this column implies that this evidence is not very reproducible. It is therefore only possible for broad generalizations to be made about changes in this transition with different alkyl chain lengths. From PDHI to PDUI inclusive the relative magnitude of the  $(1/P^2)$  gradient associated with B increases with increase in the size of the alkyl group, as shown in Figures 2 and 3. There is also an overall trend of increasing relative magnitude of  $(1/n)$  associated with B compared with the maximum  $(1/n)$  values observed for these polymers, a  $(1/n)$  peak being more clearly defined for those with longer pendant groups. Contrary to this general trend, both types of PDDoI data, when compared with that of PDUI, clearly indicate a decreased relative importance of transition B. Table 8 and Figures 2 and 3 also indicate that for this transition, there is an overall trend of increasing temperature with increase of the n-alkyl chain length.

PDHI, PDHpI and PDDI are the only series members with samples of differing molecular weight and for which more than one thermogram was obtained. For each polymer it was observed that for a well defined maximum, the two largest  $(1/n)$  values occurred at lower temperatures than those of a shoulder. No consistent correlation of sample molecular weight with the shape of transition B, and therefore its median temperature,

was apparent in the PDHI and PDHpI thermograms. In PDDI thermograms, increase in sample molecular weight results in a change in the  $(1/n)$  outline from a maximum to a shoulder, increases the width of the transition and shifts it to slightly higher temperatures. As described earlier, the magnitude of  $(1/n)$  associated with transition B relative to that associated with A increases with decrease in molecular weight, a trend that is supported by the variation in relative  $(1/P^2)$  gradients with molecular weight.

Transitions (1) and (2) are only visible for PDMI to PDBI inclusive; for higher series members it is assumed that high damping associated with A and the glass transition masks any smaller transitions. These small transitions, in the vicinity of  $0^{\circ}\text{C}$ , are not at all reproducible in form, magnitude or temperature location. The PDMI 80/25 thermogram in Figure 1 was obtained under drier conditions than usual, and both transitions are clearly visible, as for a drier PDMI 37/100 sample. As dry-box conditions were not achieved, it is feasible that water is at least partially responsible for these transitions. In region (2), data for the higher molecular weight sample of PDMI is poor, but thermograms for the other sample clearly show a maximum of varying magnitude and temperature. The transition in region (1) is not well defined for PDEI and, with depression in temperature of the large  $(1/n)$  peak, there is merely the hint of a shoulder in this region for PDPI and complete masking in PDBI thermograms. In the PDEI thermograms damping evidence for transition (2) is irregular, but the only PDPI thermogram shows a relatively large and well defined maximum.

Shoulders differing in temperature and indistinctly outlined on the large (1/n) maxima, are the only sign of transition (2) for PDBI.

With the exception of transition B, transitions within region (3) are also non-uniform, the limitations of a large summary table therefore being more apparent. As indicated in Table 8, two transitions are visible above about  $-130^{\circ}\text{C}$  in the (1/n) data of three of the eight PDMI thermograms. All thermograms indicate a shoulder or maximum which is relatively large and broad, but which does change its magnitude and position randomly. An additional transition is sometimes visible at lower temperatures as a smaller (1/n) shoulder and, as indicated in Figure 1 for PDMI 80/25, can decrease the definition of the adjacent increase in (1/n). Some PDMI thermograms also indicate a possible shoulder within  $-120^{\circ}$  and  $-150^{\circ}\text{C}$ . Above  $-100^{\circ}\text{C}$  PDEI and PDPI thermograms contain anisotropic (1/n) data with poorly defined shoulders differing in magnitude and temperature with run and anisotropy. For PDEI, Table 8 contains the average of the median temperature for the most convincing shoulder in each thermogram. A much more reproducible transition occurs at  $-141^{\circ}\text{C}$  for PDEI, both thermograms indicating a small, but significant (1/n) maximum. As shown in Figure 2, where the median course between the different (1/n) graphs of the odd and even numbered oscillations is given, a smaller damping fluctuation occurs at similar temperatures for PDPI. Reference to Table 8 indicates the apparent difference in transition temperature, between the mean temperatures for differing anisotropic data and the position

manifest in Figure 2, which can occur when interpreting small changes in  $(1/n)$ . The PDPI transition temperature in region (4) being unusually low, it is not surprising that for the higher series members the transition should not, in general, be obvious below  $-110^{\circ}\text{C}$  in region (3). However the thermograms sketched in Figure 2 for PDBI 70/100 and PDHI 55/100 show the hint of a shoulder in one set of anisotropic data and a small  $(1/n)$  maximum respectively between  $-130^{\circ}$  and  $-150^{\circ}\text{C}$ .

PDBI 35/25 has a very high molecular weight and shows unusual  $(1/n)$  behaviour in regions (3) and (4). A minimum is defined between  $-45^{\circ}$  and  $-25^{\circ}\text{C}$  and with decreasing temperature,  $(1/n)$  increases to a constant  $(1/n)$  region which extends from  $-190^{\circ}$  to  $-100^{\circ}\text{C}$ , as if transitions (3) and (4) had coalesced. Above  $-110^{\circ}\text{C}$ , the illustrated PDBI thermogram shows a small, but obvious shoulder, whose temperature parameters are quoted for transition (3) in Table 8. Due to the absence of a definite decrease in  $(1/P^2)$  within  $-110^{\circ}$  and  $-30^{\circ}\text{C}$ , transition (3) has not been classed as transition B for PDBI. Reference to Figure 2 emphasizes the difference between the  $(1/P^2)$  vs. T graphs of PDHI and PDBI in this region. It is apparent from Table 8, that the location of the  $(1/n)$  shoulder for PDBI approximately fits the general trends for transition B, implying that this transition may occur for polymers with four or more carbon atoms in the n-alkyl chain. For PDBI, the lack of concurrent  $(1/P^2)$  decrease and the smallness of the temperature span of high  $(1/n)$  associated with transition (3) may merely be a result of the critically smaller length of the alkyl group. For series members PDMI to PDBI

inclusive, only small barely noteworthy changes in  $(1/P^2)$  occur between the glass transition region and region (4). As shown in Figure 2, a small minimum in  $(1/P^2)$  is visible within region (2) for PDPI. The existence, in only one of the PDEI thermograms, of small  $(1/P^2)$  minima in regions (2) and (3) raises doubts about their importance. In the PDMI thermograms a small  $(1/P^2)$  minimum was indicated at least once for each of transitions (1), (2) and (3).

The  $(1/n)$  data does not indicate the existence of a transition in the vicinity of  $-190^\circ\text{C}$  for PDMI and PDEI. The absence of a substantial decrease in  $(1/P^2)$  within region (4), provides confirmation of this interpretation, particularly useful when  $(1/n)$  data is scattered at the beginning of the run. Transition (4) is visible as a large  $(1/n)$  peak for all other poly(di-n-alkylitaconates). Occasionally, as for PDPI, the entire apex is not revealed due to its approximate coincidence with the lowest temperature attained for that run. As shown in Figures 2 and 3 a substantial decrease in  $(1/P^2)$  is always associated with the  $(1/n)$  maximum; this steeper gradient ceases randomly between  $-145^\circ$  and  $-180^\circ\text{C}$ . The PDBI  $(1/P^2)$  data is unusual: as shown in Figure 2 the steeper gradient persists until  $-130^\circ\text{C}$  for PDBI 70/100 and it extends to approximately  $-115^\circ\text{C}$  for the PDBI sample with continuous high damping between  $-190^\circ$  and  $-100^\circ\text{C}$ . The PDHI and PDDI  $(1/n)$  data for this broad transition were scattered and anisotropic giving slightly poorer reproducibility of the temperature parameters quoted in Table 8. Fluctuations in the large temperature differential between the sample and the thermocouple junction

may contribute to the random variation of median temperatures within the sample group PDBI to PDDI. Transition temperature differences, presumably meaningless, may also be due to the breadth of the transition, to which a temperature differential across the braid, also large and changeable at these low temperatures, may contribute. However, inspection of the thermograms does indicate a general trend of increasing temperature of transition (4) with increasing length of the alkyl group. The (1/n) peak is more completely displayed in Figures 2 and 3 when it occurs at higher temperatures and therefore any obvious trends in the shape of this maximum may only reflect changes in the temperature of transition (4), not itself a very reliable parameter.

Two temperature regions are of interest with respect to small less reproducible (1/n) variations in a few of the poly(di-n-alkylitaconate) thermograms. For samples PDMI to PDHI inclusive, features between  $-120^{\circ}$  and  $-150^{\circ}\text{C}$  in their (1/n) thermograms have already been described. From Figures 2 and 3 it is obvious that PDMI is the only series member which could reveal a secondary transition within  $40^{\circ}\text{C}$  and  $T_g$ . The PDMI 37/100 thermogram in Figure 1 indicates such a transition, as a possible (1/n) shoulder, most clearly of all the PDMI thermograms; this insubstantial shoulder is also evident at slightly lower temperatures and could therefore be confused with transition (1).

PMMA data have been described in terms of the four main temperature regions of Table 8 although, as expected from the difference in backbone structure, and as illustrated in Figure 1, the transitions differ from those of PDMI. The

transitions in regions (1) and (2) are characterized by substantial damping with concurrent changes in  $(1/P^2)$ . These transitions occur at higher temperatures than the average PDMI temperatures and the difference between the associated damping and  $(1/n)$  within region (3) is larger than for PDMI. Within transition region (3) damping changes are small and like the PDMI thermograms with indistinct transitions within region (3), an additional shoulder is suggested between  $-167^\circ$  and  $-147^\circ\text{C}$ . As with PDMI, neither  $(1/n)$  nor  $(1/P^2)$  data indicate the existence of transition (4).

Damping thermograms indicate that transitions B and (4) are the most noteworthy of the secondary transitions summarized in Table 8. The frequencies of the composite oscillations were evaluated at the median temperatures for these two transitions as given in Table 8. The results indicated a direct correlation between frequency and concentration of the impregnating solution, small frequency differences implying that actual composite concentration may more accurately be the relevant parameter. A decrease in frequency with increase in alkyl chain length was evident for braids impregnated in solutions of similar concentrations. The braid impregnated in a PDPI solution of approximate concentration 6 per cent, %, oscillated at approximately 0.27 Hz at  $-190^\circ\text{C}$ , frequencies at transition (4) median temperatures being approximately 0.43 Hz for PDHI, with a solution concentration of 12%, and about 0.56 Hz for PDDoI with a solution concentration of 22%. The trends are similarly illustrated for transition B, the limiting frequency values being associated with 8% PDDI (0.21 Hz) and 22% PDDoI (0.33 Hz). With the fundamental decrease in  $(1/P^2)$ ,

and hence frequency, with increase in temperature, and also the overall trend of an increase in temperature for transitions B and (4) with increase in alkyl chain length, the implied inverse relationship between frequency and median transition temperature is reasonable. However the decrease in frequency with increase in temperature from (4) to B, also varies with braid concentration: frequencies decreased by approximately 0.10 Hz for PDHI and PDHpI 12% braids and by 0.06 Hz for the 8% PDDI braid. Evaluation of the oscillation frequency at transition (3) for PDBI 70/100 (10%), and hence the frequency decrease of 0.05 Hz with a 100 degree temperature increase from transition (4), does not reveal whether the classification of the transition with the higher temperature is correct or not. The relatively small decrease compared with that of 0.10 Hz for 10% PDDI, could perhaps be related to the smaller temperature increase involved. That the difference in frequency which occurs between the two transition regions merely appears to reflect the  $(1/P^2)$  behaviour for PDBI, confirms the criterion for B; the lack of a large  $(1/P^2)$  decrease within region (3), precluding the identification of transition (3) with B for PDBI.

FIGURE 4

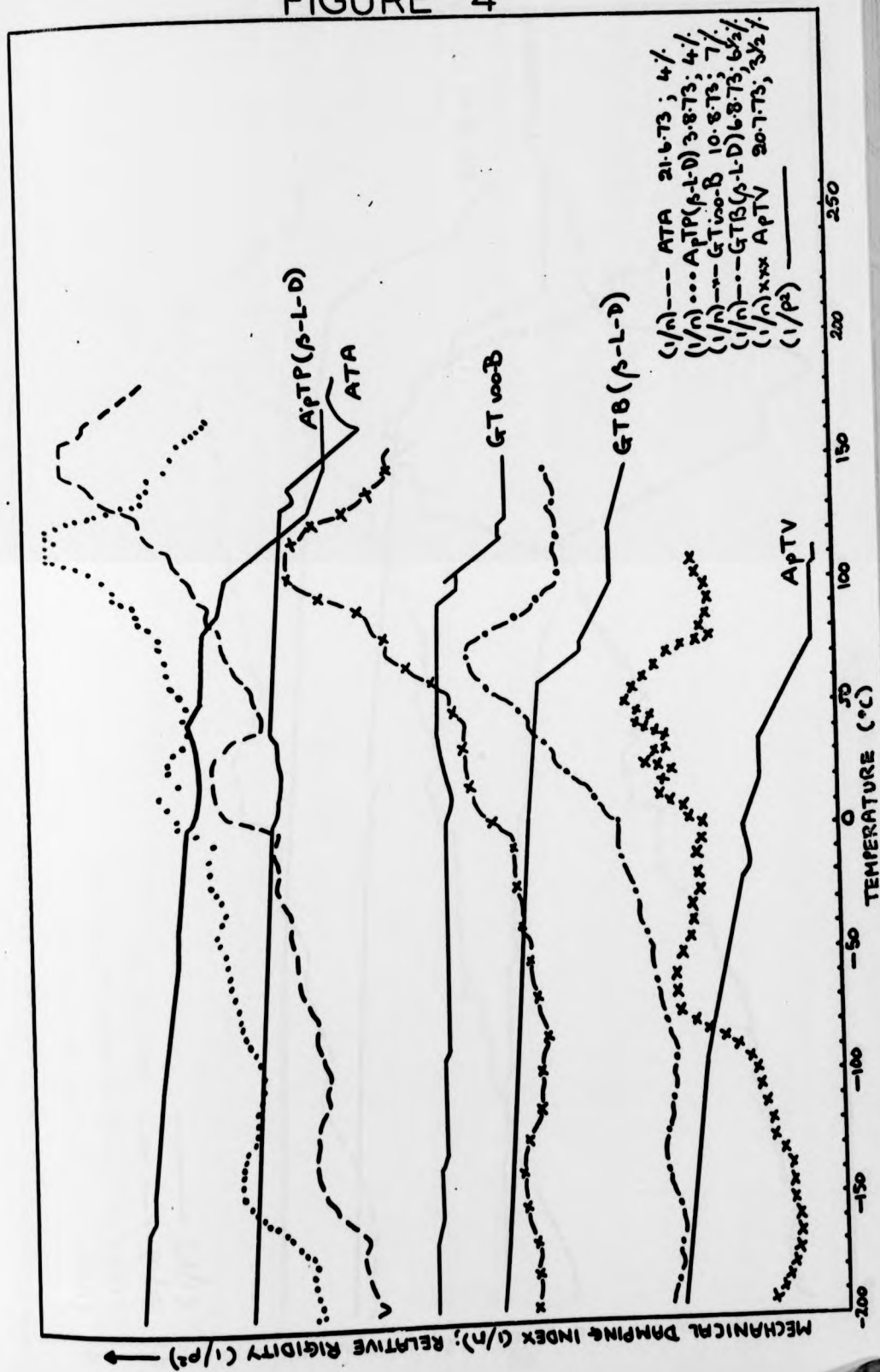


FIGURE 5

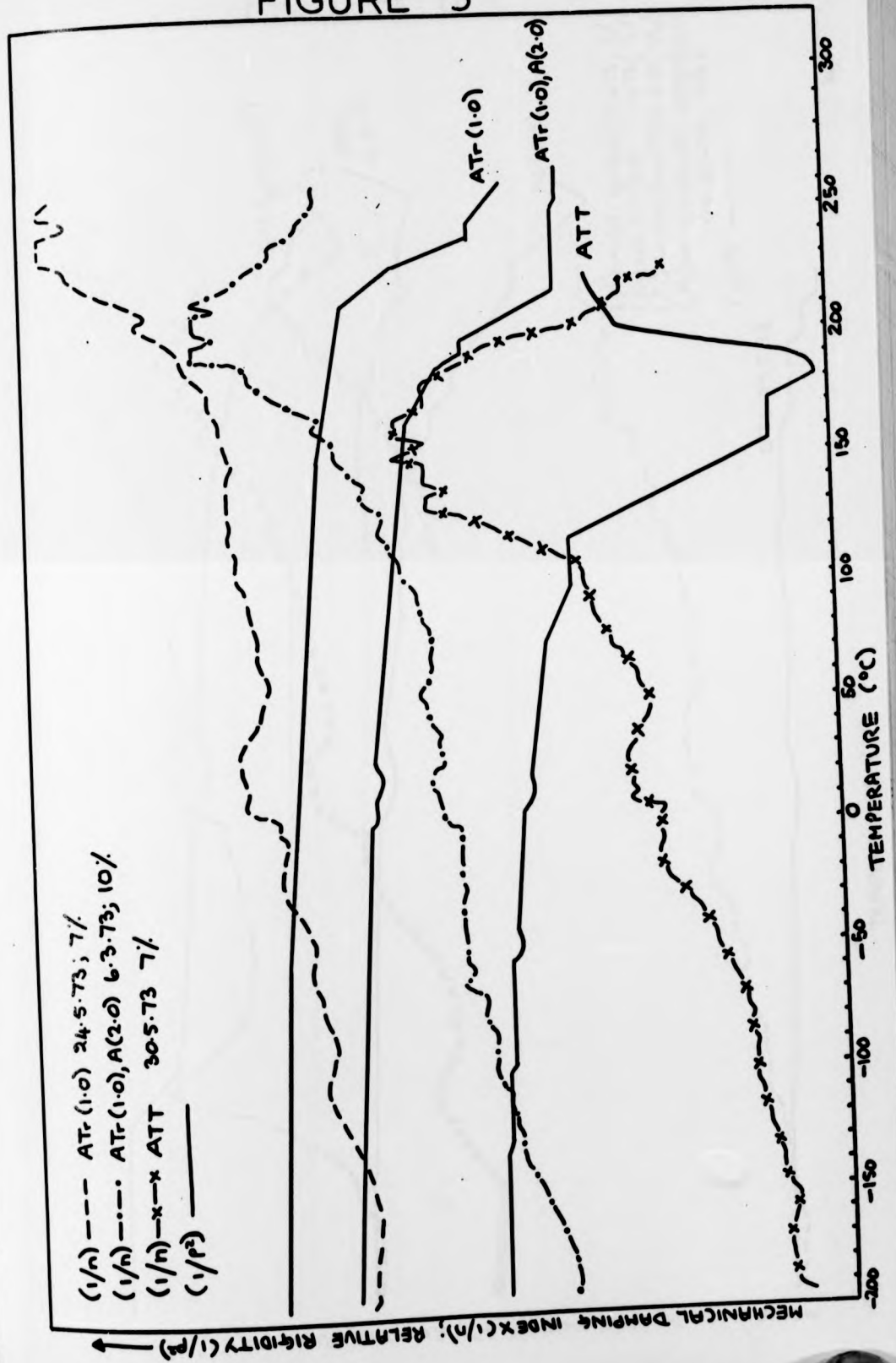


FIGURE 6

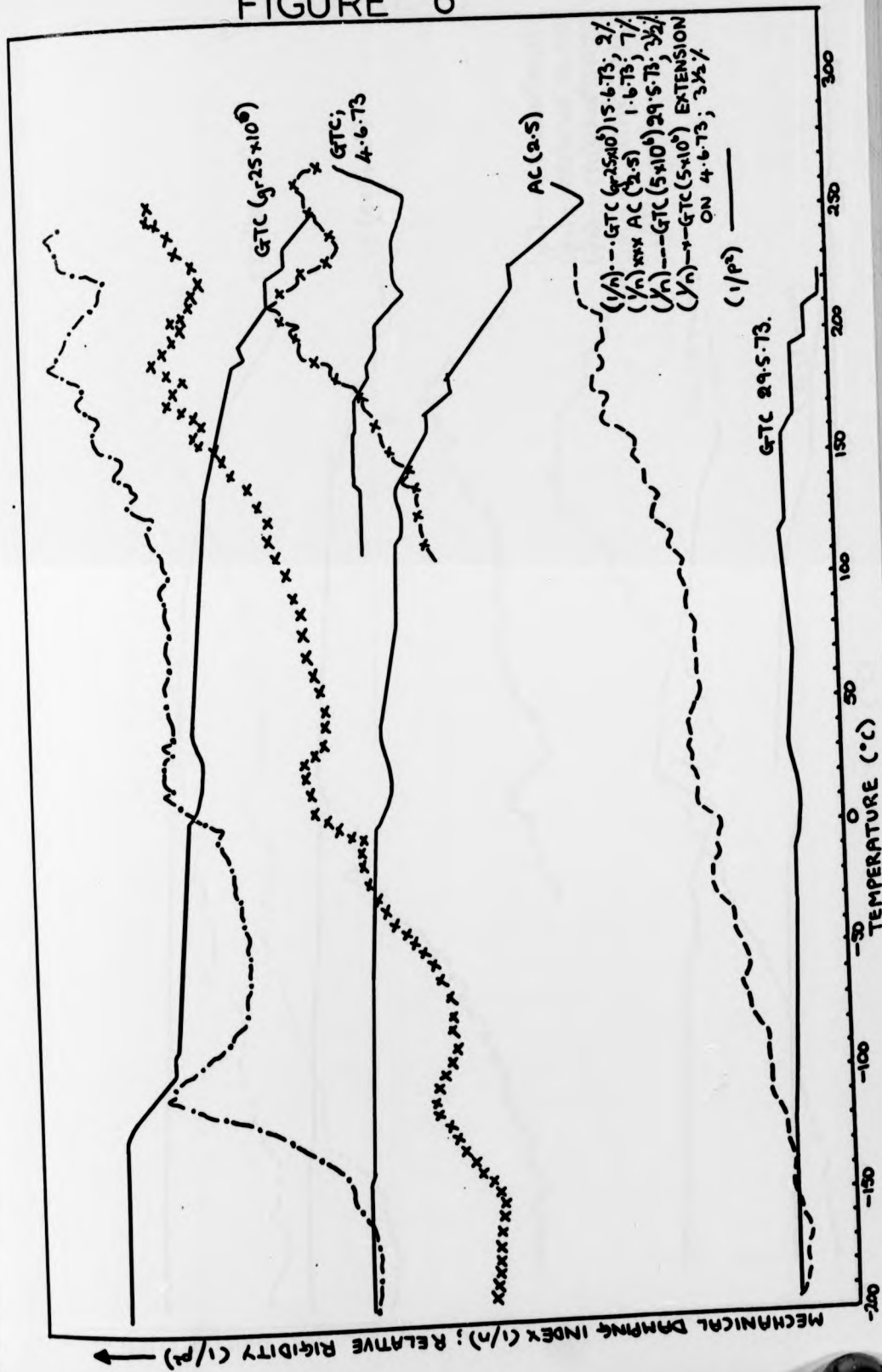


FIGURE 7

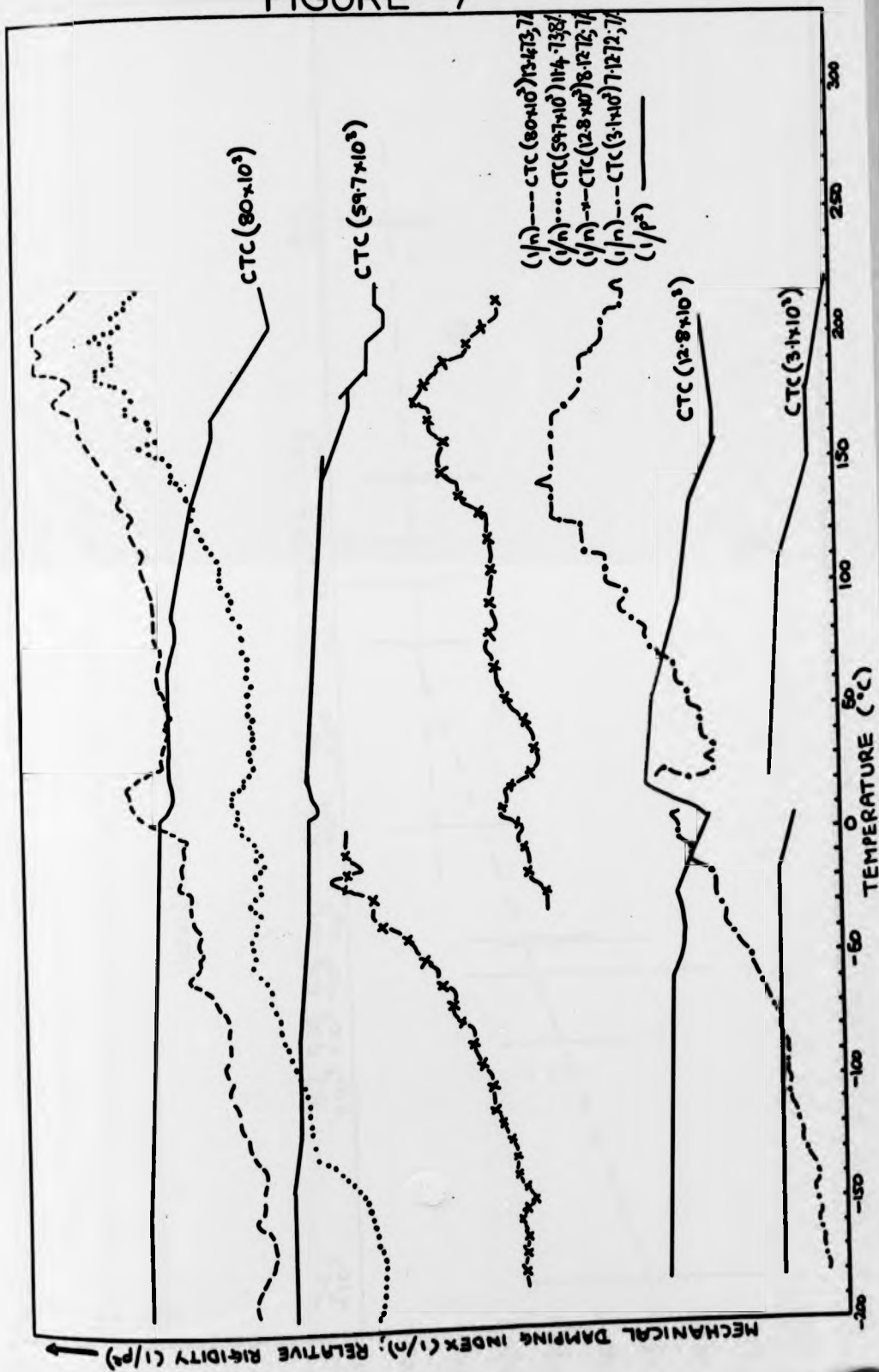


FIGURE 8

Cellulose Triacetate  $T_g$  vs.  $\log_{10} \frac{M_w}{M_n}$   
 Vertical lines represent the temperature span of the two largest  $(1/n)$  values,  
 for every thermogram Weight-average molecular weight

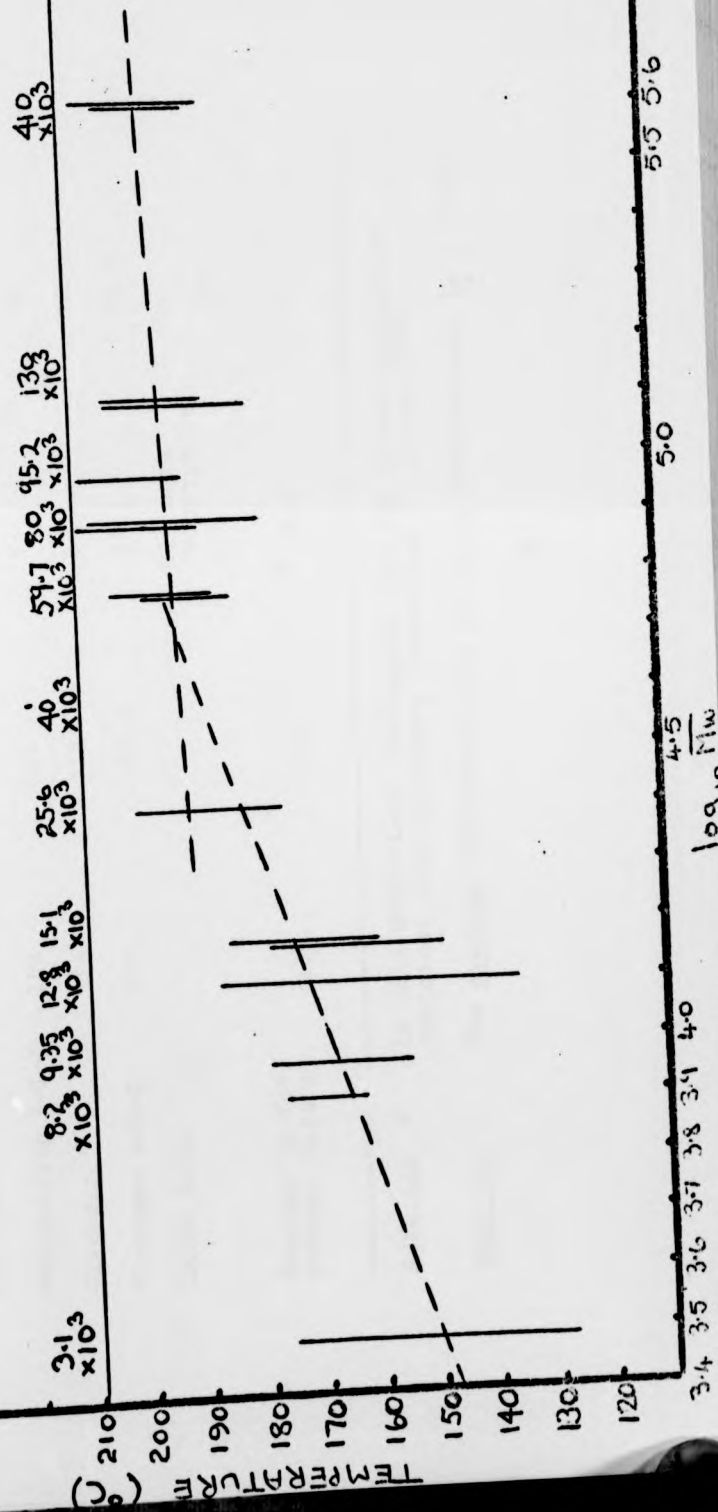


TABLE 9

Median Temperatures ( $^{\circ}\text{C}$ ) for Large (l/n) Values, Associated with the Glass Transition, for Carboxylic Acid Derivatives of Linear and Branched  $\alpha$ -D-(1  $\rightarrow$  4)-linked Polyglucans

Parent Polysaccharide	Acetate Ester	Propionate Ester	n-Butyrate Ester	n-Valerate Ester
Amylose	156	117.5	80	62
Amylopectin	161	122	69	56
Amylopectin $\beta$ -L-D	159	121	73	49
Glycogen	155	114	63	40
Glycogen $\beta$ -L-D	147	105.5	68	42.5
Extra Data			Glycogen Isobutyrate 111	33*
Average Tg for n-Alkyl Esters	156	116	70.5	47

Note (1). \* In this GTV( $\beta$ -L-D) thermogram, has the glass transition coalesced with secondary transition I, as for GTV?

Note (2). The average reproducibility of these temperatures is  $\pm 2.5^{\circ}\text{C}$

TABLE 9

Median Temperatures ( $^{\circ}\text{C}$ ) for Large (1/n) Values, Associated with the Glass Transition, for Carboxylic Acid Derivatives of Linear and Branched  $\alpha$ -D-(1  $\rightarrow$  4)-linked Polyglucans

Parent Polysaccharide	Acetate Ester	Propionate Ester	n-Butyrate Ester	n-Valerate Ester
Amylose	156	117.5	80	62
Amylopectin	161	122	69	56
Amylopectin $\beta$ -L-D	159	121	73	49
Glycogen	155	114	63	40
Glycogen $\beta$ -L-D	147	105.5	68	42.5
Extra Data			Glycogen Isobutyrate 111	33*
Average Tg for n-Alkyl Esters	156	116	70.5	47

Note (1). \* In this GTV( $\beta$ -L-D) thermogram, has the glass transition coalesced with secondary transition I, as for GTV?

Note (2). The average reproducibility of these temperatures is  $\pm 2.5^{\circ}\text{C}$

TABLE 10

Median Temperatures (°C) for Large (1/n) Values Associated with Tg for a Variety of Polysaccharide Esters

Cellulose Triacetate	2,3-di-0-acetyl, 6-0-trityl amylose [ATr(1.0), A(2.0)]	6-0-trityl amylose [ATr(1.0)]	Tri-0-tosyl amylose [ATT]
184 (+ 4)	212 (-6) (+ 3)	234.5 (+ 5.5)	155 (+ 4)
195 (+ 12) (- 6)	Glycogen and amylose-grafted- glycogen tricarbanilate	Glycogen tri- carbanilate, after prior heating to Tg	Cellulose tri- carbanilate; molecular weight- independent Tg
	195 (+ 9)	213 (+ 2)	195.5 (+ 3.5)

Note. Brackets contain reproducibility estimates for the quoted Tg's.

Section B: TBA Data of Several Polysaccharide Derivatives

(i) The glass transition region

Table 9 contains glass transition temperatures of carboxylic acid derivatives of linear and branched  $\alpha$ -D-(1  $\rightarrow$  4)-linked glucan chains. Between June and August 1973 one thermogram was obtained for each ester, five of these being shown in Figure 4. In general, the (1/n) maximum is clearly outlined for these esters, Table 9 containing median temperatures for the two largest (1/n) values observed. Two thermograms were obtained for ApTV, due to badly scattered data in the first thermogram which has therefore not been evaluated for Tg. Data obtained for ATA in November 1972 has also been omitted from Table 9 ; this early run gave a median temperature of 153.5°C despite unusual boundary amplitudes.

Two braids were impregnated in ATP solutions of similar concentration. Evaluation of their damped oscillations with boundary amplitudes of 2 cm and 0.5 cm (amplitude ratio equals 4.0) gave median temperatures for the largest damped oscillations of 119°C and 116.5°C, their approximate mean value being quoted in Table 9 . Therefore a TBA experiment repeated under similar conditions yields median temperatures for maximum (1/n), associated with the glass transition, within approximately 2.5 degrees. This reproducibility estimate includes the effect of experimental errors, such as those occurring in temperature evaluation; estimated maximum temperature errors for each ester group average between  $\pm 1.5^\circ$  and  $\pm 2.5^\circ$ C. The damped oscillations of one of the ATP composites mentioned above, were also evaluated

with boundary amplitudes of 3 cm and 1 cm (amplitude ratio equals 3.0); the resulting Tg's differed by approximately 5 degrees for a unit change in the amplitude ratio. For each type of ester, thermograms were obtained with a maximum divergence of amplitude ratio between approximately 0.5 and 1.0. From the available reproducibility estimates, it has been assumed that a difference in Tg of about 5 degrees is meaningful.

Therefore, from Table 9, differences in the branching of the polysaccharide backbone result in these trends for the median temperatures of each ester type, in order of decreasing temperature:

acetate

amylopectin > amylopectin  $\beta$ -L-D > amylose > glycogen > glycogen  $\beta$ -L-D.

propionate

amylopectin > amylopectin  $\beta$ -L-D > amylose > glycogen > glycogen  $\beta$ -L-D.

n-butyrate

amylose > amylopectin  $\beta$ -L-D > amylopectin > glycogen  $\beta$ -L-D > glycogen .

n-valerate

amylose > amylopectin > amylopectin  $\beta$ -L-D (> glycogen  $\beta$ -L-D > glycogen) .

Lower Tg's are indicated for all esters of highly branched glycogen and glycogen  $\beta$ -L-D. The last row in Table 9 contains the average of the median temperatures quoted in the first five

rows, where a decrease in average  $T_g$  with increase in length of the ester group is apparent. Row six contains the  $T_g$  of glycogen isobutyrate, almost identical to the average  $T_g$  for n-propionate esters. Row six also contains the result for an additional GTV ( $\beta$ -L-D) thermogram. The  $(1/n)$  vs.  $T$  graphs for this GTV ( $\beta$ -L-D) composite and for the GTV composite show irregularity of the  $(1/n)$  maximum, which suggests the coalescence of the glass transition with secondary transition I (to be discussed below). This possible explanation for the depression of  $T_g$  for this GTV ( $\beta$ -L-D) sample implies that the true  $T_g$  for GTV may be higher than that indicated in Table 9 .

The median temperature for the largest, steepest linear decrease in  $(1/P^2)$  usually occurs within a few degrees of the median temperature for maximum  $(1/n)$ . GTV and GTV ( $\beta$ -L-D) are exceptions to this generalization: the median temperatures of the two parameters differ by more than 10 degrees, the GTV ( $\beta$ -L-D)  $(1/n)$  maximum having the higher temperature but for the other ester it has the lower location. Identifying the greatest rate of molecular motion onset with  $T_g$ , gives further support to the idea that the value in Table 9 may be erroneously low for GTV. As a further  $(1/P^2)$  decrease occurs at slightly higher temperatures for GTV ( $\beta$ -L-D), the situation of the slightly larger or steeper decrease is of dubious significance. For the remaining valerate esters, secondary transition I is clearly perceptible as a separate entity, and the median maximum  $(1/n)$  temperature occurs on average 1.5 degrees below the median temperature for the steepest, largest  $(1/P^2)$  decrease. The average difference is 2.5 degrees for all the butyrate esters and for the acetate esters the median  $(1/P^2)$  temperature is on

average 3.0 degrees lower than the temperatures in Table 9 . The breadth of the shallow ATP (1/n) maximum could be related to the unusually large average difference, of 10.0 degrees, between median temperatures of its two parameters; for the remaining propionate esters the median temperature for maximum (1/n) is likewise higher than that for the linear (1/P<sup>2</sup>) decrease, but the temperature difference is, on average, only 2.0 degrees.

The frequencies of the maximum damped oscillations in each thermogram were evaluated. The oscillation frequency of an impregnated braid is directly proportional to its relative rigidity and, in general, the latter decreases gradually with increase in temperature. However, despite large variations in T<sub>g</sub> with ester group, their average frequency at T<sub>g</sub> was almost constant, being 0.15 Hz for the acetate esters, 0.17 Hz for the valerates and 0.16 Hz for both the propionate and the butyrate esters. Within each set of samples containing the same ester group, data suggest that the frequency at which the composite oscillates at T<sub>g</sub> is directly proportional to sample concentration and inversely proportional to T<sub>g</sub>. Amylopectin and amylopectin β-L-D composites were impregnated with dispersions of the insoluble samples in concentrations of about 4% and all soluble samples were impregnated with solutions of concentrations within the 4% to 8% range. For each type of ester the insoluble samples often oscillated, at their relatively high T<sub>g</sub>'s, at the minimum observed frequency, of about 0.13 Hz. ATP, with a T<sub>g</sub> almost identical to the average temperature for propionate esters,

oscillated, at that temperature, at the maximum evaluated frequency of 0.20 Hz; GTP and GTP ( $\beta$ -L-D) braids were also impregnated with 7% solutions and, despite their lower Tg's, these composites oscillated at lower frequencies. Despite the implied dependence of composite frequency on the proportion of  $\alpha$ (1  $\rightarrow$  6) linkages in the sample, frequency at Tg is still only affected by two independent variables: composite concentration and degree of branching, the latter being a cause of the Tg differences between samples containing the same ester group.

Table 9 contains the mean of the median temperatures for the two largest (1/n) values of odd and even numbered oscillations, considered separately due to the lack of more than one thermogram for most of the samples. These Tg's are thought to be reliable to about  $\pm 2.5^\circ\text{C}$ . With the exception of ATT, Tg's given in Table 10 were averaged from at least two thermograms and therefore odd and even numbered oscillations were not considered separately; a reproducibility estimate is given in brackets beneath the average Tg. The standard deviation of the eleven CTA values is quoted and four repeat runs for high molecular weight samples of CTC enabled evaluation of an average discrepancy of  $\pm 3.5^\circ\text{C}$ . These reproducibility estimates are approximately 1 degree smaller than the value obtained by halving the maximum difference between Tg values. This latter procedure was adopted for amylose and glycogen carbanilates and for ATr(1.0). For ATr(1.0), A(2.0) the Tg discrepancy was smaller than the maximum estimated error for temperature evaluation; the latter parameter is therefore quoted for this sample, for ATT, and for GTC on further heating. When

comparing Tg's, it should be remembered that these reproducibility estimates are themselves very approximate.

All possibly relevant thermogram details are provided as many variables affect TBA data and exceptions to generalized trends are therefore common.

Due to non-exponential damping of the oscillations of CTA composites, which was particularly noticeable in samples that had been cooled to sub-ambient temperatures, none of the thermograms have been reproduced in the thesis. The resulting scatter in the data diminished with increase in temperature and therefore the largest  $(1/n)$  peak is well defined over an average temperature range of 10 degrees. The largest, steepest decrease in  $(1/P^2)$  has a median temperature between 2 and 10 degrees below that for the  $(1/n)$  maximum. A braid impregnated in a heterogeneous system containing non-dissolved sample, showed discontinuities in the oscillation damping and the consequent thermogram displays a  $(1/n)$  maximum of width about 70 degrees and median temperature  $185^{\circ}\text{C}$ . The structure of the CTA composite itself, possibly affected by cooling, is thought to be responsible for the unsatisfactory form of the oscillations which caused eleven thermograms to be obtained between June 1972 and May 1973. Sample concentrations varied between 5% and 10% and the frequencies of maximum damped oscillations between 0.18 and 0.26 Hz, the higher frequencies being usually associated with higher composite concentrations. The data suggest that incomplete sample dissolution results in absorption of greater sample mass onto the braid and hence in greater effective composite concentration and frequency at Tg.

The median temperature for the two largest  $(1/n)$  values, of the ATr(1.0), A(2.0) thermogram sketched in Figure 5 is  $206^{\circ}\text{C}$ . Another thermogram obtained for the same sample, but with a lower composite concentration, has a median high  $(1/n)$  temperature of  $205.5^{\circ}\text{C}$ . However, in the latter thermogram there is a fluctuating high  $(1/n)$  profile; the peak, for which  $(1/n)$  is slightly greater, has a median temperature of  $213.5^{\circ}\text{C}$ , large  $(1/n)$  values also being centred on  $194^{\circ}\text{C}$ . In both thermograms the steep  $(1/P^2)$  gradient related to  $T_g$  is interrupted by constant  $(1/P^2)$  values at about  $195^{\circ}\text{C}$ . The  $(1/n)$  maximum of the illustrated thermogram can also be divided into two parts with equal  $(1/n)$  and median temperatures of  $195.5^{\circ}$  and  $210.5^{\circ}\text{C}$ . The largest, steepest  $(1/P^2)$  reduction occurs at temperatures above  $195^{\circ}\text{C}$  and therefore the average  $T_g$  is quoted as  $212^{\circ}\text{C}$  in Table 10 . As shown in Figure 5 a division in the maximum  $(1/n)$  data is not always clearly perceptible and consequently  $T_g$  could have been quoted as  $206^{\circ}\text{C}$ . During both maximum  $(1/n)$  processes the average frequency of oscillation for the 10% composite was 0.19 Hz; at  $213.5^{\circ}\text{C}$  the 7% composite was oscillating at 0.15 Hz. Similar boundary amplitudes were used in the data evaluation.

The median temperature for maximum damped oscillations in the ATr(1.0) thermogram (see Figure 5) is  $240^{\circ}\text{C}$ , the steepest, largest decrease in  $(1/P^2)$  having a median temperature 7 degrees lower. The  $(1/n)$  maximum was more distinct in another thermogram, where the median temperature for maximum  $(1/n)$  was  $229^{\circ}\text{C}$  and for the steepest  $(1/P^2)$  gradient,  $224^{\circ}\text{C}$ . The approximate equality of the differences between median temperatures (of the two

parameters) supports this interpretation of the  $(1/n)$  peak in the traced thermogram, where high  $(1/n)$  persists to above  $250^{\circ}\text{C}$ . It is possible that inadequate drying of one of the braids could have contributed to its low median temperatures, and therefore to the 11 degree difference between median temperatures for maximum  $(1/n)$ , averaged in Table 10 . Both braids, impregnated with 7% solutions, oscillated at 0.14 Hz when  $(1/n)$  was a maximum. Both sets of data were evaluated with boundary amplitudes of 2 cm and 0.5 cm.

The very large, broad  $(1/n)$  maximum indicated in Figure 5 for ATT has a median temperature of  $155^{\circ}\text{C}$ . The steepest and largest linear  $(1/P^2)$  decrease, generally used to identify the glass transition region, occurs from  $115^{\circ}$  to  $155^{\circ}\text{C}$ , its median temperature occurring 20 degrees lower than  $T_g$ . With temperature increase above  $180^{\circ}\text{C}$ ,  $(1/n)$  quickly decreases, and  $(1/P^2)$  displays exceptional behaviour by increasing rapidly to attain, by  $210^{\circ}\text{C}$ , a value only slightly less than that at  $115^{\circ}\text{C}$ . The  $(1/P^2)$  recovery signifies a concurrent increase in the density of the composite, also implied by the observed twisting of the braid from  $180^{\circ}\text{C}$ . An unusually large amount of untwisting had occurred with the onset of the glass transition, alternate oscillation decays being off-scale from  $150^{\circ}$  to  $195^{\circ}\text{C}$ . Heating ceased at  $225^{\circ}\text{C}$  and on removal from the instrument the braid was black. A 7% solution had been used in the preparation of the ATT composite which oscillated at approximately 0.13 Hz at the  $T_g$  quoted in Table 10 .

$T_g$  was identified with the median temperature for the two largest  $(1/n)$  values in amylose carbanilate thermograms, 7% solutions and a boundary amplitude ratio of 4.0 being used

in the preparation and data evaluation of all but one composite. The fully substituted samples oscillated at frequencies close to their mean frequency, of 0.21 Hz, their mean Tg being 196°C. Two sets of data gave a value of 194°C for Tg despite differences in composite concentration and amplitude ratio. However, the other two composites, with identical concentration and boundary amplitudes gave thermograms exhibiting the extreme values of 43 and 14 degrees for the width of the (1/n) maximum, for which median temperatures differed by 17.5 degrees. From approximately 140° to 220°C, the large (1/P<sup>2</sup>) reduction in ATC thermograms can be described by three gradients, the most unusual feature being the short second decrease spanning 180° or 190°C. Changes in the relative (1/n) magnitude of the implied additional molecular process could account for the differences in breadth, and therefore temperature, of the apparent glass transition region; in general, the narrower the (1/n) maximum, the higher the median temperature. Non-exponential amplitude decay occurred for the oscillations of an ATC composite whose external water content may have been reduced; the scattered (1/n) data suggests a possible Tg-elevation to approximately 207°C, the median temperature for the narrowest maximum observed. Figure 6 contains the thermogram obtained for an AC(2.5) sample. The data was evaluated with a boundary amplitude ratio of 3.0, and the composite, prepared with a 7% solution, oscillated at 0.16 Hz at the apparent Tg. The median temperature for maximum (1/n) is 192°C. A secondary high (1/n) process could be affecting the glass transition region for this sample as well: the second decrease in (1/P<sup>2</sup>) is evident from 170° to 180°C and

the (1/n) peak is broader than that of several fully-substituted samples. The possible condensation of water on this composite could also account for its slightly lower Tg, remembering the implications of the scattered "dry-run" data. The poor reproducibility of the ATC data does not allow identification of any significant change in Tg with variation of the degree of substitution of amylose carbanilate. The median high (1/n) temperatures of all five thermograms have therefore been averaged in Table 10 and their maximum range has been unequally divided, to indicate that the true Tg may well be higher than 195°C.

The first thermogram obtained for GTC, on 29.5.73, is sketched in Figure 6 and shows high (1/n) at 180°C, only slightly less than that of the maximum damped oscillations which occur from 214°C until the end of the run. The two largest (1/n) values, visible between 165° and at least 225°C, have a median temperature of at least 195°C. After fairly rapid cooling from 225°C and reheating from 100°C, this composite yielded a partial thermogram which displays a distinct and symmetrical (1/n) peak of width approximately 20 degrees and median temperature 213°C. ATC chains were grafted on to GTC, with a molecular weight of ( $5 \times 10^6$ ), to give samples of approximate molecular weight ( $8 \times 10^6$ ), ( $25 \times 10^6$ ) and ( $100 \times 10^6$ ). With increase in sample molecular weight, the median temperature for highly damped oscillations decreased from 204° to 187°C, a 17 degree depression. In addition, the breadth of the (1/n) maximum increased with molecular weight: the GTC ( $100 \times 10^6$ ) thermogram has a shallow, high (1/n) profile of width approximately 60 degrees, resembling the 29.5.73 thermogram, whereas the GTC

(gr  $8 \times 10^6$ ) peak width is similar to that of the GTC re-run. The median temperature trend merely reflects a depression in temperature of the onset of high (1/n); substantial (1/n) ceases between  $210^\circ$  and  $216^\circ\text{C}$  for all three samples. The amylose carbanilate data also suggests an additional high (1/n) process in the vicinity of  $180^\circ\text{C}$ , and that a variation in median temperature of  $\pm 9$  degrees is not necessarily meaningful. As there is only one thermogram for each sample, the reproducibility of the median temperatures is unknown. The mean Tg for the four GTC and GTC (gr) thermograms, obtained by heating the sample to Tg for the first time, is given in Table 10 and has the same value, of  $195^\circ\text{C}$ , as the mean temperature for amylose carbanilate. Thermogram complexity in the glass transition region evidently precludes the detection of a significant difference between Tg's of amylose and glycogen carbanilates. The existence of additional high (1/n), which disappears with heating to Tg, is indicated by GTC; it is possible that changes in the relative magnitude of this (1/n) are responsible for the different median temperatures which apparently indicate a decrease in Tg with decrease in branching of the backbone structure. It is also feasible that this variable high (1/n) is masking a real trend; the narrow (1/n) peaks, of width 20 degrees, of GTC ( $5 \times 10^6$ ) and GTC (gr  $8 \times 10^6$ ) have median temperatures of  $213^\circ$  and  $204^\circ\text{C}$  respectively. The mean frequency of the maximum damped oscillations was 0.16 Hz, extreme values being 0.19 Hz for GTC (gr  $100 \times 10^6$ ) and GTC (gr  $8 \times 10^6$ ) composites and 0.12 Hz for GTC. The GTC composite was impregnated in a solution of concentration 3.5%; for the GTC (gr) samples

the concentration decreased from 3.5% to 1% with increase in sample molecular weight. A boundary amplitude ratio of approximately 4.0 was used for all the data evaluation.

Thermograms of CTC samples contain  $(1/n)$  maxima which differ considerably in relative height and breadth, as illustrated in Figure 7. The glass transition region, identified as usual with the two highest  $(1/n)$  values, apparently extends over 50 degrees for samples of molecular weight  $(3.1 \times 10^3)$  and  $(12.8 \times 10^3)$  and over about 20 degrees for the higher molecular weight samples. Asymmetry of the  $(1/n)$  maximum, evident in three of the traced thermograms, suggests the existence of a secondary process just below Tg. As precise definition of the glass transition region is obviously impossible, Figure 8 summarizes the temperature spans of highest oscillation  $(1/n)$  for all CTC samples. The glass transition is clearly depressed in temperature with decrease in sample molecular weight below  $(25.6 \times 10^3)$ . Composites were impregnated in 7% solutions of the low molecular weight fractions ( $\overline{M}_w < 40 \times 10^3$ ) and there was little variation in the frequencies of maximum damped oscillations despite their differing temperatures, the mean frequency being 0.16 Hz. Practically all CTC data was evaluated with a larger boundary amplitude of 2.0 cm, but with amplitude ratios varying between 10.0 and 2.66. There is no clear correlation of this ratio with the breadth of the  $(1/n)$  maximum, which seems to be narrower for the higher molecular weight samples, average temperature spans of 33 and 21 degrees

being displayed by samples below and above ( $40 \times 10^3$ ) in molecular weight respectively.  $T_g$  is almost constant for higher molecular weight ( $\overline{M}_w > 40 \times 10^3$ ) CTC samples, median temperatures for high ( $1/n$ ) increasing from a mean value of  $193^\circ$ , for CTC ( $59.7 \times 10^3$ ), to  $197^\circ\text{C}$  for unfractionated CTC ( $410 \times 10^3$ ). These effectively molecular-weight-independent  $T_g$ 's have an average value of  $195.5^\circ\text{C}$ , quoted in Table 10. Solutions with concentrations of 3% to 8% were used to impregnate braids with higher molecular weight samples. The frequencies of the maximum damped oscillations varied between 0.13 and 0.23 Hz and were apparently independent of sample concentration, the mean frequency being 0.18 Hz.

The large ( $1/P^2$ ) reduction occurs by a steeper gradient than the gradual decrease caused by thermal expansion and often ceases within a few degrees of the median temperature for high ( $1/n$ ). In general, the temperature range and therefore the magnitude of this  $T_g$ -related decrease differs considerably. The presentation of  $T_g$  data in Tables 9 and 10 is inevitably unsatisfactory; the thermograms necessitated subjective interpretation and were, unfortunately, far too numerous to be totally reproduced. In general, two or more ( $1/n$ ) vs.  $T$  and/or ( $1/P^2$ ) vs.  $T$  graphs for the same sample are not consistent and therefore possible causes for their differences have been described above. Any correlations, evident between a parameter such as the width of the ( $1/n$ ) maximum and a variable such as molecular weight or sample concentration, have been mentioned; the absence of such a correlation may merely indicate the existence of a more dominant variable such as the postulated  $180^\circ\text{C}$  high ( $1/n$ ) process of the carbanilates.

TABLE 11

## Summary Table of Secondary Transitions of Polysaccharide Esters

Sample	I $5^{\circ}\text{C} < T < 50^{\circ}\text{C}$			II $-100^{\circ}\text{C} < T < 5^{\circ}\text{C}$			III $-160^{\circ}\text{C} < T < -100^{\circ}\text{C}$			IV $\text{Run Onset Temperature} < T < -160^{\circ}\text{C}$		
	a	b	c	a	b	c	a	b	c	a	b	c
	(degrees)	(degrees)	(degrees)	(degrees)	(degrees)	(degrees)	(degrees)	(degrees)	(degrees)	(degrees)	(degrees)	(degrees)
Acetate esters of $\alpha$ -(1 $\rightarrow$ 4) linked polyglucans	( $\bar{m}$ ) 17	22		IIa; (m/s) -	-16.5		$\bar{m}$ 19.5	-133				
Propionate and isobutyrate esters of $\alpha$ -(1 $\rightarrow$ 4) linked polyglucans	( $\bar{m}$ ) 17.5	28.5		IIa; (m/s) -	-13.5		$\bar{m}$ 16.5	-136.5				
n-Butyrate esters of $\alpha$ -(1 $\rightarrow$ 4) linked polyglucans	( $\bar{m}$ ) 24	32.5		IIa; (m/s) -	-9		m 19.5	-131	m	-	-	< -190
n-Valerate esters of $\alpha$ -(1 $\rightarrow$ 4) linked polyglucans	( $\bar{m}$ ) 21	26.5		IIa; (m/s) -	-11		(m/s) 22.5	-122.5	m	-	-	< -190
Cellulose Triacetate	(m) 20	28		Existence of II and III is possible but data is very poor. See written details.								

TABLE II (continued)

Sample	I $5^{\circ}\text{C} < T < 50^{\circ}\text{C}$			II $-75^{\circ}\text{C} < T < 5^{\circ}\text{C}$			III $-130^{\circ}\text{C} < T < -75^{\circ}\text{C}$			IV Run Onset $< T < -160^{\circ}\text{C}$ Temperature		
	a	b	c	a	b	c	a	b	c	a	b	c
2,3-di-O-acetyl, 6-O-tritylamylose	( <u>m</u> )	17	17	(m/s)	50	-30	(m/s)	11	-96.5			
				(see written details)								
6-O-tritylamylose	<u>m</u>	28	24.5	IIa; m	14	-18.5	m/s	19	-101			
				m/s	17	-55						
Tri-O-tosyl- amylose	<u>m</u>	27	22	IIa; m/s	30	-8	<u>s</u>	23	-101			
Amylose Carbanilate	<u>m</u>	21	21	IIa; <u>s</u>	21	-11.5	<u>m</u>	17.5	-107			
				(m)	9	-58.5						
Glycogen and amylose-grafted- glycogen tricarbanilate	( <u>m</u> )	25.5	26	IIa; (m)	16	-13	m/s	16	-98			
				(m)	19	-63						
Cellulose Tricarbanilate	<u>m</u>	16	14.5	IIa; (m/s)	19.5	-20.5	(m/s)	19.5	-102			
				(m)	10	-49						

TABLE 11 (continued)

Key: In column a, the letter "m" or "s" indicates that the most frequent (l/n) outline is a maximum or shoulder respectively, brackets indicating poor transition reproducibility, i.e. (l/n) evidence varies in temperature and/or magnitude with detailed sample structure and/or run and/or initial oscillation direction. This letter is underlined if the associated (l/n) change is substantial. Columns b and c contain the width of the temperature range and the median temperature respectively of the two largest (l/n) values associated with the transition. Average values for these parameters are quoted.

(ii) The secondary transition regions

The main (1/n) characteristics of the polysaccharide esters at temperatures lower than their Tg's have been summarized in Table 11. Transition temperatures can be expected to differ with sample structure and therefore the temperature limits which define the four regions of particular interest are variable by as much as  $\pm 10$  degrees. Region II is very broad and may contain more than one transition, a transition occurring within  $-30^{\circ}$  and  $+5^{\circ}\text{C}$  being described as "IIa" in column a. Transition region III occurs at lower temperatures for esters of the  $\alpha$ -(1  $\rightarrow$  4)-linked polyglucans. Region IV corresponds to region (4) of the poly(di-n-alkylitaconates) (see Table 8), where the transition is obvious as a large (1/n) maximum with an associated (1/P<sup>2</sup>) decrease. Some of the thermograms for the polysaccharide esters were obtained in the autumn of 1972, when slower warming rates in regions I and II may have affected the data; the poly(di-n-alkylitaconates) were studied during 1973 and the transition temperatures quoted in Table 11 have therefore been solely derived from 1973 thermograms. The following pages contain details of the summarized transitions, describing the effects of variables such as the rate of warming and the degree of backbone branching.

Initially, the secondary transitions of the fully substituted  $\alpha$ -(1  $\rightarrow$  4)-linked glucans whose Tg's are given in Table 9, are discussed in order of decreasing temperature. In general, the thermograms of these esters exhibit a small transition in region I. Brackets are shown in the relevant column a of Table 11 to indicate that the average values quoted in columns b and c are only approximate guides to the

width and median temperature of that transition. A variation in the median temperature with repeat run of at least 10 degrees has been observed, differences for samples including the same ester group being of the same order of magnitude. A clear correlation between transition temperature and the proportion of  $\alpha$ -(1  $\rightarrow$  6)-linkages could not be discerned, although for each ester type the amylopectin  $\beta$ -L-D derivative has the lowest median temperature and the glycogen transition is found at relatively high temperatures. In addition, the average value in column b is not very meaningful; the width of the transition, and hence its median temperature, is extremely sensitive to the effects of anisotropy in  $(1/n)$  and irregularity in the shape of the peak. Thermograms of the acetate and propionate esters most frequently contain signs of a shoulder on this broad maximum at 10° to 20°C, actually shown most clearly in Figure 4 by the GTB ( $\beta$ -L-D) tracing. The only thermogram obtained in 1972 for ATA displays a narrower maximum for this transition at lower temperatures than in the 1973 ATA thermogram. This maximum is clearly perceptible, the letter "m" therefore being underlined in column a. There is, however, a gradation in the  $(1/n)$  amplitude in region I relative to that associated with the glass transition, the former transition becoming more important with increase in the length of the n-alkyl group. As shown in Figure 4 for ATA and ApTP( $\beta$ -L-D), typifying thermograms for these ester types,  $(1/n)$  associated with transition I is considerably less than the maximum  $(1/n)$  values. In the GT iso-B thermogram, the small relative magnitude of  $(1/n)$  in region I justifies, for this transition, the grouping of this ester with the propionate samples. It is evident in Figure 4 that  $(1/n)$  in

region I is larger for the butyrates, the transition being visible as a shoulder on the  $(1/n)$  maximum for GTB and GTB ( $\beta$ -L-D) and as a discrete maximum for the less highly branched butyrate esters. Transition I cannot be identified for GTV and GTV ( $\beta$ -L-D), presumably merging with the glass transition, as previously suggested. The ATV thermogram shows a distinct  $(1/n)$  peak, with a large concurrent  $(1/P^2)$  decrease and the associated  $(1/n)$  equal to that of the adjacent glass transition. As shown in Figure 4 for ApTV and ApTV ( $\beta$ -L-D), the relative magnitude of the transition within region I is slightly smaller than the described ATV transition. As well as the difference in character of the  $(1/n)$  vs. T graph in region I, the broad shallow minimum in  $(1/P^2)$ , observed there for all acetates, some propionates and for GT iso-B, is not usually visible for the higher esters.

As indicated in Figure 4 for esters of the  $\alpha$ -(1 + 4) polyglucans evidence for a transition within region II is provided by the  $(1/n)$  increase at temperatures higher than that of the  $(1/n)$  peak within region III. In general, there is an overall  $(1/n)$  increase concurrently with temperature within region II; at least two coalescent transitions are implied, the  $(1/n)$  change at higher temperatures being attributed to transition IIa. The magnitude of  $(1/n)$  associated with transition II differs greatly and the  $(1/n)$  contribution of transition IIa often appears to be small; it is consequently difficult to distinguish the temperature extent of each transition, and width parameters for these transitions, being meaningless, have therefore not been included in Table 11. As indicated by " $m/s$ ", the outline, relative amplitude and

temperature of these (1/n) transitions vary with initial oscillation direction, run and sample. Underlining has been omitted as significant (1/n) evidence is not consistently associated with either transition. Median temperatures give only a rough indication of the disposition of these transitions; discrepancies in the apparent location of transitions II and IIa of the order of 30 and 10 degrees respectively have been observed between data of a different initial oscillation direction, run or sample backbone structure. Due to (1/n) inconsistency, it was impossible to detect a correlation between median temperature and degree of backbone branching, for samples including the same ester groups. The earlier run for ATA yielded a thermogram which clearly indicated II and IIa with median temperatures approximately 15 degrees lower than those given in Table 11 for the 1973 acetate thermograms. The tracings in Figure 4 illustrate that (1/n) changes related to transitions IIa, II and III are frequently very small. Nevertheless in the majority of thermograms it is evident that the higher the temperature of the transition, the greater the amplitude of the associated (1/n). Exceptions to this generalization are due to variations in the evidence for transition II; in this region, (1/n) can be less than in region III, or very much greater and with a concurrent increase in the  $(1/P^2)$  gradient, as illustrated by the GT iso-B and ApTV thermograms respectively. It has been observed that (1/n) associated with transition II is most frequently greater than that of IIa for amylopectin and amylopectin  $\beta$ -L-D esters; this is the only backbone structure effect that could be detected in the irregular (1/n) variations within region II.

As indicated in Figure 4, the  $(1/n)$  amplitude within region III varies unevenly with ester group;  $(1/n)$  differences within regions II and IV, themselves related to the size of the ester group, may be, at least partially, responsible. A broad  $(1/n)$  maximum is clearly outlined for the acetates, propionates and butyrates, their median temperatures being very reproducible: the maximum divergence within each set of samples increased systematically from about 10 to 20 degrees with ester group enlargement. There is no obvious correlation of median temperature with degree of branching. For GT iso-B the height of the  $(1/n)$  peak associated with transition III resembles the smaller maxima of the n-butyrate more closely than the significantly larger  $(1/n)$  evident in region III of the propionate and acetate thermograms (hence the underlining of "m" in column a for these two esters). Transition III is not well defined in the  $(1/n)$  vs. T graphs of the valerate derivatives and median temperatures for the shallow peaks or shoulders are therefore unreliable. It is evident from Figure 4 that identification of this transition from ApTV data is particularly difficult and median temperatures evaluated from the two available thermograms, deviated by 30 degrees. Transition temperatures are apparently affected by both the rate of warming and the temperature at the run onset, the key variable possibly being the temperature differential across the chamber. Cooling was only achieved to  $-145^{\circ}\text{C}$  in the early ATA run, and the resulting thermogram indicated a broader  $(1/n)$  maximum at least 10 degrees higher than transition III for the later acetate runs.

For the n-butyrate and n-valerate esters, the existence of a large transition below  $-190^{\circ}\text{C}$  is indicated by a

clearly perceptible increase in  $(1/n)$  and/or  $(1/P^2)$  with decrease in temperature within region IV. Thermogram interpretation for transition IV is complicated by scattered data at the beginning of the run and by the hint of a small additional transition, to be discussed later, in the vicinity of  $-170^\circ\text{C}$  for some acetates and propionates. Nevertheless, as shown in Figure 4, the absence of transition IV is substantiated, in the acetate, propionate and GT iso-B thermograms, by an approximately horizontal  $(1/P^2)$  graph and/or the lack of a systematic  $(1/n)$  increase by  $-190^\circ\text{C}$ .

The contents of each remaining row in Table 11 are described in sequence below. As mentioned earlier, CTA data obtained at sub-ambient temperatures is badly scattered and relevant details have therefore been derived from the two clearest thermograms. Transition I is distinct in only one of these thermograms; the width and median temperature of the associated maximum damped oscillations were quoted because the two largest  $(1/n)$  values extend from  $0^\circ$  to  $69^\circ\text{C}$ . A related minimum in  $(1/P^2)$  occurs within  $5^\circ$  and  $40^\circ\text{C}$ . The transition evidence for CTA visually resembles the ATA  $(1/n)$  and  $(1/P^2)$  characteristics in region I. In one thermogram the dominant  $(1/n)$  feature within  $+5^\circ$  and  $-160^\circ\text{C}$  occurs between  $-60^\circ$  and  $-90^\circ\text{C}$  with an associated  $(1/P^2)$  reduction. Transition III is suggested, on the low temperature side of this peak, by a slight shoulder at approximately  $-125^\circ\text{C}$ . The other thermogram is quite different; the main  $(1/n)$  peak is indicated between  $-120^\circ$  and  $-165^\circ\text{C}$ , whereas merely the existence of finite  $(1/n)$  is revealed within region II. It

is evident that a large transition does not exist in the vicinity of  $-190^{\circ}\text{C}$ .

The data given in Table 11 for ATr(1.0), A(2.0) is derived from the thermogram illustrated in Figure 5. Any discrepancies between this data and the results of the other, 1972 run are described below. It is noteworthy that the change-over temperature, for the temperature programming method, and the sub-ambient rates of warming were similar on both runs. As shown in Figure 5, a  $(1/P^2)$  minimum is related to transition I, also obvious as a small  $(1/n)$  maximum, whose median temperature varies by 14 degrees with initial oscillation direction; in the earlier data the analogous temperature, of  $11.5^{\circ}\text{C}$ , approximates to one of these differing values. It is evident in Figure 5 that region II contains almost constant  $(1/n)$ ; detailed examination of the thermogram reveals, however, the possible existence of a slight  $(1/n)$  minimum at  $-25^{\circ}\text{C}$  which could locate IIa and II at  $-15^{\circ}$  and  $-40^{\circ}\text{C}$  respectively. The main feature of the other thermogram is a  $(1/n)$  peak at about  $-20^{\circ}\text{C}$ . As displayed in the tracing, a  $(1/n)$  maximum and/or shoulder is perceptible in region III, its median temperature being confirmed by the situation of the small shoulder in the original thermogram. Transition IV is obviously absent.

The main transitions of the illustrated ATr(1.0) thermogram have likewise been summarized in Table 11. For the most part, this thermogram was obtained with sub-ambient warming rates of about one degree per minute: as usual, the 1972 run involved a slower rate. Transition I is clearly visible

in the original thermogram but cannot be characterized due to a gap in the data. For the more distinct transition at the higher temperatures in region II, a slower warming rate resulted in a median temperature 10 degrees lower than the value given for IIa in Table 11. In both thermograms the definition of transition II is poor. With increase in temperature from approximately  $-145^{\circ}\text{C}$ , a  $(1/n)$  increase is obvious in both thermograms; the slightly scattered data of the early run, which began at  $-175^{\circ}\text{C}$ , indicates a slightly higher temperature for transition III. As shown in Figure 5, there is no sign of a large transition in the vicinity of  $-190^{\circ}\text{C}$ .

Figure 5 also contains a tracing of the ATT thermogram. There is a tangible  $(1/P^2)$  decrease in region I and the associated  $(1/n)$  maximum includes the hint of a shoulder at approximately  $10^{\circ}\text{C}$ . High  $(1/n)$  is visible at the upper temperatures of region II, the implied transition being therefore designated IIa. The existence of transition II is dubious; a small  $(1/P^2)$  minimum occurs in the vicinity of  $-50^{\circ}\text{C}$ , where the slightest hint of a  $(1/n)$  shoulder can be detected. The absence of a large transition within region IV is confirmed by the horizontality of the  $(1/P^2)$  vs. T graph.

The main characteristics of the best thermogram obtained in 1973 for ATC and of the thermogram illustrated in Figure 6 for AC(2.5) are summarized in Table 11. Transition region I contains a distinct  $(1/n)$  peak with an associated  $(1/P^2)$  minimum, the evidence for this transition being particularly similar to that of the  $\alpha$ -(1  $\rightarrow$  4)-linked glucan acetate esters. The position of the large shoulder within region II is invariant,

despite differences in the degree of substitution. The only hint of transition II is found in a thermogram for ATC the median temperature of the  $(1/n)$  fluctuation being quoted in Table 11 . Transition III is well defined as a large  $(1/n)$  maximum, which apparently occurs a few degrees lower for the partially substituted sample. In general, thermograms of the amylose carbanilate samples show a cumulative  $(1/n)$  increase with increase in temperature, and consequently the  $(1/n)$  amplitude within transition regions I, IIa and III decreases in that order. Within region IV,  $(1/n)$  data, frequently scattered, suggest the existence of a small transition, to be described later. The approximately horizontal  $(1/P^2)$  vs. T graph in region IV, proves that a notable transition does not take place in the vicinity of  $-190^{\circ}\text{C}$ .

Several ATC thermograms were obtained in 1972 and due to instrument malfunction some of the early runs were interrupted at approximately room temperature. Detailed experimental conditions were much more variable in 1972 and differed from those of later runs. In 1973, the compensating heater was used routinely to minimise the temperature differential across the sample at sub-ambient temperatures. In 1972, temperatures of  $-190^{\circ}\text{C}$  were not always achieved on cooling, and usually, the subsequent warming rate was slower than in 1973 runs. As described for ATA, these other differences in run conditions affect the shape and location of transitions I, II and III, key variables probably being the temperature differentials within the sample chamber. In amylose acetate and carbanilate thermograms obtained in 1973,

evidence for transition I is provided by the significant  $(1/n)$  maximum and concurrent  $(1/P^2)$  shallow minimum; normally, the curved region for both parameters is broad and extends over much of region I, but differences in shape and width have occasionally been observed. This description is at variance with the appearance of the earlier thermograms, especially in the vicinity of region I, where the transition is identified with the substantial  $(1/n)$  maximum and the related variation in  $(1/P^2)$ . Usually, the  $(1/n)$  maximum is narrower and has a lower median temperature than in 1973 thermograms. The associated  $(1/P^2)$  data frequently decrease at temperatures lower than the onset temperature of high  $(1/n)$ , the magnitude of the subsequent  $(1/P^2)$  recovery, and therefore the minimum which it defines, being inconstant. As already mentioned, the 1972 thermogram for ATA, obtained with a warming rate of less than one degree per minute, showed transitions I, II and IIa with median temperatures approximately 15 degrees lower than the values given in row one of Table 11. Except for carbanilate derivatives, ATr(1.0) is the only other sample to be studied in 1972 with a slower warming rate; in the resulting thermogram, IIa occurs about 10 degrees lower than indicated by the analogous 1973 tracing in Figure 5. Transition IIa is presumably masked by transition I in two early ATC thermograms, the remaining data suggesting the existence of a shoulder in the vicinity of  $-20^{\circ}\text{C}$ . It is therefore evident that for the most part, the earlier runs, with slower rates of warming, display transitions I, II and IIa at lower temperatures. This summary of the main differences

between thermograms obtained in 1972 and 1973 is completed with a description of the effect on region III data of both the sub-ambient warming rate and the run onset temperature. Two of the amylose carbanilate composites were cooled to  $-175^{\circ}\text{C}$  and their thermograms showed transition III at temperatures similar to and slightly higher than the median temperature in Table 11, derived from more recent data. This is in agreement with the increase in transition temperature already noticed in region III for ATr(1.0) and ATA runs with higher onset temperatures. The earliest ATC data, obtained after a minimum temperature of  $-125^{\circ}\text{C}$ , suggests that the rate of warming may nevertheless be a pertinent variable within region III; transition I shows a large depression in temperature of at least 20 degrees, a comparable transition temperature decrease being implied for the incompletely-defined (1/n) maximum within region III.

The thermograms for GTC and GTC(gr) samples reveal no obvious correlation between secondary transition temperature and the proportion of grafted-ATC in the sample structure. Therefore, the principal transition temperatures for three of these derivatives are summarized in Table 11 and any divergence of the 1972 data for GTC(gr  $8 \times 10^6$ ) will be reported below. Transition I is clearly perceptible as a (1/n) maximum whose shape and median temperature varies with sample, necessitating brackets in column a. Both thermograms for the samples without, and with the greatest proportion of grafted-ATC, contain signs of a shoulder at approximately  $10^{\circ}\text{C}$ . The latter sample has, for 1973 data, an unusually narrow maximum with a median temperature (and width)

10 degrees lower than the average(s) quoted in Table 11 , the associated  $(1/P^2)$  minimum being clearly outlined from  $0^\circ$  to  $30^\circ\text{C}$ . As shown in Figure 6, the remaining 1973 thermograms display shallow  $(1/P^2)$  minima of similar breadth; the GTC minimum does not span the related highly damped region in the usual way, but appears to be displaced to slightly lower temperatures. Within region I, the  $(1/n)$  vs. T and  $(1/P^2)$  vs. T graphs of GTC(gr  $8 \times 10^6$ ) are similar to those of other early thermograms, the median temperature being depressed by approximately 15 degrees as for 1972, ATA data. For GTC ( $5 \times 10^6$ ) and GTC(gr  $100 \times 10^6$ ) region IIa contains a small  $(1/n)$  maximum in the vicinity of  $-20^\circ\text{C}$  and an approximately horizontal  $(1/P^2)$  vs. T trace. In the traced GTC(gr  $25 \times 10^6$ ) thermogram, transition IIa is poorly defined by the  $(1/n)$  data between  $-25^\circ$  and  $5^\circ\text{C}$ , and over this region a very slight decrease in  $(1/P^2)$  is implied. A reduction in  $(1/P^2)$  within  $-30^\circ$  and  $-10^\circ\text{C}$  is the clearest evidence of transition IIa in the 1972 thermogram. Transition II is indicated by a small  $(1/n)$  maximum in the thermograms for GTC ( $5 \times 10^6$ ) and GTC(gr  $100 \times 10^6$ ), their average median temperature being quoted in Table 11 . The observed similarity of these thermograms within region II demonstrates the effect of constancy of transitions II and IIa despite a change in the proportion of  $\alpha$ - $(1 \rightarrow 6)$  branch points within each sample. Transition II is not clearly perceptible in the illustrated GTC(gr  $25 \times 10^6$ ) data; when this ununiform transition is visible, the height of associated  $(1/n)$  is less than that indicating transition IIa. As with the early ATC data, the

1972 GTC(gr  $8 \times 10^6$ ) thermogram hints at transition II within the approximate region of  $-80^\circ$  to  $-50^\circ\text{C}$ . In general, 1972 and 1973 thermograms for samples with varying degrees of backbone branching, contain small and irregular  $(1/n)$  changes in region II, which result in differences in transition visibility and temperature. Within region III, the resemblance of the thermograms for GTC ( $5 \times 10^6$ ) and GTC(gr  $100 \times 10^6$ ) persists as does the exceptional behaviour of the grafted sample of intermediate molecular weight whose 1973 thermogram, shown in Figure 6, displays a large  $(1/n)$  maximum and an associated reduction in  $(1/P^2)$ . Transition III is least conspicuous in the sketched GTC thermogram;  $(1/n)$  vs. T graphs of the two, at least partial, GTC samples with extreme molecular weights reveal a shoulder approximately centred on  $-96^\circ\text{C}$ : the  $(1/n)$  maximum in the GTC(gr  $25 \times 10^6$ ) thermogram has a median temperature of about  $-101^\circ\text{C}$ , as does the peak in the 1972 thermogram of GTC(gr  $8 \times 10^6$ ). As in two of the early ATC runs, the latter sample was only cooled to  $-175^\circ\text{C}$ , and the combination of several run condition differences, such as a slightly slower warming rate and higher run onset temperature than usual in 1973 runs, has resulted in the lack of any significant discrepancy between the 1972 and 1973 temperature data for transition III. The horizontal  $(1/n)$  vs. T and  $(1/P^2)$  vs. T graphs within region IV, illustrated in Figure 6, by the GTC(gr  $25 \times 10^6$ ) thermogram do not signify a transition. As shown in the GTC thermogram, initial  $(1/n)$  scatter in the other 1973 thermograms is a little confusing, but the implied absence of transition IV is confirmed by the constancy of the  $(1/P^2)$  data.

There are eight CTC thermograms extending over sub-ambient temperatures and four of these were obtained in 1972. Two of the 1973 thermograms are illustrated in Figure 7 and transition temperatures averaged in the last row of Table 11 are normally derived from the more recent data. Transition I is evident as a significant maximum in the  $(1/n)$  vs.  $T$  graphs of 1973; for CTC samples of molecular weight  $(80 \times 10^3)$ ,  $(59.7 \times 10^3)$  and  $(8.2 \times 10^3)$ , the average median temperature is  $14.5^\circ\text{C}$ . It is reasonable to assume that when a sample has only been cooled to about  $-40^\circ\text{C}$ , the temperature differentials within the sample chamber will not be identical to those that usually exist after cooling to  $-190^\circ\text{C}$ . For the CTC  $(15.1 \times 10^3)$  composite, surveyed during a TBA run which began at about  $-40^\circ\text{C}$ , the median temperature for transition I is approximately 10 degrees lower than the average value in Table 11. In all four thermograms, transition region I displays an effective modulus minimum of varying breadth, the temperature at its nadir being approximately coincident with the median temperature for the concurrent high  $(1/n)$ . The general differences between the 1972 and 1973 CTC data within region I, are as described in the above summary of this effect. The displacement of the narrower  $(1/n)$  maximum to lower temperatures is illustrated in Figure 7 by the CTC  $(12.8 \times 10^3)$  thermogram, the two  $(1/n)$  vs.  $T$  traces resulting from the use of two sets of boundary amplitudes for evaluation of  $n$  from the damped oscillations.

Within region II,  $(1/n)$  is generally scattered and inconsistent and therefore, with the lack of any obvious discrepancies between the 1972 and 1973 thermograms, the clearest features of all eight thermograms have been summarized.

The  $(1/n)$  data illustrated in Figure 7 for CTC ( $59.7 \times 10^3$ ) and CTC ( $80 \times 10^3$ ), indicates the existence of transition II within the  $-60^\circ$  to  $-30^\circ\text{C}$  region; their average temperature for the indistinct transition can be found in Table 11. As a consequence of the insubstantiality of the CTC ( $80 \times 10^3$ ) evidence combined with the variations in visibility of transition II already described for carbanilates of differing backbone structures, the absence of transition II from the 1972 thermograms for CTC ( $80 \times 10^3$ ) and CTC ( $410 \times 10^3$ ) is not too surprising. In addition, the illustrated thermograms for the higher molecular weight samples display a small maximum within region IIa, approximately equivalent to transition II in  $(1/n)$  amplitude. For CTC ( $80 \times 10^3$ ) and CTC ( $410 \times 10^3$ ), thermograms obtained in 1972 show one distinct transition within region II, approximately centred on  $-16^\circ\text{C}$ , the average median temperature derived for transition IIa from the 1973 thermograms. As with the other early carbanilate data, these thermograms contain the suggestion of a small  $(1/n)$  change within  $-70^\circ$  and  $-50^\circ\text{C}$ ; the identification of two transitions within region II in the scattered 1973  $(1/n)$  vs.  $T$  graphs of CTC ( $80 \times 10^3$ ) and CTC ( $59.7 \times 10^3$ ) is therefore justified. Thermograms obtained for CTC samples of lower molecular weight differ visually from those described above. In the four thermograms obtained for CTC samples of greater molecular size, the only large  $(1/P^2)$  variation is associated with transition I: CTC ( $8.2 \times 10^3$ ), CTC ( $12.8 \times 10^3$ ) and CTC ( $15.1 \times 10^3$ ) thermograms display two  $(1/P^2)$  minima within regions I and II, the  $(1/P^2)$  variation being as large as the  $T_g$ -related decrease. The thermogram

obtained in 1973 by warming the CTC ( $15.1 \times 10^3$ ) composite from  $-190^\circ\text{C}$ , shows a single  $(1/n)$  maximum within region II, with a median temperature of  $-24^\circ\text{C}$ ; the initial  $(1/P^2)$  minimum, found within  $-50^\circ$  and  $-10^\circ\text{C}$ , is therefore clearly associated with transition IIa. The additional  $(1/P^2)$  minimum occurring from about  $-60^\circ$  to  $-25^\circ\text{C}$  and  $-45^\circ$  to  $0^\circ\text{C}$  in CTC ( $12.8 \times 10^3$ ) and CTC ( $8.2 \times 10^3$ ) thermograms respectively, are their clearest evidence of a transition within region II. The 1973  $(1/n)$  data for the latter sample is very scattered; the existence of IIa is implied in the vicinity of  $-10^\circ\text{C}$ , but this median temperature is too unreliable to be averaged for Table 11. As in most 1972 thermograms, CTC ( $12.8 \times 10^3$ )  $(1/n)$  evidence for transition I is depressed in temperature and, as shown in Figure 7, the associated  $(1/P^2)$  variation extends to  $-20^\circ\text{C}$ .  $(1/n)$  vs. T graphs have not provided sufficient information to indicate which of transitions II and IIa is to be associated with the large additional  $(1/P^2)$  minimum. The CTC ( $3.1 \times 10^3$ )  $(1/P^2)$  vs. T tracing in Figure 7 contains a single variation which fits the general description of 1972  $(1/P^2)$  data related to transition I; transition IIa has been identified as a  $(1/n)$  shoulder centred on  $-26^\circ\text{C}$ . The median temperature quoted in Table 11 has been averaged from this value for CTC ( $3.1 \times 10^3$ ) and from values derived from 1973 thermograms of CTC ( $15.1 \times 10^3$ ), CTC ( $59.7 \times 10^3$ ) and CTC ( $80 \times 10^3$ ). Transition IIa occurs at lower temperatures for the lower molecular weight samples, but this trend, based on few thermograms, may be related to the varying visibility of transition II, itself apparently more distinct for higher molecular weight samples.

All eight thermograms show substantial (1/n) within region III, a shoulder being more frequently outlined for the lower molecular weight samples in particular. As there is no obvious correlation between median temperature and either the sample molecular weight or the date of the run, the average of all eight median temperatures has been quoted. Differences in the shape of transition III may be partially responsible for the divergence of these temperatures, which necessitated brackets in column a; the maximum difference in transition temperature, of 25 degrees, occurs between CTC ( $59.7 \times 10^3$ ) and CTC ( $80 \times 10^3$ ), the relevant thermograms being illustrated in Figure 7. With cooling to a minimum temperature of  $-125^\circ\text{C}$ , a CTC ( $80 \times 10^3$ ) composite showed greatest (1/n) within region III, in the vicinity of  $-110^\circ\text{C}$ . Although within the range of temperatures derived from 1973 thermograms for samples of identical and similar molecular weight, this median temperature is lower than the average value, and therefore does not contradict the effect described above for ATC data after limiting cooling. The constant and approximately horizontal ( $1/P^2$ ) vs. T gradients within region IV provide the clearest evidence for the absence of this large transition in the CTC thermograms.

In addition to the main transitions summarized in Table 11, there are several small (1/n) variations, which indicate the possible existence of less obvious transitions. None of the TBA transition evidence has been very reproducible and inevitably the smaller the (1/n) shoulders or maxima the less reliable are the temperature parameters of the implied

All eight thermograms show substantial  $(1/n)$  within region III, a shoulder being more frequently outlined for the lower molecular weight samples in particular. As there is no obvious correlation between median temperature and either the sample molecular weight or the date of the run, the average of all eight median temperatures has been quoted. Differences in the shape of transition III may be partially responsible for the divergence of these temperatures, which necessitated brackets in column a; the maximum difference in transition temperature, of 25 degrees, occurs between CTC ( $59.7 \times 10^3$ ) and CTC ( $80 \times 10^3$ ), the relevant thermograms being illustrated in Figure 7. With cooling to a minimum temperature of  $-125^\circ\text{C}$ , a CTC ( $80 \times 10^3$ ) composite showed greatest  $(1/n)$  within region III, in the vicinity of  $-110^\circ\text{C}$ . Although within the range of temperatures derived from 1973 thermograms for samples of identical and similar molecular weight, this median temperature is lower than the average value, and therefore does not contradict the effect described above for ATC data after limiting cooling. The constant and approximately horizontal  $(1/P^2)$  vs. T gradients within region IV provide the clearest evidence for the absence of this large transition in the CTC thermograms.

In addition to the main transitions summarized in Table 11, there are several small  $(1/n)$  variations, which indicate the possible existence of less obvious transitions. None of the TBA transition evidence has been very reproducible and inevitably the smaller the  $(1/n)$  shoulders or maxima the less reliable are the temperature parameters of the implied

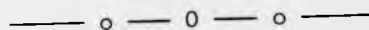
transitions. The transitions being of dubious significance, minimal details are given below. There is a varying temperature distribution along the braid; at temperatures above 0°C the top of the braid is, on average, cooler than the bottom. In addition, the programmed heating of the sample chamber above ambient temperatures is not uniform, cycling of the chamber temperature being obvious by 100°C. Within 50 degrees of T<sub>g</sub>, (1/n) fluctuations have therefore been ignored, as they may merely be due to the combined effect of uneven warming of the braid and the onset of high (1/n). Thermograms for the two esters which contain a trityl group and have the highest T<sub>g</sub>'s, show signs of a transition within the 110° to 170°C region. The analogous region for the carbanilates, about 110° to 145°C, may also contain a small transition which is most obvious in some of the thermograms for higher molecular weight CTC samples. Polysaccharide samples, with the exception of the propionate, butyrate and valerate esters of α-(1 → 4)-linked glucans, have T<sub>g</sub>'s above 150°C and, in general, their thermograms display at least one small transition between transition I and about 110°C, the related (1/n) differing with initial oscillation direction, run and sample. Evidence for this transition is more substantial in 1972 thermograms, where a shallow, characteristically broad (1/n) maximum is apparent. It was noted previously that differences in run conditions affect the magnitude and shape of (1/n) variations; the higher temperature and broader span of transition I in 1973 data may therefore be masking this less reproducible (1/n) feature. A few thermograms indicate a smooth (1/n) increase from approximately 30°C to the apex of the T<sub>g</sub> peak, whereas those of some α-(1 → 4)-linked) glucan carbanilate derivatives and

A(1.0), A(2.0) suggest a second process above  $80^{\circ}\text{C}$ . Some 1972 thermograms obtained by heating the composite from room temperature, show a  $(1/P^2)$  minimum within  $20^{\circ}$  and  $65^{\circ}\text{C}$ ; this phenomenon was observed for one CTC composite, of molecular weight  $(95.2 \times 10^3)$ , one ATC composite and several CTA composites. The random occurrence of this effect in 1972 thermograms which only begin at about  $20^{\circ}\text{C}$ , suggest that it may be spurious, although,  $(1/n)$  evidence for a transition in this region is also more obvious in early data. This  $(1/P^2)$  minimum occurs at higher temperatures than the minimum associated with transition I. In general, many of the thermograms for samples listed in Table 11 contain small  $(1/n)$  fluctuations within the main secondary transition regions. As mentioned above, in the vicinity of  $10^{\circ}\text{C}$ , some 1973 thermograms display an irregularity in the  $(1/n)$  evidence for transition I. Within  $-190^{\circ}$  and  $-150^{\circ}\text{C}$  another barely significant  $(1/n)$  variation is often apparent, the lack of an associated change in  $(1/P^2)$  confirming the absence of a main secondary transition. The presence of transition IV in butyrate and valerate thermograms masks the  $(1/n)$  evidence of any smaller transition. Not all thermograms reveal the small  $(1/n)$  variation within region IV and hence nothing may be deduced from its absence for a sample such as A(1.0), A(2.0).

Some thermograms show interesting  $(1/n)$  or  $(1/P^2)$  patterns at temperatures above  $T_g$ . With increase in temperature above  $85^{\circ}\text{C}$ , the ATV composite experiences a concurrent  $(1/n)$  change until the  $(1/n)$  amplitude at  $T_g$  ( $62^{\circ}\text{C}$ ) is matched. In addition, scattered data in both GTV (8-L-D) and only one of the ApTV thermograms indicates fairly high

( $1/n$ ) above  $T_g$ . As illustrated in Figure 6, amylose and glycogen carbanilate composites, in general experience greater ( $1/n$ ) at temperatures above  $230^\circ\text{C}$  approximately. CTC data does not exist at temperatures above  $230^\circ\text{C}$ , but thermograms for samples with lower  $T_g$ 's do not suggest further ( $1/n$ ) increases. The AC(2.5) tracing also displays a large, rapid decrease in ( $1/P^2$ ) from  $230^\circ\text{C}$ , with a subsequent increase in the vicinity of  $260^\circ\text{C}$ . The thermogram for GTC( $\text{gr } 100 \times 10^6$ ) contains the large, steep ( $1/P^2$ ) reduction from approximately  $230^\circ\text{C}$ , but it is not evident in the GTC ( $5 \times 10^6$ ) thermogram. GTC ( $5 \times 10^6$ ) ( $1/P^2$ ) data increases with heating above  $260^\circ\text{C}$ , as illustrated in the Figure 6 tracing of the only GTC thermogram to extend to these temperatures.

Evaluation of the oscillation frequency of poly(di-n-alkylitaconate) composites at transitions B and (4) revealed an apparent correlation between frequency and both composite concentration and transition temperature. Transition region (4) corresponds to region IV for the polysaccharide esters, but the transition indicated within this region by n-butyrate and n-valerate derivatives occurs below the run onset temperature. It is therefore impossible to gauge the effect of the difference in backbone structure on the frequency of composite oscillation at the median temperature of this highly damped transition. Frequency data for the most significant poly(di-n-alkylitaconate) transitions yielded no information in addition to that provided by ( $1/P^2$ ) behaviour and therefore oscillation frequencies during smaller transitions have not been evaluated.



The iterative procedure required to summarize these TBA results, necessitated identification of the features and trends to be reported, before all the details could be assembled from the raw thermogram data. In particular, effort was directed at optimizing the equivalence of the secondary transition regions for all esters studied; the resulting correlation between the regions defined in Tables 8 and 11, and any obvious similarity in their transition features are described below.

Differences in polymer structure can result in transition temperature variation, and therefore the transition regions defined in Table 8 for the poly(di-n-alkylitaconates) do not correspond exactly to those of the polysaccharide esters. Remembering that the temperature limits for polysaccharide transition regions in Table 11 are variable by as much as  $\pm 10$  degrees, the approximate equivalence of the main secondary transition regions is indicated in this small Table.

Temperature Limits of the Secondary Transition Regions. (°C)	Nomenclature in Table 8	Nomenclature of Equivalent Regions in Table 11
$0 < T < 40$	(1)	I
$-30 < T < +5$	(2)	IIa
$-160 < T < -30$	(3)	II (when IIa occurs at $T > -30^{\circ}\text{C}$ ) III
Run onset temperature $< T < -160$	(4)	IV

Region (3) of Table 8 effectively corresponds to the combined span of regions III, and of II below  $-30^{\circ}\text{C}$ . In Table 11, the lower temperature limit of region II and the upper limit of region III is either  $-100^{\circ}\text{C}$  or  $-75^{\circ}\text{C}$ ; when the division between regions II and III occurs at  $-100^{\circ}\text{C}$ , transition B and transitions at higher temperatures in region (3) effectively occur within region II.

For all polysaccharide derivatives, except the n-butyrate and n-valerate esters, region I normally contains a broad  $(1/n)$  maximum, of small magnitude relative to the  $(1/n)$  amplitude at  $T_g$ , and with a frequently-associated  $(1/P^2)$  minimum. For PDMI and PDEI the shape of the  $(1/n)$  maximum or shoulder within region (1) is not distinct or consistent and comparison with  $(1/n)$  data within the corresponding region for the polysaccharide esters merely reveals that their transitions do not look too dissimilar.

For the polysaccharide derivatives, transition region II extends over a wide temperature range, necessitated by the difficulty experienced in identifying the  $(1/n)$  maxima or shoulders attributed to two transitions of varying visibility. The relative amplitude of  $(1/n)$  associated with the transition (II) at lower temperatures is extremely variable. Transition II is most pronounced in thermograms for the carboxylic acid esters of  $\alpha$ -(1 + 4) polyglucans, relatively high  $(1/n)$  being most frequently displayed within the region by amylopectin and amylopectin  $\beta$ -L-D derivatives. Nevertheless, within region II oscillations are usually more highly damped above  $-30^{\circ}\text{C}$ , transition IIa being dominant in many carbanilate thermograms and those of ATr(1.0) and ATT. Because of the large differences in  $(1/n)$  evidence for transition II, it is impossible to estimate the magnitude of the  $(1/n)$  change caused by transition IIa. The median temperatures for transition IIa, given in Table 11, are similar to those of transition (2) in Table 8. As indicated in Table 8, transition (2) [and (1)] is not very reproducible in  $(1/n)$  magnitude, shape or temperature for series members PDMI to PDBI inclusive. Therefore, although absolute confirmation is not provided, the  $(1/n)$  data does not preclude the possible identification of transition (2) with IIa;  $(1/P^2)$  minima have been attributed to this transition for samples with either type of backbone structure. Between  $-100^{\circ}$  and  $+5^{\circ}\text{C}$ , transition region II for some polysaccharide esters, the PDMI and PDEI  $(1/n)$  vs. T graphs visually resemble those of the polysaccharide esters. In particular, for PDMI the transition within region (3), with median temperature  $-66^{\circ}\text{C}$ ,

shows large differences in form and magnitude, which are similar to those observed for transition II; for PDEI, the median temperature of  $-54^{\circ}\text{C}$  approximates to many of the temperatures quoted for this transition in Table 11.

Transition region (3) of the poly(di-n-alkylitaconates) spans region III, as well as much of region II, of the polysaccharide esters. In thermograms for all polysaccharide esters except the n-butyrate and n-valerate derivatives, transition III was identified as the main secondary transition at the lowest temperature: comparison with (1/n) evidence in the thermograms of acetate and propionate esters reveals that this transition is relatively small for n-butyrate and n-valerate esters of the  $\alpha$ -(1  $\rightarrow$  4) polyglucans, the only polysaccharide samples to demonstrate transition IV. For esters other than the carboxylic acid derivatives of  $\alpha$ -(1  $\rightarrow$  4)-linked glucans, substantial (1/n) associated with transition III occurs at higher temperatures and the form and relative height of its outline is less consistent. The esters for which transition region III occurs between  $-130^{\circ}$  and  $-75^{\circ}\text{C}$ , have median temperatures within 10 degrees of  $-106^{\circ}\text{C}$ , the temperature quoted in Table 8 for the second (1/n) change apparent within region (3) in a few of the PDMI thermograms.

A large (1/n) maximum with an associated reduction in  $(1/P^2)$  occurs in transition region (4) for all poly(di-n-alkylitaconates) except PDMI and PDEI; similar (1/n) and  $(1/P^2)$  patterns for only the n-butyrate and n-valerate polysaccharide esters indicate the existence, below  $-190^{\circ}\text{C}$ , of the analogous transition. For poly(di-n-hexylitaconate) and higher series members, region (4) contains the only secondary transition that can be correlated with those of the polysaccharide esters;

transitions A and B mask any smaller variations in the  $(1/n)$  vs. T graphs of these poly(di-n-alkylitaconates).

For higher poly(di-n-alkylitaconates), the maximum  $(1/n)$  region was complicated by both the possible existence of transition A and by high  $(1/n)$  that persisted to temperatures above the postulated  $T_g$ . In the remaining poly(di-n-alkylitaconate thermograms and in those of all the polysaccharide esters, identification of  $T_g$  from the position of the largest  $(1/n)$  peak was relatively straightforward, although, as described above, the detailed shape, magnitude and relative location of the associated  $(1/P^2)$  decrease vary with sample structure and even with thermogram.

Section C: Differential Scanning Calorimeter Data

Because instrument time was limited, available Differential Scanning Calorimeter (DSC) thermograms are inadequate in quantity and quality. In general, thermograms were not obtained for two samples of the same polymer and therefore the reproducibility of apparent transitions is unknown. As it was not always possible to scan the same sample twice, or over both sub-ambient and above-ambient temperature regions, the data is also incomplete. Optimum run conditions with respect to sensitivity and stability of the baseline, were not achieved; samples, usually of mass 12 to 13 mg, were normally scanned over a wide temperature interval on one of the least sensitive of the differential power ranges. Smaller sample mass and greater instrument sensitivity could have resulted in better temperature resolution, but with greater sensitivity, it is more difficult and time-consuming to achieve a linear baseline, even over narrow temperature intervals. Baseline curvature, reported to be frequently S-shaped over the full sub-ambient temperature range, is evident in the thermograms of reference samples, composed of aluminium sample pan lids. To allow for this lack of linearity, it was necessary to estimate the average magnitude of the random gradient changes which separate approximately linear baseline portions. As these reference sample baselines are not usually parallel to the temperature axis, the angular displacements were measured instead of their tangents. From the data of three reference sample thermograms, obtained under the usual run conditions and over the full sub-ambient temperature range, it appeared that the average angle between different

gradients varied approximately directly with the sensitivity of the recorder range and approximately inversely with the sample mass. With reference sample data as the basis, these observations enabled evaluation of a critical angular displacement for a given set of experimental conditions. It was assumed that the average angle between different gradients would also vary directly with the instrument sensitivity. However, there was considerable dubiety about the method of extrapolation for differing sample masses; for samples of low mass, arithmetic extrapolation yielded a smaller critical value than the implied geometric extrapolation, but combination with the effect of the required increase in instrument sensitivity still resulted in a large estimate for the critical angular change. Due to the sparseness of reference sample data, this procedure for the evaluation of a significant angular displacement is not satisfactory; nevertheless, the criterion simplified the interpretation of these complex DSC thermograms, by enabling some of the small gradient changes to be ignored. Because none of the reference sample thermograms extend over the above-ambient temperature range, the sub-ambient significance criterion was even more arbitrarily applied to gradient changes at higher temperatures. Features at the extremes of the scanned temperature range have been ignored, because these thermogram variations could be due to slight differences in the operation of the instrument at the beginning and end of the run. Reference sample data indicates that, in general, a linear baseline is not established until 20 degrees above the temperature at which the instrument is in control

of temperature programming, and that, within this region, features such as gradient changes and endothermic peaks are not necessarily significant. For a given set of run conditions, adjustment of the "slope" control enables the constant baseline gradient to be aligned parallel to the temperature axis of the chart. As there was insufficient time to obtain either baseline gradient constancy or horizontality, interpretation of the thermograms was difficult. An iterative procedure was adopted, as for interpretation of the TBA data, to compensate for ignorance of both the actual baseline and the effect on the thermogram features of its finite and varying gradient. With identification of similar characteristics in the thermograms of related polymers scanned under similar run conditions, a new interpretation which improved their correlation often became apparent.

The DSC temperature read-out is in degrees Kelvin; the temperatures given below have been converted to degrees Celsius by subtraction of 273 degrees from the original temperatures. All quoted temperatures are those for extrapolated gradient changes, unless otherwise stated. Diagram 3 illustrates the procedure used to obtain the extrapolated onset, peak and end temperatures for a typical endothermic shift and a typical peak involving a net shift, an overall shift being characterized by the median of its onset and end temperatures. The selection of extrapolating lines is frequently rather arbitrary due to the existence of many, often apparently insignificant, gradient changes. Although the final thermogram interpretation may be

erroneous, their analysis involved considerable effort, as it was hoped that the DSC thermograms would provide transition data which confirms some of the TBA results. Correlation of the transitions revealed by the two techniques may prove impossible, but the form and temperature of DSC thermogram features may aid interpretation of the molecular processes responsible for the reported dynamic mechanical transitions. Therefore, many of the DSC thermograms have been traced and are presented in Figures 9 to 16; with the exception of Figure 12, their overall dimensions have been photographically reduced by a factor of two. Because the individual thermograms are vertically spaced along the ordinate in these Figures, only the direction of the endothermic heat flow rate is indicated. The actual thermograms were traced with continuous lines; baseline extrapolations are shown, by dashed lines, to aid identification of their intersection temperatures. Illustrated thermograms do not contain the portion within 20 degrees of the onset of temperature control. Main characteristics of both sub- and above-ambient thermograms are described below; it is feasible that, due to the inadequate basis of the gradient change significance criterion or their location at the run extremities, some noteworthy features are among those rather arbitrarily ignored. In TBA, the sample is not simply an encapsulated solid, as for the DSC, but intermingles with the glass braid; consequently the stresses inherent in the two sample forms and their effects on the data may differ. As the former technique yields effectively first run data, DSC thermograms resulting from first temperature scans are, in general,

illustrated in order to optimise any possible result correlation. Thermogram features caused by sample stress are removed by the initial scanning cycle and in the field of thermal analysis, temperature parameters from re-run thermograms are therefore considered to be more reliable. Samples were usually scanned twice in the DSC and principal features of the re-run thermograms are also described below. During sub-ambient runs, first and re-run thermograms were normally obtained with a heating rate of forty degrees per minute, after fast cooling from approximately  $20^{\circ}\text{C}$  or a maximum temperature of  $150^{\circ}\text{C}$  respectively to about  $-170^{\circ}\text{C}$ . Similarly, for above-ambient runs samples were, in general, quickly cooled to approximately  $-30^{\circ}\text{C}$  before being scanned at forty degrees per minute. Unless otherwise stated in Tables summarizing the main thermogram features, the illustrated thermograms were obtained with instrument and recorder ranges of 5 milli-calories per second (mcal/sec) and 10 mV full-scale deflection (fsd) respectively.

DIAGRAM 3

Temperature Extrapolations in DSC Thermograms

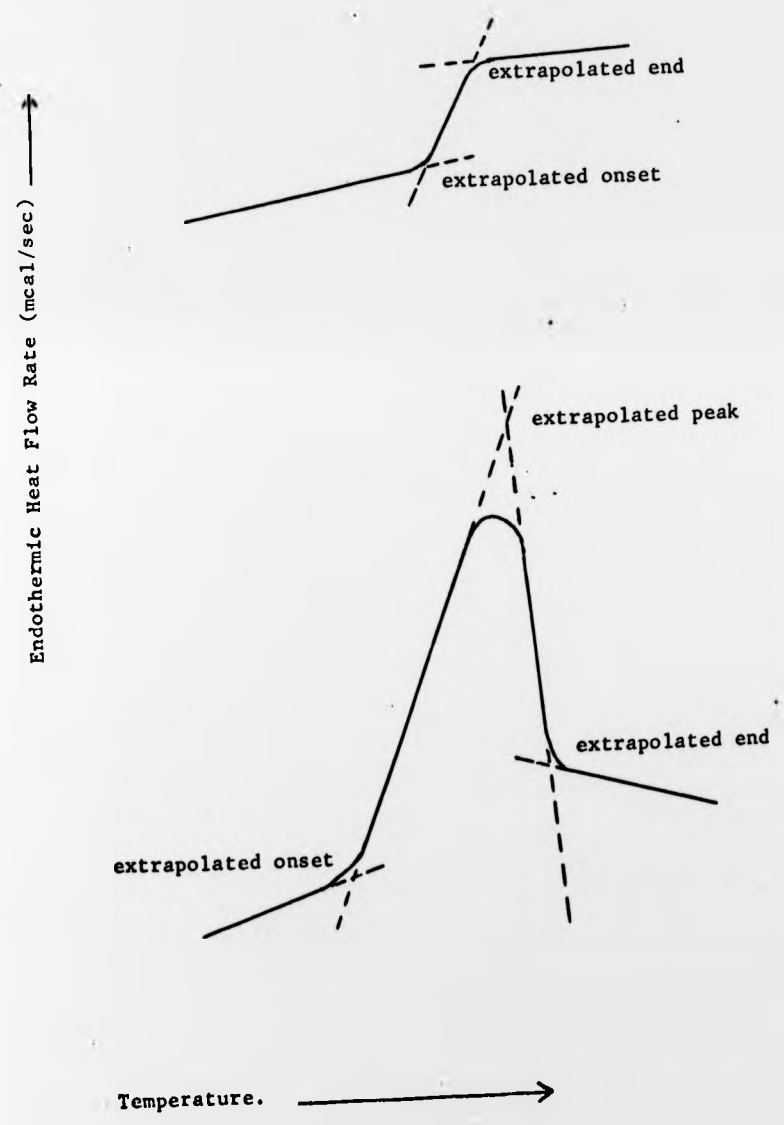


FIGURE 9

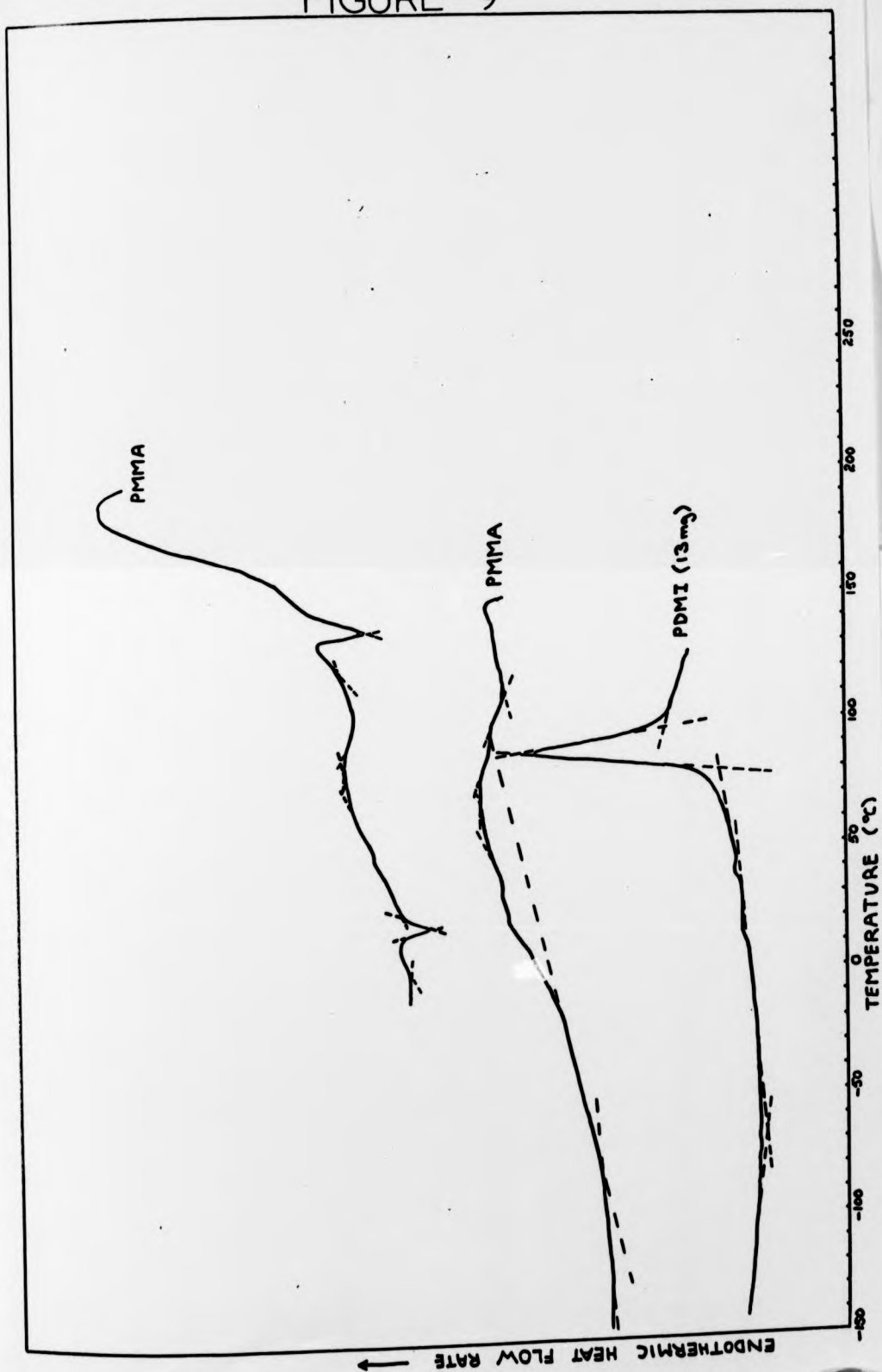


FIGURE 10

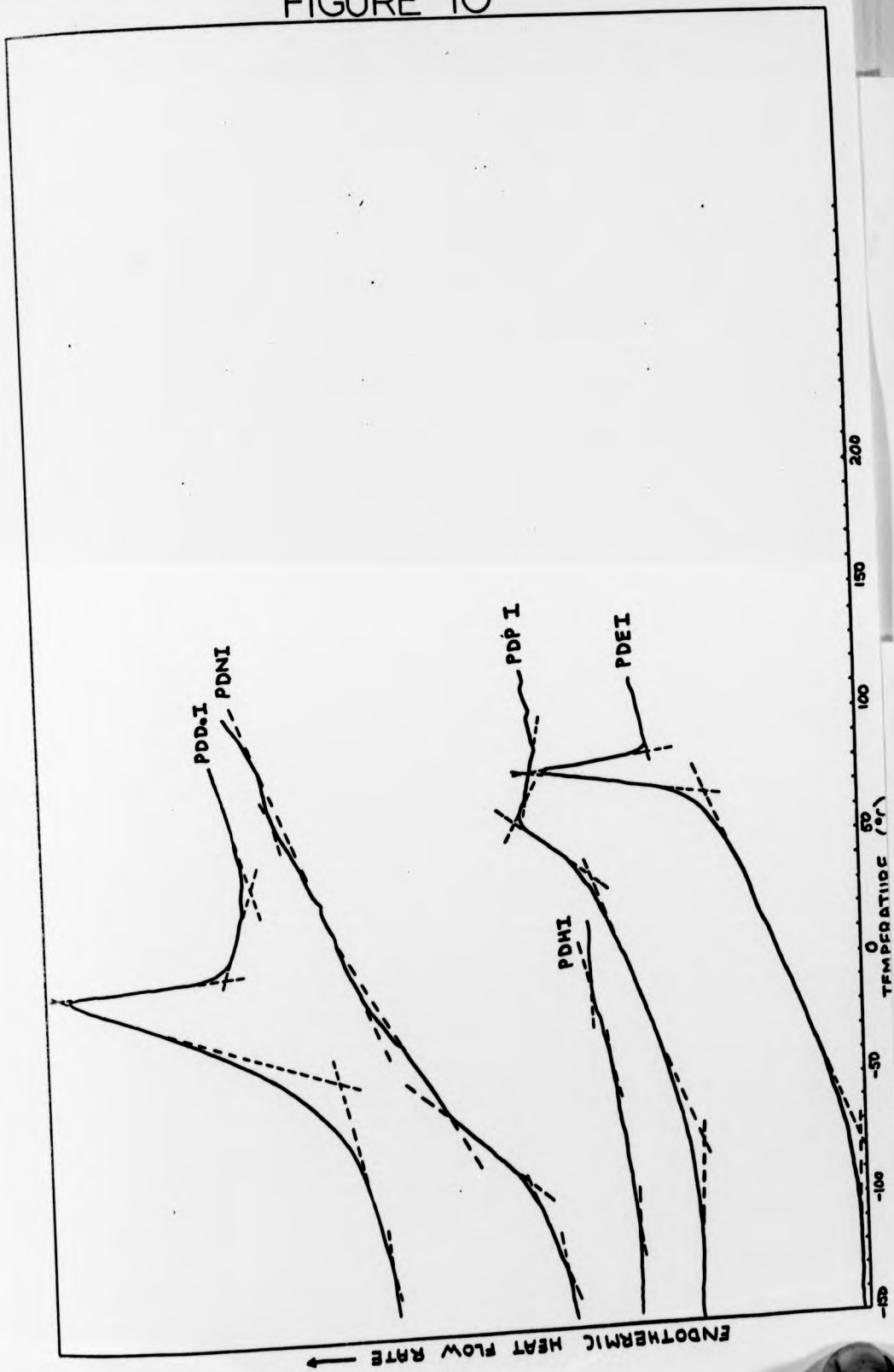


FIGURE 11

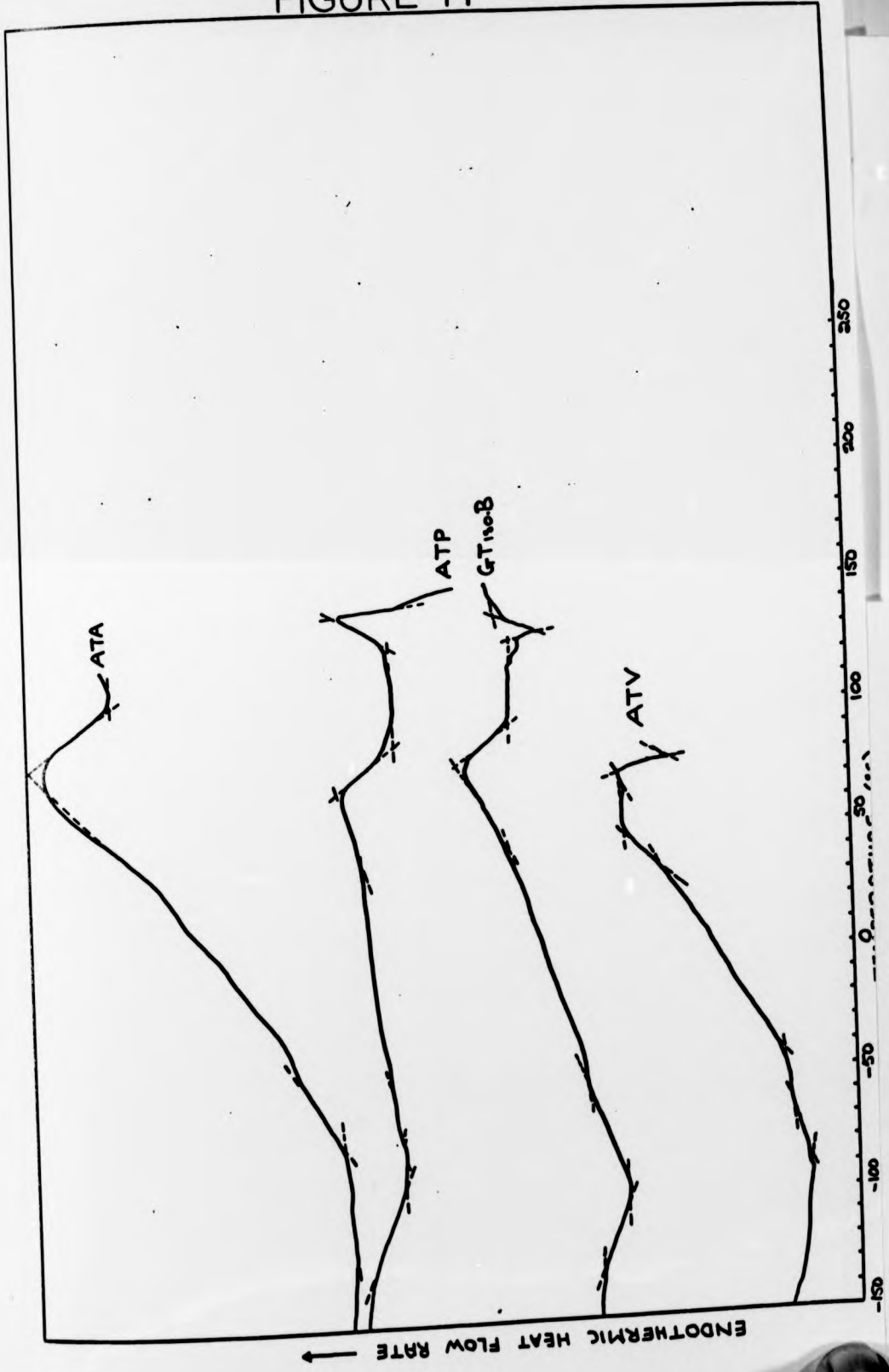


FIGURE 11

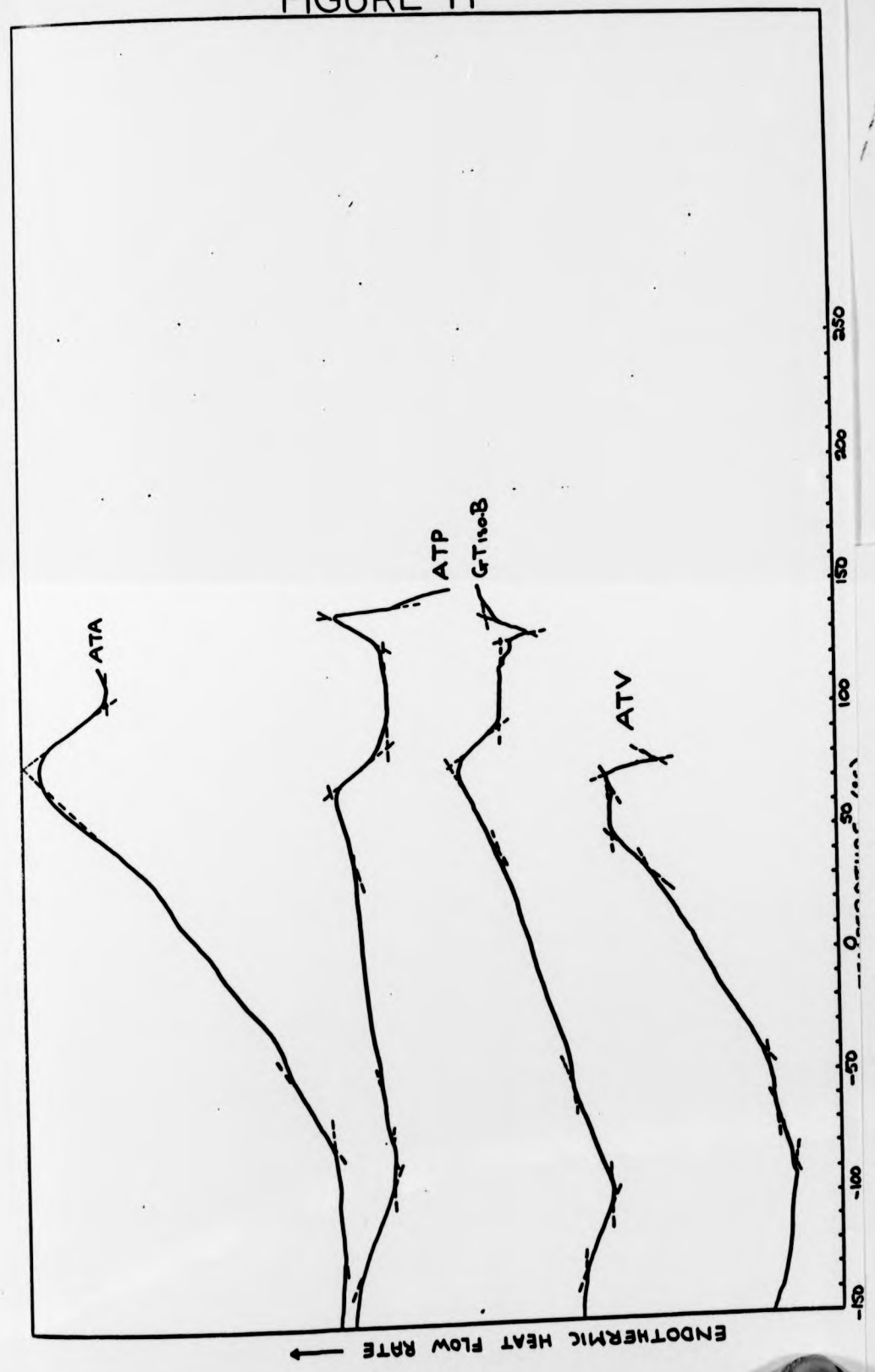


FIGURE 12

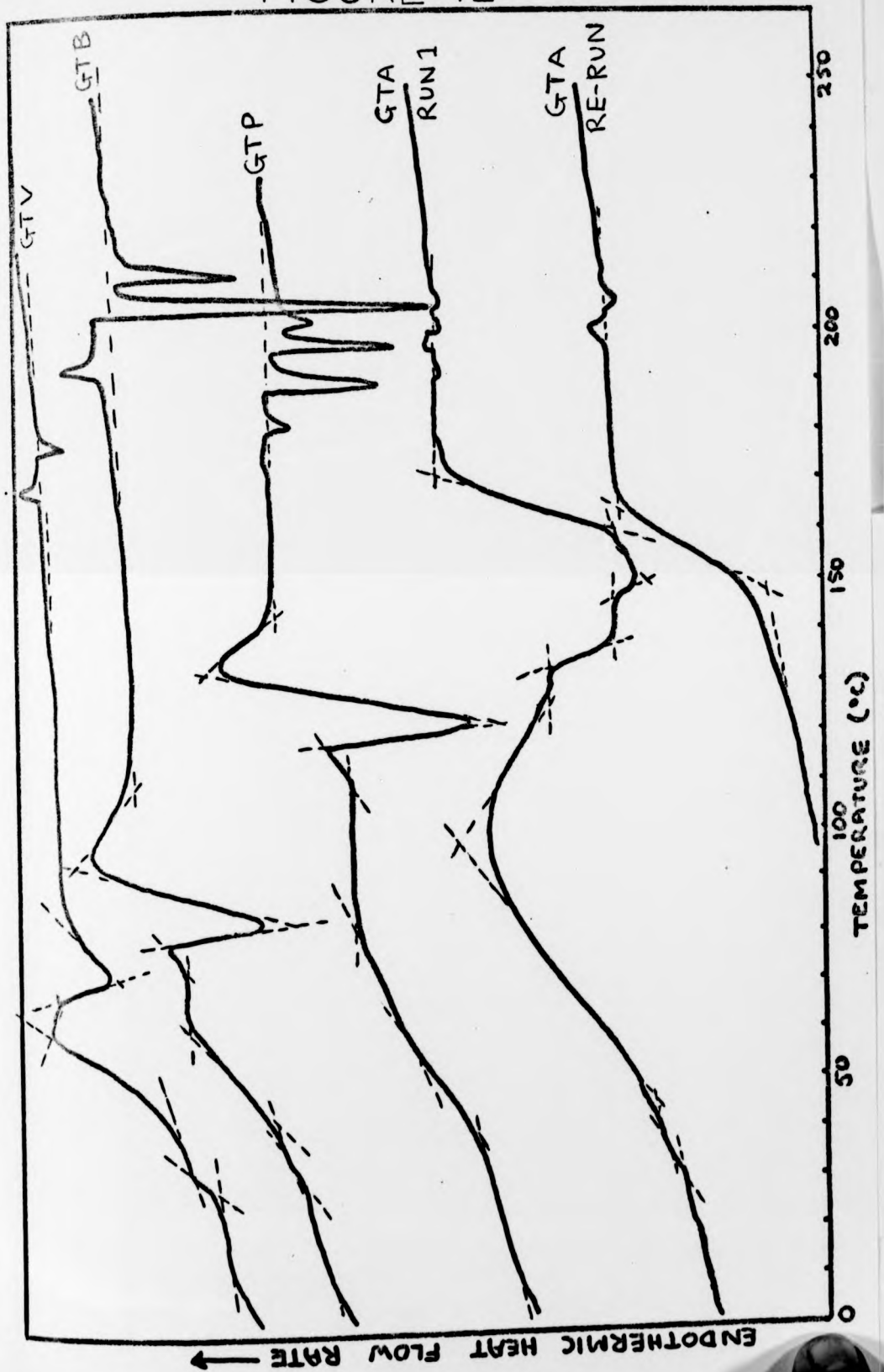


FIGURE 13

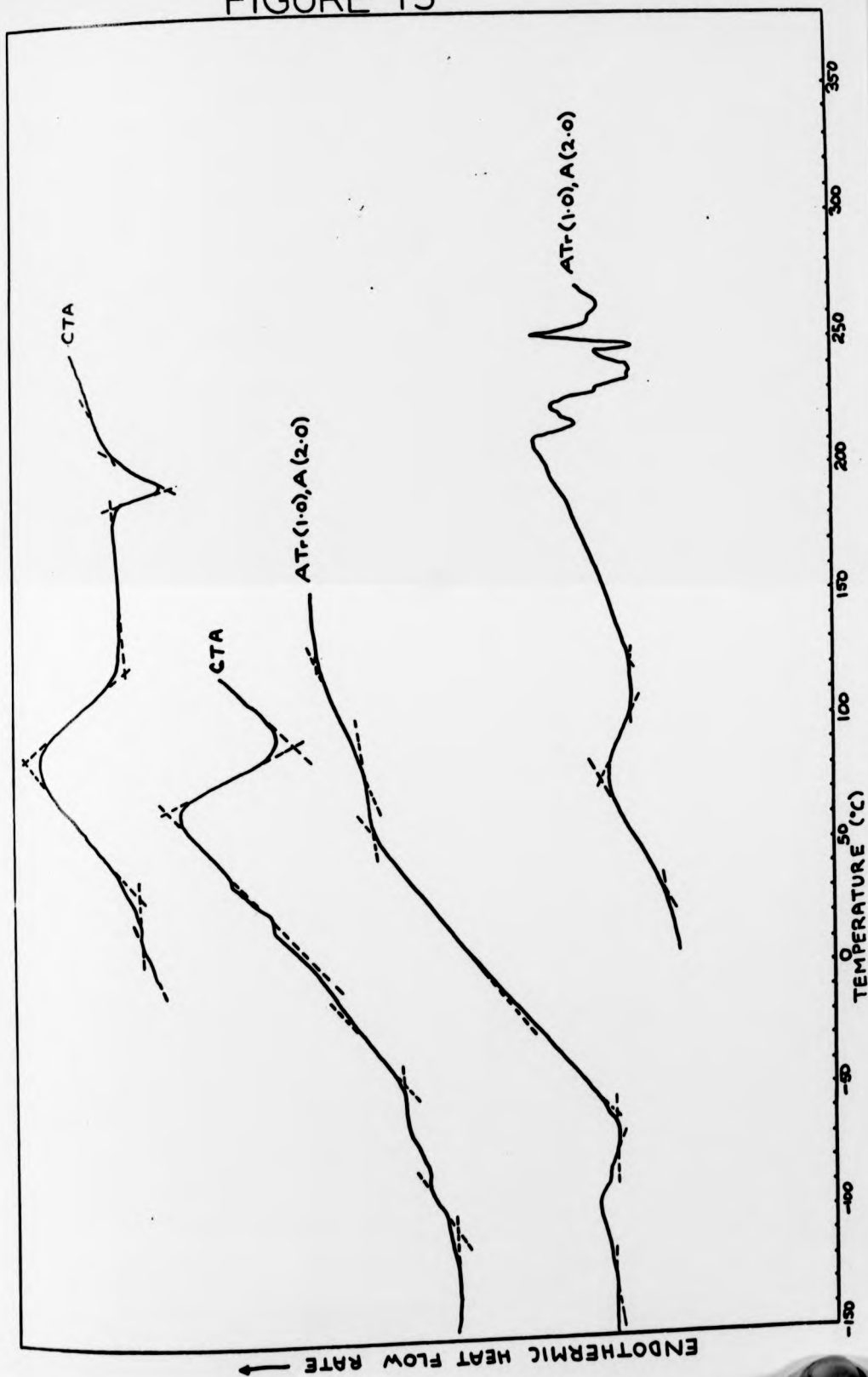


FIGURE 14

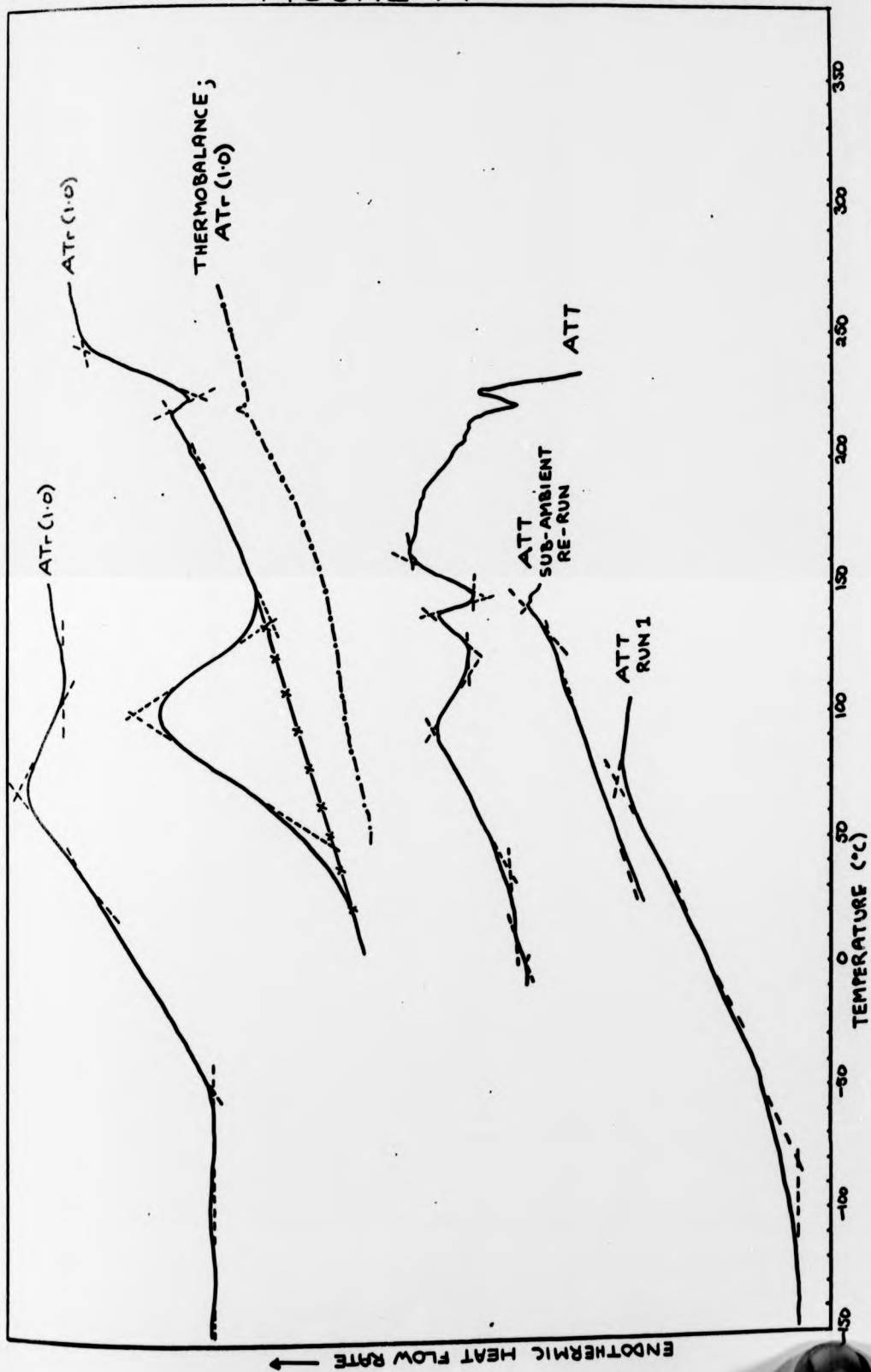


FIGURE 15

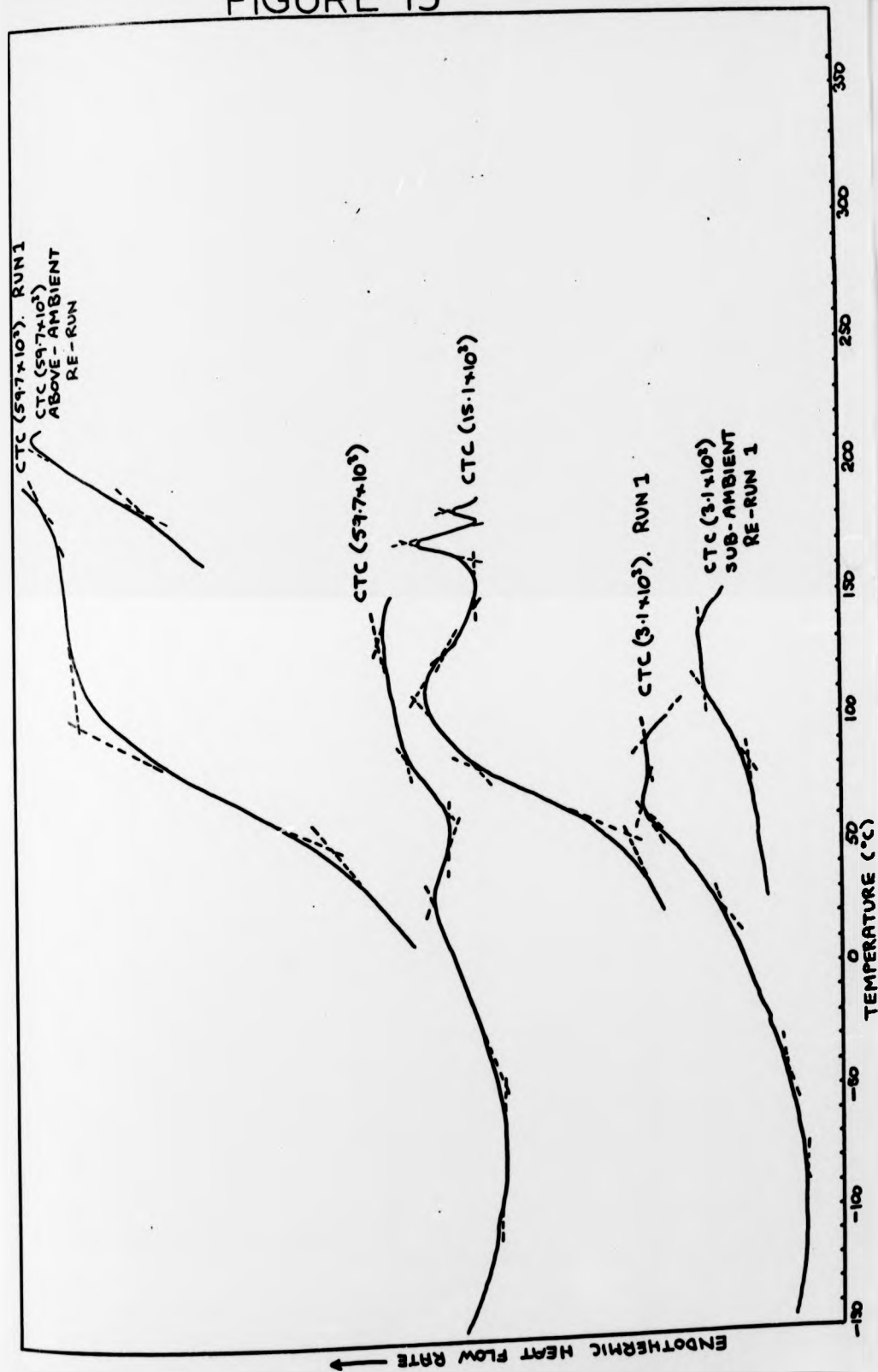


FIGURE 16

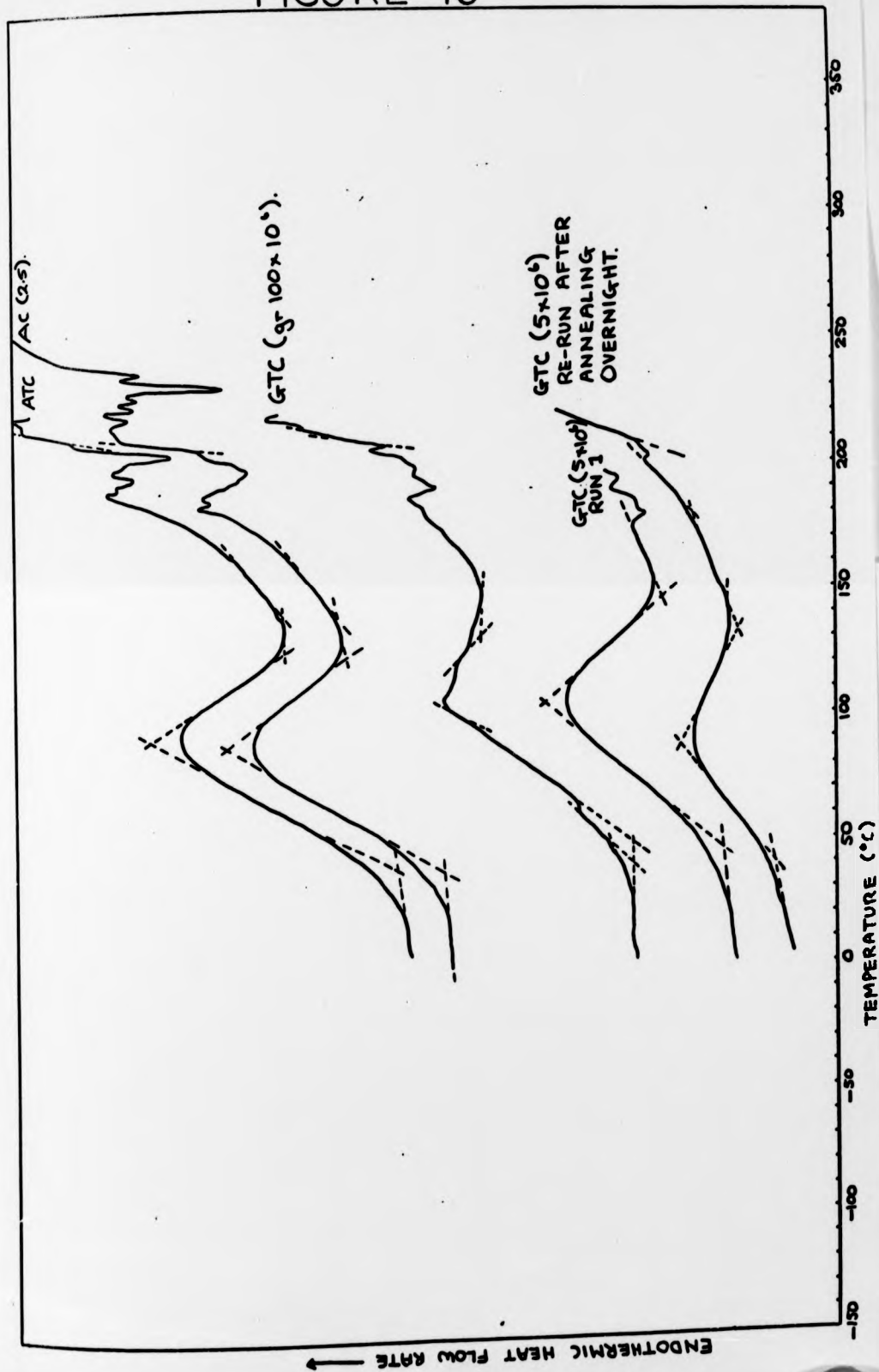


TABLE 12

Summary Table of the Main Endothermic Features of Poly(di-n-alkylitaconate) Thermograms over the Sub-ambient Temperature Region

Sample	Sample Mass (mg)	Run 1 re-run	Extrapolated Peak	Extrapolated Onset	Extrapolated End	(°C) Shift Median	Net Shift (Onset→End) (Sub-divisions)	Additional Details (Peak height is given in sub-divisions)
PDMI 37/100	13	run 1	87	79	96	87.5	9.5	Peak height = 26.5; 10mV fsd recorder range assumed for both runs
PDMI 37/100	13	re-run 1	-	67	92	79.5	13.5	
PDMI 37/100	26	re-run 3	87	69	107	88	13	Peak height = 4; slow cooling, see text; instrument range 10m cal/sec fsd; 10 mV fsd recorder range assumed
PDEI	12.8	re-run 1	78	67	85	76	10	Peak height = 22.5; 10 mV fsd recorder range assumed; run 1 ended at 70°C
PDPI	13.1	re-run 1	58	34	66	50	11.5	Peak height = 2; 10 mV fsd recorder range assumed; run 1 ended at 50°C
PDHI 45/100	24	run 1	-	-39	-11	-25	(3.5)	Scanned at 20°/min both runs; cooling rate unknown, probably fast. Instrument range 10m cal/sec fsd; recorder range unknown both runs
PDHI 45/100	24	re-run 1	-	-34	0	-17	(4)	

Table continued:

TABLE 12 (continued)

Sample	Sample Mass (mg)	Run 1 re-run	Extrapolated Peak	Onset	End	Shift Median (°C)	Net Shift (Onset→End) (Sub-divisions)	Additional Details (Peak height is given in sub-divisions)
PDNI	10.8	run 1	-	-89	-60	-74.5	14.5	10 mV fsd recorder range assumed; temperatures define largest shift
PDDoI	13.9	run 1	-6	-44	1	-21.5	20	Peak height = 30; 10 mV fsd recorder range for both runs;
PDDoI	13.9	re-run 1	-6	-48	2	-23	15	Peak height = 32.5

TABLE 13  
Summary of Poly(methyl methacrylate) Thermogram Features

Feature Description	Sub-ambient thermogram (sample mass=13.1 mg)				Above-ambient thermogram (sample mass=7.5 mg)				
	Extrapolated Peak	Extrapolated Onset	Extrapolated End	Extrapolated Shift Median	Extrapolated Peak	Extrapolated Onset	Extrapolated End	Extrapolated Shift Median	Additional Details
Simple endothermic shift on re-run; glass transition?	-	132	146	139	-	114	133	123.5	See text for first run description
Broad, shallow endothermic peak; first run only	67	-15	88	-	80	23	97	-	Exothermic gradient changes define shoulders about the peak at 65° and 91°C
Small features within 0°C and 40°C; first run temperatures	20	8	23	-	-	1	9	5	Two effectively first run features a) endothermic shift b) exothermic peak
	31	23	38	-	19	16	23	-	

(i) Thermogram features of several poly(di-n-alkyl-itaconates) and of poly(methyl methacrylate)

Temperatures quoted in Table 12 were derived from the illustrated first run thermograms and those of their re-runs; this Table also details the sample mass and any divergence from the general run conditions described above. Figure 9 shows the thermogram obtained by scanning a 13 mg sample of PDMI 37/100 over the sub-ambient temperature range for the first time. The magnitude of the net endothermic shift was estimated by counting the number of sub-divisions (equivalent to one hundredth of the ordinate fsd on the original chart) between the intersection points of extrapolating lines at the shift onset and end temperatures. A measure of the peak height was similarly evaluated between the intersections at the peak and end temperatures. On reheating, this sample only caused a simple, and slightly larger, endothermic baseline shift. Another PDMI 37/100 sample, with twice the usual sample mass, was scanned with half the normal instrument sensitivity; for both samples the employed recorder range is unknown, but it is reasonable to assume that the fsd was 10 mV. During the first run of the larger sample, a large endothermic peak was recorded at 87°C, with a peak height of 24 sub-divisions; the baseline shift, of 11 sub-divisions, spans a slightly wider temperature region, but its median temperature is only 0.5 degrees higher than that in row one of Table 12. After fast cooling, the first and second re-runs, gave thermograms which contain simple endothermic shifts of magnitude 13 and 14 sub-divisions and median temperatures 79° and 79.5° respectively. Loss of

the endothermic peak with heating and quick cooling and enlargement of the persistent endothermic shift occurred for both samples, and their peak and median shift temperatures are effectively identical. After the second re-run the larger PDMI sample was slowly cooled, overnight at less than one degree per minute and before re-run 3 to about  $-170^{\circ}\text{C}$  at five degrees per minute. The subsequent thermogram displays an endothermic shift with a shallow peak and resembles the PDPI thermogram shown in Figure 10, where the coincidence of shift and peak temperatures indicated in Table 12, and typical of PDMI thermograms, is not evident. The thermogram, obtained by scanning a PDMI 37/100 sample, of mass 13.5 mg, over the above-ambient range for the first time, is identical to that illustrated in Figure 9 and has therefore not been reproduced: a large endothermic peak occurs at  $86^{\circ}\text{C}$  and includes a net shift spanning 20 degrees and centred on  $87^{\circ}\text{C}$ . In general,  $150^{\circ}\text{C}$  was the maximum sample temperature attained during sub-ambient runs; on the only above-ambient runs for a poly(di-n-alkylitaconate), PDMI was heated to about  $200^{\circ}\text{C}$ . With re-scanning under the usual run conditions, the enlarged endothermic shift for this sample was not depressed in temperature with the absence of the peak, as in sub-ambient runs, the mid-point occurring at  $87.5^{\circ}\text{C}$ .

Two small endothermic peaks are visible in the PDMI sub-ambient, first run thermogram illustrated in Figure 9. The shallower peak at  $16^{\circ}\text{C}$ , is visible, although slightly diminished, in the re-run thermogram, but the analogous residue of the narrower peak at  $37^{\circ}\text{C}$  is barely perceptible. In addition to varying with re-run, these small features differ with sample

the endothermic peak with heating and quick cooling and enlargement of the persistent endothermic shift occurred for both samples, and their peak and median shift temperatures are effectively identical. After the second re-run the larger PDMI sample was slowly cooled, overnight at less than one degree per minute and before re-run 3 to about  $-170^{\circ}\text{C}$  at five degrees per minute. The subsequent thermogram displays an endothermic shift with a shallow peak and resembles the PDPI thermogram shown in Figure 10, where the coincidence of shift and peak temperatures indicated in Table 12, and typical of PDMI thermograms, is not evident. The thermogram, obtained by scanning a PDMI 37/100 sample, of mass 13.5 mg, over the above-ambient range for the first time, is identical to that illustrated in Figure 9 and has therefore not been reproduced: a large endothermic peak occurs at  $86^{\circ}\text{C}$  and includes a net shift spanning 20 degrees and centred on  $87^{\circ}\text{C}$ . In general,  $150^{\circ}\text{C}$  was the maximum sample temperature attained during sub-ambient runs; on the only above-ambient runs for a poly(di-n-alkylitaconate), PDMI was heated to about  $200^{\circ}\text{C}$ . With re-scanning under the usual run conditions, the enlarged endothermic shift for this sample was not depressed in temperature with the absence of the peak, as in sub-ambient runs, the mid-point occurring at  $87.5^{\circ}\text{C}$ .

Two small endothermic peaks are visible in the PDMI sub-ambient, first run thermogram illustrated in Figure 9. The shallower peak at  $16^{\circ}\text{C}$ , is visible, although slightly diminished, in the re-run thermogram, but the analogous residue of the narrower peak at  $37^{\circ}\text{C}$  is barely perceptible. In addition to varying with re-run, these small features differ with sample

mass. The first run thermogram for the larger PDMI sample shows a shallow, complex endothermic peak at about  $39^{\circ}\text{C}$ , slight shoulders being outlined from the peak to  $49^{\circ}\text{C}$  and between  $29^{\circ}$  and  $36^{\circ}\text{C}$ . This shallow endotherm extends from  $8^{\circ}$  to  $63^{\circ}\text{C}$ , but only the first re-run revealed a narrow endothermic peak within this region, at  $46^{\circ}\text{C}$ ; in the third re-run thermogram there is merely an additional endothermic gradient increase at  $39^{\circ}\text{C}$ . The above-ambient thermograms do not contain any endothermic peaks at temperatures lower than the large endothermic shift; an exothermic and subsequent endothermic gradient change was obvious during the second run at  $10^{\circ}$  and  $36^{\circ}\text{C}$ .

Figure 10 illustrates the main endothermic features of thermograms obtained at sub-ambient temperatures for other poly(di-n-alkylitaconates). For both PDEI and PDPI the first sample scan was stopped at too low a temperature; for both series members, the (first and only) re-run temperature for the onset of the endotherm was identical with the first run value, and therefore the re-run thermogram has been interpreted as effectively that of a first run. As a result, Figure 10 illustrates the re-run thermograms of PDEI and PDPI, Table 12 containing the relevant details.

Because PDHI 45/100 was the first sample to be scanned in the DSC, the experimental conditions were not those generally used in subsequent runs. As illustrated in the first run thermogram, the baseline has a less endothermic gradient after the simple shift, which therefore resembles the manifestation of a glass transition as reported in the thermal analysis literature. The recorder range being unknown, the

actual shift magnitude should not be compared with those of other samples; the values quoted in Table 12 indicate that both a slight increase in shift magnitude and median temperature occurred on reheating this sample. Subsequent re-runs showed that extrapolated temperatures for the baseline shift were apparently affected by differences in the scan speed, the ratio of scan to chart speed, and recorder and instrument sensitivity. On the second and fifth re-runs, the scan speed was double the chart speed, their ratio usually being 1.0; the second re-run, with a scan speed of twenty degrees per minute, resulted in a shift of width 32 degrees and median temperature  $-17^{\circ}\text{C}$ , while on the fifth re-run, with a scan speed of forty degrees per minute, a narrower shift of width 27 degrees spanned  $-21.5^{\circ}\text{C}$ . During the fifth re-run, an increase in the recorder sensitivity, possibly by a factor of 5, increased the median shift temperature by approximately 2 degrees to about  $-19^{\circ}\text{C}$ , temperature error being enlarged with compression of the temperature scale on the abscissa.

As shown in Figure 10, there are several endothermic features in the first (and only) thermogram obtained for PDNI; the extrapolated temperatures which characterize the largest shift are quoted in Table 12. The large endothermic peak and overall shift, traced in Figure 10 for PDDoI, is repeated almost identically in the re-run thermogram. Differences in the estimates of the shift and peak magnitudes, given in Table 12, may have been caused by differences in the gradients of baselines bordering the peak: during the first run the initial baseline persisted from an endothermic gradient change at  $-120^{\circ}\text{C}$  and on the re-run from an additional gradient increase

at  $-87^{\circ}\text{C}$ ; in the illustrated thermogram the final baseline gradient is not constant, as in the re-run thermogram, but shows endothermic curvature resulting in an extrapolated gradient change at  $37^{\circ}\text{C}$ .

As shown in the traced PDNI thermogram, after the largest shift at  $-74.5^{\circ}\text{C}$  the baseline has a more endothermic gradient; a smaller endothermic feature subsequently occurs which, when interpreted as a shift from  $-32^{\circ}$  to  $-10^{\circ}\text{C}$ , leads to a less endothermic baseline gradient. This final baseline defines a shallow endothermic peak at  $61^{\circ}\text{C}$ , which extends from about  $41^{\circ}$  to  $84^{\circ}\text{C}$ . The baseline is not very smooth above  $-60^{\circ}\text{C}$  and it is therefore possible that the subsequent, slightly irregular shift could be interpreted as an endothermic peak at  $-10^{\circ}\text{C}$ .

The extrapolated endothermic gradient change at about  $-110^{\circ}\text{C}$ , in the illustrated first run thermogram for PDHI, is a consequence of the general endothermic curvature which extends over this temperature region and ceases in the vicinity of  $-70^{\circ}\text{C}$ , this change in baseline form being more clearly outlined during subsequent runs. In the compressed thermogram of the fifth re-run, the beginning of a linear baseline portion is defined by a small endothermic shift between  $-82^{\circ}$  and  $-74^{\circ}\text{C}$ : the more sensitive record of the fifth re-run, which similarly shows initial endothermic baseline curvature, merely displays an exothermic gradient change at  $-65^{\circ}\text{C}$ . This variation in the outline and temperature of a small thermogram feature with differences in recorder range, demonstrates the importance

of achieving optimum run conditions for each sample. It is believed that with more time, the DSC would have revealed a greater number of secondary transitions than the few tentatively described above.

Endothermic baseline curvature is a general feature of the sub-ambient poly(di-n-alkylitaconate) thermograms. The resulting extrapolated gradient change occurs at  $-125^{\circ}\text{C}$  for PDNI and, as already mentioned, at  $-120^{\circ}\text{C}$  and approximately  $-110^{\circ}\text{C}$  in the first run thermograms of PDDoI and PDHI respectively. For both PDPI and PDEI, the curvature is pronounced, extrapolating to an endothermic gradient change at  $-76^{\circ}$  and  $-72^{\circ}\text{C}$  respectively on their first runs. A similar extrapolation for the first run thermogram of the 13 mg PDMI sample, reveals a smaller, but significant, overall gradient change at  $-65^{\circ}\text{C}$ .

Poly(methyl methacrylate) was scanned under the usual run conditions over both the sub- and above-ambient temperature ranges, the thermograms resulting from the initial runs being illustrated in Figure 9. A simple endothermic shift, indicative of the glass transition, occurs in the above-ambient re-run thermogram at the temperatures quoted in Table 13. As shown in the tracing, during the first run the portion of this shift from  $120^{\circ}$  to  $130^{\circ}\text{C}$  was interrupted by an exothermic peak at  $137^{\circ}\text{C}$ , which spanned the  $133^{\circ}$  to  $145^{\circ}\text{C}$  region. On re-scanning another PMMA sample over sub-ambient temperatures, significant endothermic curvature was evident from  $92^{\circ}\text{C}$ , although the steepest shift occurred from  $132^{\circ}\text{C}$  to define a median shift temperature of  $139^{\circ}\text{C}$ . It is apparent

from the illustrated thermogram that in this region the first run only revealed a very small endothermic peak at  $144^{\circ}\text{C}$ , of width 9 degrees.

The broad complex endothermic peak, evident from  $-15^{\circ}$  to  $88^{\circ}\text{C}$  in the sub-ambient tracing, does not occur on sample re-heating. The subsequent exothermic shift from  $99^{\circ}$  to  $111^{\circ}\text{C}$  is another feature that is only visible in the first run thermogram. The extension of the baseline at temperatures below the peak onset, intersects the thermogram at about  $100^{\circ}\text{C}$ , confirming this thermogram interpretation; alternatively the endothermic gradient change at  $111^{\circ}\text{C}$  could be taken as the end of the broad peak. The illustrated above-ambient thermogram shows a similar endothermic peak at  $80^{\circ}\text{C}$  and subsequent increase in the final baseline gradient at  $108^{\circ}\text{C}$ , both features being absent in the re-run thermogram. The outline of this endotherm is similarly complicated, in the two initial thermograms, by the existence of an exothermic gradient change on either side of the peak at temperatures given in row two of Table 13 .

As shown in Figure 9, the onset of the broad endotherm in the above-ambient thermogram is complicated by the presence of a small endothermic baseline shift and subsequent exothermic peak, neither feature being reproduced in the re-run thermogram. In the illustrated sub-ambient thermogram, two endothermic peaks are visible at  $20^{\circ}$  and  $31^{\circ}\text{C}$  on the low temperature side of the broad endotherm at  $67^{\circ}\text{C}$ ; unlike the broader peak, they are reproduced in the re-run thermogram at  $21^{\circ}$  and  $33^{\circ}\text{C}$ , where they have coalesced slightly and the

height of the smaller peak, originally at  $31^{\circ}\text{C}$ , has decreased a little. Figure 9 reveals the visual similarity of the PMMA and PDMI sub-ambient thermograms within  $0^{\circ}$  and  $40^{\circ}\text{C}$ ; for both 13 mg samples, the smaller, higher-temperature feature is less reproducible after the first heating cycle. Resembling the sub-ambient poly(di-n-alkylitaconate) thermograms, the initial PMMA baseline becomes increasingly endothermic, the extrapolated gradient change being evident at about  $-80^{\circ}\text{C}$  in the illustrated thermogram. With reference to the other temperature extreme in Figure 9, the above-ambient thermogram for PMMA shows a large endothermic movement from  $160^{\circ}$  to  $190^{\circ}\text{C}$ , the concurrent thermobalance trace indicating an increased rate of weight loss from about  $170^{\circ}\text{C}$ , and a total weight loss of about 2% by the end of the first run. It is therefore possible that a very small amount of sample degradation could have occurred and could have caused the depression in onset temperature of the reproducible endothermic shift from  $120^{\circ}$  to  $114^{\circ}\text{C}$  in the subsequent thermogram.

TABLE 14

Broad Endothermic Peak; a General Feature of only the First Run Thermograms of Polysaccharide Esters

Sub-ambient thermogram data				Above-ambient thermogram data						
Sample	Sample Mass (mg)	Additional Details	Onset Temp. (°C)	End Temp. (°C)	Peak Temp. (°C)	Onset Temp. (°C)	End Temp. (°C)	Additional Details	Sample Mass (mg)	Sample
PMMA	13.1	Peak complicated by two shoulders at 45° & 77°C	-15	88	67	80	97	Peak complicated by two shoulders at 65° & 91°C	7.5	PMMA
CTA	4.1		-44	93	67	87	123		3.3	CTA
ATA	6.0	Onset not clearly defined	-	105	77	98	125		13.1	GTA
ATP	12.9		39	86	68	-	60	Shift and subsequent exothermic gradient change at 83°C; peak at 60°C?	12.9	GTP
Gtiso-B	12.9	Shoulder at 61°C	42	92	76	-	63	Simple endothermic shift, 12.9 containing insignificant exothermic gradient change at 58°C	12.9	GTB
ATB	12.2	Shift from 58° to 69°C?	58	80	69	-	61	Endothermic shift with insignificant endothermic gradient change at 54°C	13.7	GTV
ATV	9.9	Shift from 33° to 47°C?	33	Approx. 47	47	89	124	Apparently insignificant endothermic gradient change on re-run at 37°C	4.0	AC(2.5)

TABLE 14 (continued)

Sub-ambient thermogram data			Above-ambient thermogram data					Sample			
Sample	Sample Mass (mg)	Additional Details	Onset Temp. (°C)	End Temp. (°C)	Peak Temp. (°C)	Peak Temp. (°C)	Onset Temp. (°C)	End Temp. (°C)	Additional Details	Sample Mass (mg)	Sample
<p>Re-run data for the above-ambient run after overnight annealing at ambient temp.</p>											
GTC( $5 \times 10^6$ )	8.8		41	133	87		105	147		8.8	GTC( $5 \times 10^6$ )
CTC( $3.1 \times 10^3$ )	13.0	Endothermic gradient increase at 48°C defines shoulder at 55° to 60°C	23	78	64		107	131	Shoulders on peak at 103° and 122°C and endothermic shift at onset: re-run gradient change at 45°C	3.5	GTC ( $100 \times 10^6$ )
CTC( $15.1 \times 10^3$ )	13.9	Endothermic gradient change at -45°C on re-run. Peak irregular with endothermic gradient change at 12°C. Baseline is very exothermic	-44	73	45		110	147	Peak complex: exothermic gradient change at 82°C and shift from 128°C to 130°C	14.0	CTC ( $15.1 \times 10^3$ )
CTC( $59.7 \times 10^3$ )	11.4	Endothermic gradient change at -43°C on re-run	-48	48	29		101	174		13.5	CTC ( $59.7 \times 10^3$ )

Table continued:

TABLE 14 (continued)

Sub-ambient thermogram data				Above-ambient thermogram data						
Sample	Sample Mass (mg)	Additional Details	Onset Temp. (°C)	End Temp. (°C)	Peak Temp. (°C)	Onset Temp. (°C)	End Temp. (°C)	Additional Details	Sample Mass (mg)	Sample
ATr(1.0), A(2.0)	13.1	Onset not clearly defined. Shift ending at 55°C?	-	78	55	75	102	Endothermic gradient change at 29°C on re-run	11.5	ATr(1.0), A(2.0)
ATr(1.0)	7.7	Onset defined by non-significant gradient change at 33°C	-	106	68	100	137		10.3	ATr(1.0)
ATT	8.0	Possible onset and end temperatures; 0° and 100°C respectively. Shift ending at 72°C?	-	-	72	94	116	Onset of endothermic process at 24°C on re-run	9.6	ATT

TABLE 15  
 Summary of Endothermic Baseline Shifts in Polysaccharide Derivative Thermograms, possibly caused by the Glass Transition

Sample	Sub-ambient thermogram data Additional Details	Run 1/ Re-Run	Onset Temp. (°C)	End Temp. (°C)	Median Temp. (°C)	Above-ambient thermogram data			Sample	
						Median Temp. (°C)	Onset Temp. (°C)	End Temp. (°C)		Run 1/ Re-Run
ATV	Upper limit for both runs of 80°C; therefore end temp. possibly too low	Re-run 1 only	68	77	72.5	53.5	38	69	Re-run 1	GTV
ATB	Thermogram absent from Fig. 11, as recorder range changed from 5 to 10 mV during run 1. Upper limit for run 1 and re-run 1 of about 100°C	Re-run 2	87	103	95	72	59	85	Re-run 1	GTB
GTiso-B		Re-run 1 only	103	130	116.5	115.5	106	125	Re-run 1	GTP
ATP	Upper limit of 150°C					156	148	164	Re-run 1	GTA
ATA	Upper limit of 120°C; instrument range 2 mcal/sec fsd									
CTA	Upper limit of 120°C; instrument range 2 mcal/sec fsd					197.5	191	204	Re-run 1	CTA
ATr(1.0) A(2.0)	Merely an exothermic gradient change at 123°C?	Run 1 only	[78	123	100.5]	110	93	127	Re-run 1	ATr(1.0) A(2.0)
ATT	Upper limit of 100° on run 1 and 150°C on re-run 1	Effectively run 1	131	142	136.5	155	149	161	Run 1 only	AIT

TABLE 15 continued

Sub-ambient thermogram data			Above-ambient thermogram data				Sample
Sample	Additional Details	Run 1/ Re-Run	Onset Temp. (°C)	End Temp. (°C)	Median Temp. (°C)	Run 1/ Re-Run	
ATr(1.0)	Upper limit of 150°C					Run 1	ATr(1.0)
CTC(15.1x 10 <sup>3</sup> )	Upper limit of at least 150°C					Re-run 1	CTC(15.1x 10 <sup>3</sup> )
CTC(3.1x 10 <sup>3</sup> )	Upper limit of 100° on run 1 and 150°C on re-run 1	Re-run 1	82	109	95.5	Re-run 1	Upper limit for both runs of 190°C; possible onset temp. of Tg-related endothermic shift
CTC(59.7x 10 <sup>3</sup> )		Run 1 only	64	85	74.5	Re-run 1	Upper limit of 197° on run 1 and 220°C on re-run 1
Above-ambient thermogram data							
AC(2.5)	Instrument range 2mcal/ sec fsd; temp. limits of shift are more distinct in run 1 thermogram	Run 1 Re-run 1	206 205	209 211	207.5 208	Run 1 Re-run 1	Instrument range 2mcal/sec fsd; temp. limits of shift are more distinct in re-run 1 thermogram
CTC(5 x 10 <sup>6</sup> )	Upper limit of 197° on run 1 and 220°C on re-run 1; possible onset temp. of Tg-related endothermic shift	Re-run 1	213	-	-	Run 1 Re-run 1	Instrument range 2mcal/sec fsd; temp. limits for run 1 are more satisfactory (gr 100x10 <sup>6</sup> )

TABLE 16  
 Multiple First Run Peaks, Approximately Coincident with the Tg-associated Re-run Shift,  
 of Several Glycogen Esters

Sample	Extrapolated Temperatures for Tg-related Re-run Shift (°C)		Extent of Peaks During First Run (°C)		Extrapolated Temperatures of Multiple Peaks Evident in First Run Alone (°C)				
	Onset	End	Onset at endothemic gradient change	Extrapolated end of final peak	i Small apparent endothemic peak at onset of ii	ii Exothermic peak of greatest height, immediately following i	iii Endothermic, broadest peak, immediately following ii		
GTP	106	125	112	145	119 (39)	(4)	123 (39)	(11)	134 (39)
GTB	59	85	74	111	80 (12)	(4)	84 (11)	(11)	95
GTV	38	69	65	84	68	(5)	73	-	-

TABLE 17

Summary of Thermobalance Records obtained simultaneously to Several Initial Above-Ambient DSC Thermograms

Sample	a		b		c		d		Additional Details
	Approx temp (°C) of wt. loss gradient change	Approx total wt. loss (%) by this temp.	Approx temp (°C) of wt. loss gradient change	Gradient	Approx total wt. loss (%) by this temp.	Approx temp (°C) of wt. loss gradient change	Approx total wt. loss (%) by this temp.	Approx temp (°C) of wt. loss gradient change	
PDMI 37/100	55	Assumed zero	123	Gradient	Decreases 0.2	141	D Effectively 0.2		Upper temp limit of 190°C; total wt. loss of 1.5%, curvature of wt. loss trace persisting after 141°C
PMMA	57	Assumed zero	117	117	0.3	172	D 0.9		Upper temp limit of 200°C; total wt. loss of 2.1%
ATA	55	Assumed zero	145	145	1.5	260	Concurrently, large endothermic movement evident	D 7.8	Upper temp limit of 360°C; total wt. loss of 9.8%. After a small peak at 292°C, involving overall loss, gradient decreases
GTA	55	Assumed zero	100	Gradient	Decreases 0.4	215	1.0		Upper temp limit of 250°C; total wt. loss of 1.3%. After a small peak at 228°C, involving overall loss, gradient decreases
GTP	57	Assumed zero	222	222	0.8		D 0.8		Upper temp limit of 232°C; total wt. loss of 1.0%. Thermobalance trace very irregular

TABLE 17 continued

Sample	a		b		c		d		Additional Details
	Approx temp (°C) of wt. loss gradient change	Approx total wt. loss (%) by this temp.	Approx temp (°C) of wt. loss gradient change	Approx total wt. loss (%) by this temp.	Approx temp (°C) of wt. loss gradient change	Approx total wt. loss (%) by this temp.	Approx temp (°C) of wt. loss gradient change	Approx total wt. loss (%) by this temp.	
GTB 57		Assumed zero	164	0.1	240	0.5			Upper temp limit of 250°C; total wt. loss of 0.6%
GIW 60		Assumed zero	Gradient 110	Decreases 0.2	200	0.4			Upper temp limit of 220°C; total wt. loss of 0.8%
ATT 80	End of endothermic shift, of Table 14, in vicinity	Assumed zero	107 Little wt. loss between 130° and 140°C, spanning much of current endothermic peak	Negligible loss between 140°C and 160°C, with end of endothermic peak	160	0.2	D 244	0.9 By this temp, DSC trace off-scale exothermically	Upper temp limit of 250°C; total wt. loss of 1.1%. Sample black on removal from thermobalance
ATr(1.0) 60		Assumed zero	97 Approx coincident with large endothermic peak, of Table 14	Decreases 0.4	135	0.6	D 330	3.3 Approx coincident with onset of final endothermic movement going off-scale	Upper temp limit of 353°C; total wt. loss of about 10%. thermobalance trace off-scale. Endothermic curvature in trace prior to small peak at 221°C, without net wt. loss

(ii) Thermogram features of several polysaccharide derivatives

Significant thermogram features for these polymers have been rationalized into seven groups within which details are at first provided for the carboxylic acid esters, with those of the carbanilate derivatives being specified last. For samples of small mass, some gradient changes, insignificant when the apparent criterion is extrapolated to small masses and high instrument sensitivity, have been included.

(a) Significant features occurring below  $0^{\circ}\text{C}$ , and therefore only visible in thermograms extending over the full sub-ambient temperature range, constitute the first group. In general, sub-ambient thermograms show initial endothermic curvature of their baselines. Due to the existence of other thermogram features, the only first run thermograms of carboxylic acid esters to show a significant, isolated extrapolated gradient change are those of ATA, at  $-75^{\circ}\text{C}$ , and ATB, at  $-95^{\circ}\text{C}$ . ATr(1.0), A(2.0); ATr(1.0) and ATT, collectively referred to as "the three amylose esters", display a large isolated endothermic gradient change by  $-45^{\circ}\text{C}$  on both first and re-run thermograms (see Figures 13 and 14). The ATr(1.0), A(2.0) tracing in Figure 13 shows an extrapolated gradient change at  $-60^{\circ}\text{C}$ , evident at  $-67^{\circ}\text{C}$  in the re-run thermogram. As shown in Figure 14, the extrapolated gradient change occurs at  $-48^{\circ}\text{C}$  in the first run thermogram for ATr(1.0). Both ATT runs revealed effectively continual endothermic curvature between about  $-110^{\circ}$  and  $-50^{\circ}\text{C}$ , the extrapolated gradient change being at  $-81^{\circ}\text{C}$  in the illustrated thermogram.

Isolated endothermic gradient changes are clearly perceptible in DSC data for the lower molecular weight CTC samples, significant extrapolations for CTC ( $3.1 \times 10^3$ ) occurring at  $-82^\circ$  and  $-43^\circ\text{C}$  in the thermogram illustrated in Figure 15, and at  $-93^\circ$  and  $-61^\circ\text{C}$  during the re-run. The only significant isolated baseline extrapolations are visible in the CTC ( $15.1 \times 10^3$ ) first run thermogram at  $-127^\circ$  and  $-91^\circ\text{C}$ , and at  $-80^\circ\text{C}$  in the CTC ( $59.7 \times 10^3$ ) re-run thermogram.

First run thermograms for ATP and GT iso-B show exothermic peaks in the region where the analogous ATA baseline displays endothermic curvature. The ATP peak occurs between  $-92^\circ$  and  $-76^\circ\text{C}$  and unlike the end of the peak, the onset, at  $-131^\circ\text{C}$ , is clearly defined. For GT iso-B the initial exothermic movement also begins at about  $-130^\circ\text{C}$  and outlines a maximum between  $-103^\circ$  and  $-92^\circ\text{C}$ , an exothermic gradient change at  $-53^\circ\text{C}$  being interpreted as the end of this peak. The main characteristics of the ATA re-run thermogram are two gradient changes, endothermic at  $-88^\circ\text{C}$  and exothermic at  $+10^\circ\text{C}$ , which separate linear baseline portions; because of the smallness of the ATA sample and the increased instrument sensitivity, these gradient changes are apparently insignificant. When re-scanned in the DSC, ATP and GT iso-B gave re-run thermograms visually similar to that of ATA: the endothermic gradient change took place at  $-84^\circ\text{C}$  for ATP, its exothermic movement at  $17^\circ\text{C}$  being not quite significant; the GT iso-B re-run revealed a significant exothermic gradient change at  $20^\circ\text{C}$ , which only persisted for a few degrees, and small endothermic movements in the vicinity of the first run peak. The shape

of these re-run thermograms suggests that the exothermic gradient change at about  $20^{\circ}\text{C}$  may be a return to the original baseline slope, possibly at the end of the endothermic movement which began in the  $-90^{\circ}$  to  $-80^{\circ}\text{C}$  region, and not the beginning of exothermic heat flow. The first CTC ( $3.1 \times 10^3$ ) run revealed a tiny exothermic shift at  $-129^{\circ}\text{C}$ , near the onset of the described exothermic peaks. The only other exothermic feature in the sub-ambient thermograms is a small bump at  $-22^{\circ}\text{C}$  in the same CTC thermogram, illustrated in Figure 15.

This paragraph contains details of the remaining features in the sub-zero region, which are all endothermic and only visible in the first run thermograms. ATB revealed a large baseline shift from  $-61^{\circ}$ , the endothermic movement ceasing at  $+21^{\circ}\text{C}$ ; as the baseline appears to be very endothermic, the exothermic gradient change at  $21^{\circ}\text{C}$  could be interpreted as an endothermic peak. The ATV thermogram shows a small shallow endothermic peak, at  $-64^{\circ}\text{C}$ , which spans the  $-89^{\circ}$  to  $-44^{\circ}\text{C}$  range, the re-run thermogram for this smallish sample containing almost significant extrapolated gradient changes at  $-95^{\circ}$ ,  $-51^{\circ}$  and  $-73^{\circ}\text{C}$ , all of which are endothermic; the reproducible endothermic curvature of the baseline may be responsible for the resemblance of this feature to a peak, alternatively interpreted as an endothermic shift between  $-89^{\circ}$  and  $-70^{\circ}\text{C}$  with a subsequent endothermic increase at  $-44^{\circ}\text{C}$ . Of the three amylose esters, only the two samples containing a trityl group in each monomer unit show an additional thermogram feature in the sub-zero region. As shown in Figure 13, the ATr(1.0), A(2.0) thermogram contains a shallow endothermic peak between  $-127^{\circ}$  and  $-74^{\circ}\text{C}$ , the irregularity of its shape preventing extrapolation for the

peak temperature. In the re-run thermogram, an endothermic gradient change at  $-120^{\circ}\text{C}$  correlates with the temperature of the peak onset in the first run and very small endothermic and exothermic peaks occur at  $-96^{\circ}$  and  $-94^{\circ}\text{C}$  respectively. The mass of the ATr(1.0) sample was 7.7 mg compared with the more usual 13 mg; its smaller mass may have been responsible for the diminished magnitude of the endothermic peak at  $-96^{\circ}\text{C}$  compared with that of the analogous peak, with a median temperature of  $-97^{\circ}\text{C}$ , which has just been described. The shallow ATr(1.0) endotherm occurs within  $-113^{\circ}$  and  $-73^{\circ}\text{C}$ , the re-run showing a corresponding gradient increase at  $-113^{\circ}\text{C}$ , also insignificant. Two smaller gradient changes are subsequently visible in the irregular ATr(1.0) re-run baseline, which becomes more exothermic at  $-98^{\circ}\text{C}$  and more endothermic at  $-85^{\circ}\text{C}$ . Both trityl derivative re-runs displayed residues of the initial, shallow peaks which slightly resemble the endotherm in the first ATV thermogram, but occur at lower temperatures. The CTC ( $59.7 \times 10^3$ ) tracing in Figure 15 contains a small endothermic peak, of width 13 degrees, at  $-102^{\circ}\text{C}$ ; a very, very small re-run residue is evident in the form of an apparent exothermic peak at  $-93^{\circ}\text{C}$ , with defining exothermic gradient changes at about  $-96^{\circ}$  and  $-89^{\circ}\text{C}$ . This endothermic first run feature, unique for the CTC thermograms below  $0^{\circ}\text{C}$ , is much narrower than the peaks shown by the trityl derivatives, but is similar with respect to its location and the existence of some residue after the initial heating cycle.

Both sub- and above-ambient thermograms for CTA were obtained with high instrument sensitivity because of the difficulty

in packing sufficient of the fibrous sample into a sample pan. The criterion for significant gradient changes is therefore not very relevant to CTA thermograms and the features now described are all apparently insignificant. The first sub-ambient run revealed an increase in the endothermic gradient at  $-121^{\circ}\text{C}$  and also during an unsymmetrical endothermic peak at  $-86^{\circ}\text{C}$ , extending from  $-97^{\circ}$  to  $-83^{\circ}\text{C}$ , the subsequent baseline being interrupted by an exothermic gradient change at  $-61^{\circ}\text{C}$ . The re-run thermogram merely shows two endothermic gradient changes at  $-121^{\circ}$  and  $-93^{\circ}\text{C}$  and some small irregularities between  $-61^{\circ}$  and  $-52^{\circ}\text{C}$ , possibly caused by two tiny endothermic shifts or peaks.

(b) In describing the first group of features, which occurred below  $0^{\circ}\text{C}$ , a relationship was suggested between initial endothermic gradient increases and subsequent decreases at about  $20^{\circ}\text{C}$ . Both first and re-run above-ambient thermograms of all four glycogen derivatives contain a simple, significant exothermic gradient change between  $13^{\circ}$  and  $17^{\circ}\text{C}$ ; a significant and reproducible isolated exothermic change is absent from this temperature region in the above-ambient thermograms of all of the other esters.

As shown in Figure 13, the above-ambient thermogram for CTA contains an exothermic gradient change at  $14^{\circ}\text{C}$  which is reproduced by the rough re-run record at approximately  $13^{\circ}\text{C}$ . These gradient changes are apparently insignificant, as are the described CTA features in the sub-zero region. A subsequent sub-ambient thermogram variation is characterized by an exothermic gradient change at  $19^{\circ}\text{C}$ , which is more obviously the peak temperature of a small endotherm in the re-run thermogram. These CTA features resemble those of PMMA and PDMI in the vicinity of  $20^{\circ}\text{C}$ .

(c) A large broad endothermic peak occurs in all sub-ambient and above-ambient first run thermograms. This endotherm is characterized by its absence in the re-run thermograms which result from immediate re-scanning of the sample, and by the breadth of the temperature region spanned by its rounded peak, which occurs between  $29^{\circ}$  and  $77^{\circ}\text{C}$  in sub-ambient thermograms and between  $60^{\circ}$  and  $110^{\circ}\text{C}$  during above-ambient runs. Occasionally the peak is complex in shape, such complications being mentioned in the "Additional Details" columns of Table 14 and described below. Alternative interpretations for baseline variations at these temperatures are also indicated in these columns. The endotherm is visible in Figures 11 to 16 and the temperatures of its defining baseline extrapolations are given in Table 14.

As shown in Figure 9 both PMMA first run thermograms, with different run onset temperatures, show a similar broad endotherm. The temperature data for this peak, absent on re-run, has been included in Table 14 in order to aid interpretation of its differing locations under sub- and above-ambient run conditions. The only poly(di-n-alkylitaconate) endotherm to resemble this general polysaccharide ester feature occurs between  $41^{\circ}$  and  $84^{\circ}\text{C}$  in the PDNI sub-ambient thermogram. The thermograms for both these samples have already been described in detail.

The onset temperatures given in Table 14 are not always reliable because the existence of several gradient changes on the low-temperature side of the peak frequently precludes

knowledge of the true initial baseline. It is assumed that the only significant overall endothermic gradient change in the CTA thermogram is associated with the onset of the large endotherm. The only apparently significant endothermic gradient change in the ATA thermogram, also obtained with high instrument sensitivity, occurs below  $-70^{\circ}\text{C}$ , which is very much lower than the generally observed onset temperature. The ATB and ATV baseline variations resemble endothermic shifts, the endothermicity of the baseline possibly being responsible. The end of the ATV peak is indicated by a shallow endothermic minimum between  $62^{\circ}$  and  $67^{\circ}\text{C}$ . As shown in Figures 12 and 13, GTA and CTA are the only simple polysaccharide esters to show the broad endothermic peak in their above-ambient thermograms. The GTP and GTB thermograms could be re-interpreted in terms of a peak at  $60^{\circ}$  and  $58^{\circ}\text{C}$ , ending at  $83^{\circ}$  and  $63^{\circ}\text{C}$  respectively. In the illustrated GTV thermogram the endothermic shift is interrupted by a gradient change in the opposite direction to the endothermic decreases at  $60^{\circ}$  and  $58^{\circ}\text{C}$ , the exothermicity of the final baseline at  $61^{\circ}\text{C}$  also being unusual and suggesting an endothermic peak at this temperature. The approximately constant location of the endothermic shift, as defined by significant gradient changes, is apparent in Table 14 .

The temperature data for the three amylose esters is given in the last three rows of Table 14 to ensure an adjacent position for the peak temperatures of the same sample from its sub- and above-ambient thermograms. The beginning of the endotherm is not clearly defined in the illustrated sub-ambient thermogram for ATr(1.0), A(2.0); there is a very small exothermic gradient change at about  $0^{\circ}\text{C}$ , but the only

significant endothermic gradient change occurs at  $-60^{\circ}\text{C}$  and is reproduced with re-run, as reported earlier in the first feature group. This peak interpretation is justified by the course of the thermogram after  $78^{\circ}\text{C}$ , parallel to the very endothermic re-run baseline: interpretation of this feature as a shift ending at  $55^{\circ}\text{C}$  defines a horizontal baseline between this temperature and a further endothermic movement from  $78^{\circ}\text{C}$ . As shown in Figure 14, the onset of the endothermic peak in the ATr(1.0) sub-ambient thermogram is clearly defined at  $33^{\circ}\text{C}$ , but the involved gradient change is not significant. This Figure also reveals the poor definition of the ATT sub-ambient peak: a non-significant endothermic change at about  $0^{\circ}\text{C}$  could be due to the beginning of the process which is interrupted by the end of the first run at  $100^{\circ}\text{C}$ ; the interpretation of this feature as a shallow peak was suggested by the very endothermic gradient of the re-run thermogram. The large peak was clearly outlined during the above-ambient runs of all three amylose esters. This endotherm appears to be a phenomenon of the first run thermograms alone, and therefore the existence of the onset endothermic gradient change in the re-run thermogram for ATr(1.0), A(2.0) is surprising. In addition, the second thermogram for ATT contains a feature between  $24^{\circ}$  and  $70^{\circ}\text{C}$ , with the end of an irregular endothermic shift or endothermic peak occurring at  $63^{\circ}\text{C}$ . Confirmation of the interpretation of sub-ambient thermograms for the two fully-substituted amylose esters, both with onset residues in their above-ambient re-run thermograms, in terms of the broad endothermic peak is provided by:

- (i) the absence of the feature in re-run thermograms
- (ii) the similarity of their peak temperatures with that of the well-defined sub-ambient ATr(1.0) peak
- (iii) the peaks are clearly outlined for all three amylose esters in their above-ambient thermograms
- (iv) the elevation of their above-ambient peak temperatures is of the same order of magnitude as indicated by CTA and ATr(1.0).

The Figure 16 tracings for both AC samples and GTC( $\text{gr } 100 \times 10^6$ ) were obtained with smaller sample masses and higher instrument sensitivity than usual, the resulting extrapolated gradient change criterion possibly being inapplicable. The illustrated above-ambient thermograms for ATC and AC(2.5) contain large endothermic peaks which are almost identical. Both re-runs revealed an apparently insignificant gradient change in the vicinity of the first run peak onset and smaller subsequent endothermic gradient increases. The net endothermic shift between the intersections of extrapolated baselines at the beginning and end of the peak is slightly smaller for the smaller sample; the overall baseline shift between the same temperatures in the re-run thermograms approximately matches the net peak shift for both samples. The magnitude of the endothermic shift in the re-run baseline is only two-thirds of the corresponding shift during the GTC( $\text{gr } 100 \times 10^6$ ) peak; extrapolation for the onset temperature of this first run endotherm spans an irregular endothermic shift between its own extrapolated onset at  $40^\circ$  and  $61^\circ\text{C}$ , an insignificant endothermic gradient increase occurring during this shift at  $48^\circ\text{C}$  and in the re-run thermogram at  $45^\circ\text{C}$ . Unusually, the first run peak is not

smoothly rounded and therefore the actual peak temperature is quoted in Table 14, where details of the two shoulders are given. The GTC ( $5 \times 10^6$ ) endothermic maximum visually resembles the ATC peak. The net endothermic shift between extrapolation intersections at the beginning and the end of the former endotherm is approximately half the peak height, similarly estimated between the peak and end temperatures. Instead of being immediately re-scanned after the usual rapid cooling, the GTC ( $5 \times 10^6$ ) sample was annealed at ambient temperature overnight. The thermogram which was obtained, under identical run conditions, on the following day contains a similar endothermic maximum at slightly lower temperatures and with a smaller area, both the net endothermic shift and the peak height being approximately half their magnitude on the first run. The above-ambient re-run temperature data for GTC ( $5 \times 10^6$ ) is given in the sub-ambient portion of Table 14, enabling easy comparison with the adjacent first run peak temperature. The broad endotherm in the above-ambient thermogram for CTC ( $15.1 \times 10^3$ ) is not smoothly rounded, being complicated by the exothermic gradient change at  $82^\circ\text{C}$  and the small exothermic shift between  $128^\circ$  and  $130^\circ\text{C}$ . Because of the sloping baseline evident in the above-ambient CTC ( $59.7 \times 10^3$ ) thermogram illustrated in Figure 15, the first run feature resembles a shift, its present interpretation being confirmed by the equality of the net endothermic shift between the peak onset and end temperatures in the first and re-run thermograms. The net endothermic baseline increase is twenty five percent greater in the initial CTC ( $15.1 \times 10^3$ ) above-ambient thermogram. Sub-ambient thermograms for CTC ( $3.1 \times 10^3$ ) and

CTC ( $59.7 \times 10^3$ ) are illustrated in Figure 15; the analogous CTC ( $15.1 \times 10^3$ ) thermogram is not included because its very exothermic baseline caused the recorder pen to move off-scale frequently. Thermograms for the two lower molecular weight samples both contain irregularly shaped peaks, as detailed in Table 14, and subsequent exothermic gradient changes 12 and 14 degrees above the end of the peak for CTC ( $15.1 \times 10^3$ ) and CTC ( $3.1 \times 10^3$ ) respectively. The first CTC ( $3.1 \times 10^3$ ) run ended at  $100^\circ\text{C}$ , but the initial CTC ( $15.1 \times 10^3$ ) thermogram shows further exothermic gradient increases at  $92^\circ$  and  $137^\circ\text{C}$ , the former coinciding with the exothermic change of the sample with lowest molecular weight. The net endothermic shift between the peak onset and end temperatures for CTC ( $3.1 \times 10^3$ ) is about three times the re-run baseline shift between the same temperatures, whereas for CTC ( $59.7 \times 10^3$ ) the baseline shift of the re-run thermogram accounts for over two-thirds of the net peak shift in the initial thermogram. The coalescence of an endothermic shift with the peak could be responsible for the complexity of the CTC ( $3.1 \times 10^3$ ) endothermic maximum.

Several characteristics of the broad endotherm are now evident from Table 14 and the thermogram details given above. The peak temperature is invariant with the degree of substitution of AC and is also unaffected by the grafting of ATC chains on to the GTC structure. Considered separately, sub- and above-ambient CTC thermograms reveal an inverse relationship between peak temperature and sample molecular weight. A small variation in above-ambient peak temperatures of carbanilate derivatives with degree and type of backbone branching is evident from Table 14; variation of the

substituent groups also affects the peak temperature. Thermal history is another pertinent variable: after annealing GTC ( $5 \times 10^6$ ) at ambient temperature overnight, a repeat scan exceptionally revealed an endotherm visually similar, but smaller in area than the first run peak and depressed in peak temperature by 18 degrees. Differences in the minimum sample temperature also change the location of the endotherm: CTA and the three amylose esters experienced peak temperature elevations of 20 to 32 degrees, with increase in the run onset temperature, CTC ( $15.1 \times 10^3$ ) and CTC ( $59.7 \times 10^3$ ) temperature data revealing an analogous change in peak temperature of 65 and 72 degrees. These CTC thermograms, obtained with similar sample masses and identical recorder and instrument sensitivity, indicate that an increased peak height was recorded during above-ambient runs, confirming the impression visually derived from thermograms for the three amylose esters of differing sample masses. Low molecular weight ( $M_w < 40 \times 10^3$ ) CTC endotherms are complicated by a gradient change on the low-temperature side of the peak; similarly, the GTC( $gr\ 100 \times 10^6$ ) thermogram displays a shoulder below the peak, the grafted ATC chains possibly being responsible for the other shoulder which extends from the GTC ( $5 \times 10^6$ ) peak temperature to the vicinity of the temperature limit of the ATC peak. Within the span of the CTA above-ambient endothermic peak, GTV, GTB and GTP thermograms contain endothermic shifts with approximately constant temperature limits; their onset temperature is similar to that for the GTA peak, which extends over 80 degrees, the shifts merely spanning up to 20 degrees. A subsequent exothermic increase in the GTP thermogram and insignificant

gradient changes during the GTB and GTV shifts complicate the unusual form of these endothermic features.

(d) This paragraph describes small features which are visible near the beginning of the large first run endotherm, defined in Table 14 . A small, but distinct endothermic shift occurs within the  $29^{\circ}$  to  $37^{\circ}\text{C}$  region in three of the glycogen ester thermograms traced in Figure 12; it spans  $30^{\circ}$  to  $36^{\circ}\text{C}$  for GTA,  $32^{\circ}$  to  $37^{\circ}\text{C}$  for GTB, and  $29^{\circ}$  to  $33^{\circ}\text{C}$  for GTV, the width of the temperature range decreasing in this order. There is no evidence of a shift in this vicinity in either of the above-ambient GTP thermograms or in the above-ambient re-run thermograms of the other glycogen esters. The first sub-ambient runs for ATB and ATV revealed nothing of interest near the beginning of the large endotherm. Extrapolation for the onset temperature of this peak in the ATP tracing spans a very small endothermic shift, absent on re-run, the baseline being irregular between this kink and the exothermic peak at lower temperatures. In addition, the ATA thermogram in Figure 11 reveals apparently insignificant gradient changes between  $47^{\circ}$  and the significant gradient change, already mentioned, at  $-75^{\circ}\text{C}$ ; the record of the first GT iso-B run shows a zig-zag baseline between the end of the exothermic peak, at  $-53^{\circ}\text{C}$ , and the beginning of the broad endotherm, at  $42^{\circ}\text{C}$ , the above text containing details of both features. The small endothermic bump visible at  $37^{\circ}\text{C}$  in the CTA sub-ambient tracing was not outlined during the re-run; in the illustrated above-ambient thermogram, extrapolation for the onset temperature of the large peak spans an irregular endothermic movement of the baseline.

The small CTA features described here and at the end of group b resemble those evident at similar temperatures in the PMMA and PDMI thermograms, the concurrent sub-ambient first and re-run thermograms of CTA and the 13 mg PDMI sample being strikingly similar. All the sub-ambient and two of the above-ambient first run thermograms of the three amylose esters contain nothing of note at temperatures below the peak of the broad endotherm. The ATT tracing in Figure 14 reveals an endothermic baseline shift between  $-1^{\circ}$  and  $11^{\circ}\text{C}$  (temperature control for this above-ambient run being achieved at  $-19^{\circ}\text{C}$ , the onset temperature could be erroneous) and the re-run thermogram shows a smaller shift between  $5^{\circ}$  and  $12^{\circ}\text{C}$ . The ATC thermogram illustrated in Figure 16 shows a tiny endothermic kink at  $7^{\circ}\text{C}$  and the re-run thermogram shows an exothermic bump at  $1^{\circ}\text{C}$ , also occurring during the AC(2.5) re-run only, at  $7^{\circ}\text{C}$ . The GTC( $\text{gr } 100 \times 10^6$ ) tracing in Figure 16 also reveals a minute endothermic shift at  $9^{\circ}\text{C}$ , the re-run thermogram containing a slightly larger exothermic shift centred on  $12^{\circ}\text{C}$ . The endothermic shift spanning  $40^{\circ}$  to  $61^{\circ}\text{C}$  in the first run thermogram for GTC( $\text{gr } 100 \times 10^6$ ) is absent on the re-run, and from all other carbanilate thermograms. Thermograms for the acyl derivatives of glycogen are, in general, characterized by a small endothermic shift with a maximum span of 6 degrees, which were outlined between  $29^{\circ}$  and  $37^{\circ}\text{C}$  on the first run only; the ATT shift occurring at lower temperatures and in the re-run thermogram, covers a wider temperature range and the GTC( $\text{gr } 100 \times 10^6$ ) shift is even broader, extending to higher temperatures.

(e) Table 15 contains extrapolated temperature limits of endothermic baseline shifts which are evident in the thermograms of polysaccharide derivatives and which may be the manifestations of the glass transition. The glass transition, being associated with amorphous regions, is known to be enhanced by rapid cooling as effected prior to a re-run; sample stresses are frequently released at  $T_g$  as demonstrated by the occurrence of peaks in the vicinity of the simple shift which is therefore only visible in the re-run thermogram. The peaks which characterize the first run thermograms near  $T_g$  are described in the next feature category. When experimental conditions differed from those generally used and described at the beginning of this section, the relevant information is included in the Additional Details column, Table 14 containing details of the sample masses.

The beginning of the simple endothermic shift was indicated in the first ATB runs, but it was only completely defined by the second re-run; although the extrapolated onset temperature increased from  $84^\circ$  on the first run to  $88^\circ\text{C}$  on the first re-run, the steepest endothermic movement actually began at about  $92^\circ\text{C}$  in all three runs. The exothermic peaks obvious in the ATV and GT iso-B tracings, in Figure 11, conceal the endothermic baseline shift which was revealed with re-heating. The sub-ambient thermograms of ATP, ATA and CTA, whose upper temperature limits are given in Table 15, contain no clear evidence of a simple endothermic shift after the broad endotherm of Table 14. As shown in the Figure 11 tracing for ATP, a distinct endothermic peak is evident at  $139^\circ\text{C}$ , extending from  $125^\circ$  to  $143^\circ\text{C}$ , and is followed by exothermic movement of the baseline, which quickly goes off-scale after a gradient increase

at 147°C, the re-run baseline merely displaying slight irregularity in this region. The illustrated ATA thermogram only contains an endothermic gradient increase at 115°C, the analogous extrapolation in the re-run thermogram, at 105°C, spanning a tiny endothermic bump. At the end of the endothermic peak in the CTA sub-ambient tracing a considerable increase in the baseline endothermicity is evident, which is not as pronounced in the subsequent thermogram, where four small coalescent endothermic peaks are apparent between 68° and 82°C.

Figure 13 also contains the above-ambient CTA tracing, an exothermic peak, to be described shortly, being the only thermogram characteristic at temperatures higher than the upper limit of the broad endotherm: the concurrent region of the re-run thermogram contains differing features. From about 154°C, the irregular baseline departs endothermically from its previous linear course, a steep linear movement occurring between 201° and 204°C, with an extrapolated onset temperature of 191°C. An irregular endothermic peak is apparently outlined between 204° and 209°C, followed by a large and fairly narrow exothermic peak at 220°C, with an extrapolated end temperature of 223°C. The steep trace between the two peaks contains a kink at about 212°C, possibly their boundary temperature, and a shoulder on the exotherm at 216°C. The temperature limits of the initial endothermic movement, possibly interrupted by the subsequent exotherm, are tentatively included in Table 15 . Above-ambient re-run thermograms for the glycogen esters display a distinct endothermic baseline shift which resembles the classic form of the glass transition as reported in thermal analysis literature, the GTA re-run thermogram being therefore reproduced in Figure 12.

In the vicinity of  $T_g$ , the illustrated first run thermograms display complex peaks, which will be described in the next feature category.

It is probable that several of the endothermic baseline shifts described below for the three amylose esters are not related to the glass transition; there is considerable doubt about the validity of identifying the sub-ambient median shift temperature for ATr(1.0), A(2.0) with  $T_g$ , brackets therefore surrounding the temperatures given in Table 15. The upper temperature limit of both ATr(1.0), A(2.0) sub-ambient runs was  $150^{\circ}\text{C}$  and the re-run thermogram is uneventful after the gradient change at  $-67^{\circ}\text{C}$ , merely consisting of a constant endothermic gradient. As shown in Figure 13, the sub-ambient baseline resembles an endothermic shift between  $78^{\circ}$  and  $123^{\circ}\text{C}$ : further examination of the DSC chart revealed that the re-run baseline is parallel to this apparent shift and that  $78^{\circ}\text{C}$  defines the end of the broad peak of Table 14, and therefore the return to the original baseline; in this context the only noteworthy characteristic of the illustrated thermogram is an exothermic gradient change at  $123^{\circ}\text{C}$ . At temperatures above  $100^{\circ}\text{C}$ , the second sub-ambient thermogram for ATT, partially reproduced in Figure 14, is effectively a first run thermogram; the irregular baseline demonstrates an endothermic shift, detailed in Table 15, which apparently ends in an endothermic peak at  $142^{\circ}\text{C}$ , with a shoulder extending to about  $147^{\circ}\text{C}$ . The only noteworthy feature above  $106^{\circ}\text{C}$  in either of the sub-ambient ATr(1.0) thermograms is an endothermic increase at  $119^{\circ}\text{C}$  in the baseline gradient of the first run.

In the vicinity of the broad endothermic peak and subsequent gradient increase at 122°C, evident in the above-ambient ATr(1.0), A(2.0) tracing, the re-run thermogram displays a large endothermic baseline shift, defined in Table 15, followed by a small shift between 145° and 150°C and persistent endothermic baseline movement with an extrapolated onset temperature of 157°C. As shown in Figure 14, the above-ambient ATT tracing contains an endothermic peak at 139°C and subsequent endothermic shift, detailed in Table 15, which apparently ends in a shallow endothermic peak. The concurrent re-run thermogram is uneventful and the irregular baseline subsequently outlines only two small, rounded exothermic peaks at 197° and 209°C, which coalesce to span the approximate region of 186° to 212°C. The upper temperature limit of both ATT runs was 250°C; the presence of a black residue over the DSC head implies that sample degradation had occurred by this temperature. It is feasible that, in the absence of the adjacent first run peaks, the endothermic shift may have occurred at slightly different temperatures. Degradation had obviously occurred by the end, at 350°C, of the first above-ambient run for ATr(1.0), as confirmed by the distribution of a black residue in the DSC sample chamber. The partially reproduced thermogram in Figure 14 displays an endothermic baseline shift from an exothermic peak at 225°C; in the absence of a re-run thermogram, the temperature limits of this shift are included in Table 15. Alternatively, the baseline immediately prior to the shift can be interpreted as an endothermic peak, with extrapolated onset and peak temperatures of 202° and 220°C; this endothermic peak occurs 14.5 degrees below the mid-point of the subsequent shift, the analogous ATT features being 16 degrees apart.

The second CTC ( $15.1 \times 10^3$ ) sub-ambient thermogram contains no evidence of an endothermic shift; as already described for the first run thermogram, the baseline is very exothermic and at temperatures above approximately  $110^\circ\text{C}$  increasing exothermic curvature results in an extrapolated gradient change at  $147^\circ\text{C}$ . The CTC ( $3.1 \times 10^3$ ) re-run thermogram, partially reproduced in Figure 15, shows a simple endothermic baseline shift which spans the upper temperature limit of the first run. As already mentioned, a net endothermic shift occurred during the broad endothermic peak of the first run and the baseline gradient became more exothermic 14 degrees above the extrapolated end temperature of this peak; the re-run thermogram, effectively that of a first run above  $100^\circ\text{C}$ , similarly displays an exothermic gradient change at  $133^\circ\text{C}$ , 24 degrees after the end of the baseline shift. As shown in the CTC ( $59.7 \times 10^3$ ) sub-ambient tracing an endothermic shift occurs 16 degrees above the upper temperature limit of the broad endothermic peak; the defining temperatures of this shift are included in Table 15 due to the complete absence of a shift in the re-run thermogram, which also extends to  $150^\circ\text{C}$ . Two minute endothermic kinks in the baseline, at about  $111^\circ$  and  $130^\circ\text{C}$  were reproduced during the second run, the only other noteworthy feature of either CTC ( $59.7 \times 10^3$ ) thermogram at above-ambient temperatures, being an exothermic baseline movement extrapolating to a gradient change at  $132^\circ\text{C}$  in the illustrated sub-ambient thermogram.

As shown in Figure 15, the large complex endotherm in the above-ambient CTC ( $15.1 \times 10^3$ ) thermogram is followed by two smaller endothermic peaks, to be detailed below; in the

vicinity of these three peaks, the re-run thermogram merely shows a very small endothermic shift, at about  $132^{\circ}\text{C}$ , and an endothermic increase in the baseline gradient, with an extrapolated temperature of about  $157^{\circ}\text{C}$  which is included in Table 15, although the resulting shift is not very steep. A similar baseline gradient increase occurred at  $189^{\circ}\text{C}$ , just before the end of the first above-ambient CTC ( $59.7 \times 10^3$ ) run. The re-run thermogram for this sample, effectively that of a first run above  $197^{\circ}\text{C}$  and therefore partially reproduced in Figure 15, contains a succession of endothermic gradient increases; the final one at  $187^{\circ}\text{C}$  involves the only significant gradient change and defines the beginning of an endothermic shift which ends in an apparent peak at  $216^{\circ}\text{C}$ . It is interesting to note that, in the initial thermogram, the spacing between the onset of this shift and the end of the broad peak is 15 degrees, an analogous temperature difference of 16 degrees being revealed by the first sub-ambient run for this sample. The first above-ambient runs for ATC and AC(2.5) both revealed an increase in the baseline gradient at  $141^{\circ}\text{C}$ , 16 and 17 degrees respectively above the end of the broad endotherm, also absent on the re-run. Both re-run thermograms show endothermic curvature, an almost significant gradient change occurring at  $165^{\circ}\text{C}$  during the second ATC run. Multiple peaks are visible towards the end of the ATC and AC(2.5) tracings in Figure 16; the re-run thermograms are similarly complex and this results in complete ignorance of the true baseline gradient and difficulty in identifying the shift caused by the glass transition. The median temperature of the endothermic shift that is visible at the upper limit of the illustrated ATC thermogram has been

vicinity of these three peaks, the re-run thermogram merely shows a very small endothermic shift, at about  $132^{\circ}\text{C}$ , and an endothermic increase in the baseline gradient, with an extrapolated temperature of about  $157^{\circ}\text{C}$  which is included in Table 15, although the resulting shift is not very steep. A similar baseline gradient increase occurred at  $189^{\circ}\text{C}$ , just before the end of the first above-ambient CTC ( $59.7 \times 10^3$ ) run. The re-run thermogram for this sample, effectively that of a first run above  $197^{\circ}\text{C}$  and therefore partially reproduced in Figure 15, contains a succession of endothermic gradient increases; the final one at  $187^{\circ}\text{C}$  involves the only significant gradient change and defines the beginning of an endothermic shift which ends in an apparent peak at  $216^{\circ}\text{C}$ . It is interesting to note that, in the initial thermogram, the spacing between the onset of this shift and the end of the broad peak is 15 degrees, an analogous temperature difference of 16 degrees being revealed by the first sub-ambient run for this sample. The first above-ambient runs for ATC and AC(2.5) both revealed an increase in the baseline gradient at  $141^{\circ}\text{C}$ , 16 and 17 degrees respectively above the end of the broad endotherm, also absent on the re-run. Both re-run thermograms show endothermic curvature, an almost significant gradient change occurring at  $165^{\circ}\text{C}$  during the second ATC run. Multiple peaks are visible towards the end of the ATC and AC(2.5) tracings in Figure 16; the re-run thermograms are similarly complex and this results in complete ignorance of the true baseline gradient and difficulty in identifying the shift caused by the glass transition. The median temperature of the endothermic shift that is visible at the upper limit of the illustrated ATC thermogram has been

interpreted as  $T_g$ ; the defining temperatures are to be found in Table 15. The beginning of the shift is identified with the shoulder at  $209^\circ\text{C}$ , although a steeper shift occurs from  $204^\circ\text{C}$ ; the analogous re-run shift has the steepest gradient of a succession of shifts and resembles the characteristic thermal evidence for the glass transition more closely than that of the first run. A large simple endothermic shift is clearly perceptible in the AC(2.5) tracing between the temperatures given in Table 15. The concurrent re-run shift is interrupted by small consecutive exothermic and endothermic gradient changes near the median shift temperature. Due to the evident difficulty in deriving extrapolated temperatures from amylose carbanilate and GTC( $\text{gr } 100 \times 10^6$ ) thermograms, the quoted temperatures approximately define the actual extent of the steepest gradients. Both GTC( $\text{gr } 100 \times 10^6$ ) endothermic shifts are irregular, being complicated by apparently insignificant exothermic gradient changes at about  $210^\circ\text{C}$  and with the steepest gradient therefore occurring below this temperature; the appearance of the re-run shift, with an additional endothermic gradient change at about  $212^\circ\text{C}$ , suggests that an end temperature of  $210^\circ\text{C}$  would be more appropriate. Between the broad endotherm and the upper limit of  $197^\circ\text{C}$ , the first GTC ( $5 \times 10^6$ ) run revealed only three exothermic features, discrete peaks being visible in the tracing at  $179^\circ$  and  $194^\circ\text{C}$ , with a shoulder on the former at  $185^\circ\text{C}$ . The second thermogram for this sample, obtained after overnight annealing, is also illustrated in Figure 16. A short linear portion is visible in this thermogram and is spanned by the extrapolating lines for the quoted upper temperature of the broad endotherm;

as indicated in the similar AC tracings, an alternative extrapolation is feasible, resulting in an end temperature 18 degrees below a further endothermic baseline gradient change at 144°C. The only other noteworthy feature, apart from a similar gradient change at 181°C and a small exothermic peak at 203°C, is a fairly steep endothermic slope which actually extends from 213° to the end of the thermogram at 220°C, an alternative onset temperature for this effectively first run feature being 207°C.

DSC runs for the acylated glycogen derivatives demonstrated a depression in median temperature for the simple re-run endothermic shifts with increase in the length of the ester group. Median temperatures for GT iso-B and GTP are almost identical, despite different run onset temperatures; comparison of other sub- and above-ambient data reveals the elevation in temperature of ATB and ATV endothermic shifts compared with their location in the above-ambient thermograms of the analogous glycogen esters. Data for the three amylose esters is unsatisfactory, the only reliable indication of the glass transition being provided by the second above-ambient thermogram for ATr(1.0), A(2.0). The absence of the reported CTC ( $59.7 \times 10^3$ ) shift during the repeat of the sub-ambient run raises doubts about the validity of associating the median temperature with Tg. There is also dubiety about the interpretation of the above-ambient carbanilate thermograms for Tg, the CTC re-run shifts more closely resembling the partially defined GTC ( $5 \times 10^6$ ) shift, than the reproducible features of the complex AC and GTC ( $gr\ 100 \times 10^6$ ) thermograms; nevertheless their median temperatures in Table 15 suggest that Tg varies with the type of (1 → 4) linkage and with the degree of substitution.

(f) Peaks which occur in first run thermograms in the vicinity of T<sub>g</sub>-associated endothermic shifts, described in the last feature category, are detailed below. The GT iso-B tracing displays an exothermic peak at 130°C, which spans the 127° to 138°C region. Identifying the shallow curved endothermic minimum, at 67°C, in the illustrated ATV thermogram with the end of the broad endotherm, implies that the baseline is outlined between 67° and 71°C, although the thermogram apparently displays a small endothermic peak at 71°C. A subsequent increase in the exothermic gradient at 75°C leads to a narrow exothermic peak at 77°C, and as with GT iso-B, this exothermic peak coincides with the end temperature for the re-run shift associated with T<sub>g</sub>. As with ATV, the first ATB thermogram contains an increase in the endothermic gradient in the vicinity of the re-run shift onset; the cessation of the first ATB run at least 6 degrees below the end temperature of the re-run shift is an explanation for the absence of an exothermic peak. Temperature data for the multiple peaks evident in the illustrated GTP, GTB and GTV thermograms and for the concurrent re-run endothermic shifts are given in Table 16 . No gradient changes are evident in the lines which connect these consecutive multiple peaks, their temperature spacing being indicated in brackets. The constancy of the lateral spacing between (i and ii) and (ii and iii) for each ester is evident; it is also noteworthy that for each peak differences between temperatures for adjacent esters are approximately equal, and less than the analogous variation in T<sub>g</sub>. First run thermograms in Figure 12, obtained under similar experimental conditions such as sample mass and instrument sensitivities, indicate that the multiple peaks decrease in

height with increase in size of the ester group; in addition, the temperature interval between the shift defined in Table 14 and the endothermic gradient change at the beginning of the peaks decreases concurrently. These two effects may explain the divergence of the GTV characteristics from those of GTP and GTB: iii is absent and the largest peak does not coincide with the end of the Tg-related shift, the latter feature corresponding to the temperature at which i is barely perceptible. Inspection of Figure 12 also reveals that ii is broadest in the GTV thermogram; although iii is broader for GTB, ii is of equal width for GTP and GTB. The temperature of peak ii, approximately coincident with the end of the concurrent Tg-related shift during GTP above-ambient and GT iso-B sub-ambient runs, differs by 7 degrees in contrast to the 1 degree discrepancy of their Tg's. Tg's for the two valerate samples differ by 19 degrees, although temperatures for i and ii deviate by only about 3 degrees: the sub-ambient ATV thermogram does not resemble the above-ambient GTV tracing; a change in gradient at 75°C distinguishes between i and ii for ATV, their relative size also differing, and the re-run endothermic shift ceases at the first run temperature of ii for ATV and i for GTV.

The only analogous features in GTA and CTA above-ambient tracings are exothermic and differ visually from those described above for the glycogen esters whose thermograms do not display a broad endothermic peak at lower temperatures. The sub-ambient PMMA thermogram, illustrated in Figure 9, displays an exothermic shift 11 degrees above the quoted end temperature for the broad endotherm, the GTA tracing in Figure 12 also implying that alternatively the limit of the large peak could be identified

with the end of the exothermic shift between 133° and 137°C. The apex of the complex GTA exotherm occurs at 150°C, with shoulders extending from 141° to 145°C and 156° to 159°C; the final baseline is achieved via an endothermic shift between 161° and 171°C, slightly larger than the analogous re-run feature with a median temperature of 156°C. A simple, broad exothermic peak is displayed by the CTA thermogram between 188° and 208°C, with an extrapolated temperature of 195°C. The median temperature, of 197.5°C, of the only visible endothermic shift in the re-run thermogram has been tentatively identified with T<sub>g</sub>, although the shift is initially irregular and apparently interrupted by an exotherm at 220°C, narrower and sharper than the illustrated first run peak. Although the illustrated exothermic peak does not coincide with the end of the T<sub>g</sub>-related shift for either acetate, its proximity to T<sub>g</sub> implies a connection between the two features; the GTA exotherm occurs 45 degrees lower than the analogous CTA first run peak, a similar temperature difference between T<sub>g</sub>'s providing indirect confirmation of the tentative CTA value. The only sample of the three amylose esters to display a T<sub>g</sub>-associated shift in a re-run thermogram is ATr(1.0), A(2.0), the concurrent first run tracing merely revealing the broad endothermic peak defined in Table 14 . CTC (15.1 x 10<sup>3</sup>) is the only carbanilate sample to show a possibly T<sub>g</sub>-related shift solely in its re-run thermogram; in its illustrated above-ambient thermogram, the baseline defines the extrapolated onset of two endothermic peaks 18 degrees after a similarly derived temperature at the end of the broad complex endotherm, the peak temperatures being 173° and 185°C.

(g) The final feature category includes all the remaining noteworthy characteristics of the above-ambient thermograms. Figure 12 displays a pattern of multiple peaks above  $165^{\circ}\text{C}$ , and therefore  $T_g$ , in the first run thermograms of the glycogen esters; the low-temperature sides of these rapid maxima are particularly steep, suggesting that phase transitions may be responsible. The GTA peaks are the smallest in height, the most dominant peak being exothermic and occurring at  $206^{\circ}\text{C}$  in the GTB thermogram. The peaks are only prominent in the first run thermograms, re-run residues being similar in magnitude to the illustrated GTA bumps. The temperature interval between these glycogen ester characteristics and the previous first run features increases with the ester group size; the small GTV peaks have the lowest temperatures, of about  $170^{\circ}$  and  $179^{\circ}\text{C}$ , and are not reproduced in the re-run thermogram. The GTB re-run displays residues that are effectively coincident with the first run exothermic peak at  $212^{\circ}\text{C}$  and endothermic bump at  $232^{\circ}\text{C}$ , the exothermic residue being diminished and the endothermic bump identical in magnitude: the only possible residue for the dominant feature at  $206^{\circ}\text{C}$  is inverted, being an endothermic bump at about  $207^{\circ}\text{C}$ . Similarly, the only re-run feature to remain in the concurrent region of the illustrated GTP peaks, is an endothermic bump at  $205^{\circ}\text{C}$ , 2 degrees higher in temperature than the fourth exothermic peak visible in the initial thermogram. The final exothermic bump, at  $206^{\circ}\text{C}$ , of the GTA tracing was reproduced identically during the re-run; exceptionally, the only other re-run feature, at about  $200^{\circ}\text{C}$ , is greater in height than the concurrent endothermic and exothermic baseline deviations of the first run.

As already mentioned, it is feasible that the

A(1.0) and ATT samples had degraded by the upper temperature limit of their first above-ambient runs. It is therefore possible that the exothermic baseline movement, prior and subsequent to the exothermic peak at 222°C in the illustrated ATT thermogram, should more correctly be described as a decrease in thermal capacity of the sample. Above 270°C, the A(1.0) baseline oscillates with increasing amplitude of the subsequent endothermic and exothermic peaks, finally moving off-scale endothermically by 334°C and returning to a thermal capacity level equivalent to fifty per cent fsd just before the end of the run. At temperatures above T<sub>g</sub>, the re-run thermogram for A(1.0), A(2.0) is not as complex as the first run tracing, two distinct, narrow exothermic peaks at 240° and 248°C being predominant, with the latter being the slightly greater in height and visually similar to the coincident exothermic peak of the illustrated thermogram. At temperatures above the broad first run endotherm, amylose and glycogen carbanilate thermograms do not resemble those of other esters: the endothermic shift attributed to the glass transition is reproducible on re-run, as are some of the adjacent multiple peaks. The narrow exothermic peak, evident 10 degrees below the quoted ATC temperature for the end of the consecutive T<sub>g</sub>-related shift, is the main first run characteristic to be absent in the re-run thermogram; similarly, the multiple exotherm whose apex spans 197° to 199°C in the illustrated AC(2.5) thermogram was not outlined during the re-run. The AC(2.5) tracing also displays a large narrow exothermic peak at 231°C, a similar exotherm occurring about 9 degrees higher in the re-run thermogram, after a large endothermic shift between about

224° and 230°C.

The complex, multiple peaks, that are evident towards the end of the illustrated amylose and glycogen carbanilate thermograms, were originally attributed to sample degradation: the apparent persistence of several peaks and the presumably Tg-related shifts during repeat DSC scans of these samples implies, however, that substantial degradation had not occurred. Unfortunately, the absence of thermobalance data for carbanilate samples precludes confirmation of the latter supposition. Table 17 summarizes details of the weight loss records that were obtained simultaneously to first run DSC thermograms for several other samples and gives particulars of features concurrently revealed by the initial DSC runs. Unless otherwise stated in the summary Table, it is assumed that increases in the weight loss gradient occur at the specified temperatures. For all samples except ATT, the thermobalance run began at 25°C; it was necessary to ignore the record during the subsequent 30 degree interval because apparent increases in sample weight were recorded at temperatures up to 55°C. As indicated weight losses are initially equally unreliable, it was assumed that the weight loss was zero at 55°C, the critical temperature being 80°C for ATT. For all samples except ATA, samples varied in mass between 1.5 and 2.3 mg, and percentage weight losses were estimated to about 0.1%; for ATA, greater instrument sensitivity resulted in a fsd equivalent to less than the usual 200 µg. The temperature estimates are

also only approximate due to:

- (i) imperfect synchronization of the thermobalance record with the DSC chart at 25°C
- (ii) irregularity of the records, resulting in rather arbitrary identification of overall changes in their gradients.

In Table 17, the total loss in sample weight is given in the Additional Details column and "D" denotes that the associated slope alteration involves a substantial increase in the rate of weight loss, therefore implying that the sample could have started to degrade at that temperature. Analysis of the CTA thermobalance record is futile; large oscillations in apparent sample weight were recorded due to contact of protruberant fibres with other parts of the balance.

Comparison of weight losses that have occurred prior to possible degradation or by the upper temperature limit in the absence of a D indicates a rough correlation with molecular polarity: thermobalance data for the four glycogen esters reveals an increase in weight loss with decrease in length of the n-alkyl group and, by about 244°C, ATr(1.0) had shown a relative mass decrease 2.5 times that of fully substituted ATT. By 250°C, the relative loss in weight for ATA was 3.0 times that for GTA, a possible explanation being the considerable difference in sample age. The ATr(1.0) thermobalance record has been included in Figure 14 because it displays pronounced gradient changes, which appear to correlate with features of the concurrent DSC thermogram; these complementary techniques suggested and enabled a calculation involving sample weight loss and the energy of the broad endothermic peak, the defining baseline for the ATr(1.0) endotherm therefore being included in Figure 14.

The results of this calculation for ATr(1.0), GTA and ATT, being relevant to interpretation of the molecular processes responsible for the broad endotherm, are given in the following chapter.

The main endothermic and exothermic features in the thermograms of all the first and second DSC runs have been systematized and described, and obvious trends have also been reported in order to aid identification of any correlation between DSC and TBA data, despite the possibility of a temperature differential between apparent temperatures for the transitions revealed by the two techniques. Details relevant to the correspondence of DSC and TBA temperature data were provided at the end of the previous chapter. Inexplicable discrepancies exist between overlapping regions of sub- and above-ambient thermograms: for example, with variation in run onset temperature, the broad peak detailed in Table 14 apparently changes its position by a temperature increment which differs for each sample; it therefore seems reasonable to compare results of sub-ambient DSC runs with those of TBA thermograms which extend from about  $-190^{\circ}\text{C}$ . It is thought that the use of more sensitive recorder and/or instrument ranges would provide more details of smaller transitions at temperatures below  $T_g$ ; in assessing the significance of thermogram features revealed with increased sensitivity, the surprising variation in form and temperature

of PDHI secondary transition evidence with merely a change in recorder range should be remembered. The inadequate DSC data reported above does imply that the time required to optimize this technique for secondary transition identification would be justified; it is anticipated that further study of these samples may produce data which conflicts with the trends gleaned from these few thermograms.

CHAPTER 4

DISCUSSION

TABLE 18  
Relationships between Transition Temperatures, in °C and Corrected for the Temperature Differential across the Torsional Braid Analyzer Sample Chamber

1 Sample	2 Transition Temp. within (4)	3	4 Tg x (3/4), when in °K	5 Tg (from Tables 4 and 5)
PDMI 80/25	—		10 ± 8	104 ± 10
PDEI	—		-31.5	49
PDPI	≤ -180		-40.5	37
PDBI	-171.5		-54	19

Sample	Transition Temp. within (4)	Transition Temp. within (4)x2, when in °K	Transition Temp. of B	Transition Temp. of B x (4/3), when in °K	Onset of A, uncorrected
PDHI	-173	-73	-66	3	-20
PDHpI	-174	-75	-63	7	-25 to -35
PDOI	-167	-61	-66.5	2.3	-30
PDNI	-171	-69	-53.5	19.6	-20
PDDI	-164	-55	-57	15	-20 to -40
PDUI	-160.5	-48	-46.5	29	-20
PDDoI	-157	-41	-43.5	33	-25

In the absence of further data, it is impossible to answer many of the questions that arise from these results, and in particular those from DSC thermograms. This Chapter therefore outlines the main conclusions that may be tentatively deduced both from main Tg trends and about the molecular motions associated with apparent sub-Tg's.

(i) The glass transition temperatures of polysaccharide derivatives

In agreement with the summary, of observed variations in Tg with sample structure, that was given in Chapter 1, Table 9 data for carboxylic acid derivatives of  $\alpha$ -(1  $\rightarrow$  4)-linked polyglucans indicate:

1. a decrease in average Tg for each ester type with increase in the length of the n-alkyl portion of the ester group.
2. GT-iso B has a higher Tg than the analogous n-butyl derivative, the glass transition of GT-iso B and GTP occurring at similar temperatures.

Comparison of TBA results for samples of the same ester type indicates that, in general, those containing a greater proportion of  $\alpha$ -(1  $\rightarrow$  6) branch points in their backbone structures have lower Tg's; however improved temperature resolution is required to enable satisfactory definition of the small temperature increments involved. In the absence of density gradient and therefore expansion coefficient data, the free volume at Tg, as defined by Simha and Boyer (6), cannot at present be evaluated for these samples. It is therefore not known whether the existence

of  $\alpha$ -(1  $\rightarrow$  6)-linked multiple branch points effectively increases the free volume at a given temperature, as suggested by Gillham for samples whose molecules are thought to be geometrically interlocked (14), enabling this Tg trend to be explained in terms of the iso-free volume theory which is applicable to "high molecular weight, non-cross linked polymers free from prominent subgroup transitions" (6), specific deviations possibly being associated with samples whose characteristics fail to satisfy these conditions. The Tg's of ATA and ATP, evaluated by TBA, are exceptions to the general trend indicated by these two ester types; this deviation may be related to the difference in their source, esterification temperature and their resulting characteristics such as molecular-weight. The length of the ester group seems to affect the variation in Tg with backbone branching: on increasing the ester group size from the propionate to the n-butyrate, there is a change in the apparent trends that is possibly associated with the increasing proximity of the adjacent secondary transition which complicates the GTV and GTV( $\beta$ -L-D) thermograms.

Comparison of the median temperatures for large damping of tri-acetate derivatives of cellulose and amylose given in Tables 10 and 9 respectively, reveals that the glass transition occurs about 30 degrees higher for CTA; from steric considerations of the (1  $\rightarrow$  4)-linkages in the cellulose and amylose chain portions represented in Diagram 2, it is evident that intramolecular rotation is energetically more feasible for the  $\alpha$ -(1  $\rightarrow$  4)-linked amylose polymer. ATr(1.0),

A(2.0) has a considerably higher Tg than ATA, an effect that could have been predicted, with reference to Chapter 1, by recognising that ATA could be converted to the former sample by the replacement, in each monomer unit, of an acetate group with a bulky inflexible trityl group. Table 10 indicates that the lack of substituent groups at C2 and C3 in ATr(1.0) results in a Tg-elevation, with respect to that of ATr(1.0), A(2.0), that is of the same order of magnitude as the difference in Tg of analogous acetylated and unsubstituted xylodextrins that was observed by Brown et al (53); this increase in the Tg is associated with the increase in the number of sites that are available for hydrogen bonding. The large, Tg-associated (1/n) values of ATA (D.S. = 3.0) and ATT (D.S. < 3.0) have effectively identical median temperatures, although the median temperature of the related (1/P<sup>2</sup>) change is relatively low for ATT, which is apparently susceptible to degradation, possibly beginning near Tg and resulting in cross-linking. Carbanilate thermograms display variable high damping in the vicinity of 180°C that could be associated with rupture of "hydrogen bonds formed between C=O and NH groups of neighbouring substituents" (21) and which precludes identification of any Tg differences between the various carbanilate samples. Figure 8 illustrates the variation in Tg with molecular weight, of CTC fractions with  $\bar{M}_w < 40 \times 10^3$ , that was expected from the summary of observed trends given in the first Chapter.

This paragraph contains a discussion of the Tg's evaluated as median temperatures of DSC endothermic shifts and summarised in Table 15. Despite the generally poor

correlation of sub-ambient DSC data with Tg's given in Tables 9 and 10, the results of some above-ambient DSC analyses are of interest. The greater discrepancy between the data in Tables 9 and 15 for GTB and GTV, of 9 and 13.5 degrees respectively, as compared to the effective coincidence of both Tg's of GTA and GTP may be additional evidence that mechanical damping values at the glass transition of butyrate and valerate samples are being affected by another molecular process. Because of sample degradation by the upper temperature of the first above-ambient DSC runs of both ATT and ATr(1.0), as confirmed by thermobalance data summarised in Table 17, Table 15 contains their run 1 median shift temperatures which coincide exactly with the median temperatures for large (1/n) given in Table 10; the complete absence of a temperature differential between Tg data from the first TBA runs and above-ambient DSC scans is therefore implied. In agreement with the TBA results of Table 9, the second DSC thermograms obtained over different temperature ranges for GT-iso B and GTP reveal approximate coincidence of their Tg's. These results imply that Tg is actually invariant with run onset temperature and that the approximately 20 degree Tg difference, evident in Table 15, between both butyrate and valerate derivatives of amylose and glycogen is meaningful; the latter observation confirms the general trend of decreasing Tg with increasing backbone branching that was revealed by TBA, despite a Tg-differential of the order of 10 degrees between TBA and DSC data for these samples. The effective coincidence of Tg-associated endothermic shifts outlined during both DSC scans of the amylose carbanilates and of GTC(gr 100 x 10<sup>6</sup>)

suggests that the postulated secondary high (1/n) process of carbanilate samples does not affect these Tg values; further DSC data may therefore be able to provide reliable evidence of variation in carbanilate Tg with type of (1 → 4)-linkage, degree of backbone branching and D.S. that is hinted at in Table 15 and in the description of the corresponding TBA results.

In general, the contents of the final sub-section in Chapter 2 should, at least partially, account for temperature differentials between the results of various Tg-evaluations: however there are irregular discrepancies between the Tg's for the amylose acetate to valerate triesters reported by Cowie et al (20) and those of this work. DSC scans of ATB and ATV (20) at one quarter or one eighth of the scan speed used in this DSC work yielded Tg's which are respectively 3 and 15.5 degrees lower than those reported in Table 15; the DSC values given in Table 2 for the amylose acetate to valerate triesters (20) also differ by 11, 15.5, 12 and -5 degrees respectively from the median temperatures for large (1/n) summarised in Table 9. The CTA Tg evaluated by TBA and given in Table 10 occurs approximately half-way between the two highest values (28,29) given for CTA in Table 2, but is 30 degrees higher than the Tg indicated by the specific volume-temperature data of Russel and Van Kerpel (30). The Tg value tentatively given in Table 15 for CTA, being 13.5 degrees higher than the analogous Table 10 result, exceeds all three literature values given in Table 2 and differs by 18.5 degrees from the DTA result (28) obtained at half the scan speed used in this work.

- (ii) The glass and sub-glass transition temperatures of poly(di-n-alkylitaconates) and of poly(methyl-methacrylate).

PMMA is the only one of these samples whose transition temperatures have been reported by other workers: the T<sub>g</sub> value given in Table 2 differs slightly less from the DSC data summarised in Table 13, where the lower of the two alternative sub-ambient median shift temperatures correlates most closely with the analogous above-ambient re-run transition temperature and with the literature value. Being more than 30 degrees lower than these DSC T<sub>g</sub>'s the median temperature of maximum (1/n) quoted in Table 4 is also 20 degrees lower than the generally accepted T<sub>g</sub> value for PMMA of 105°C.

As shown in Figure 1, high (1/n) values for PDMI and PMMA extend over a similar temperature region; further correlation of the T<sub>g</sub>'s for these structurally similar polymers is precluded by the existence of more dominant factors than the chemical structure of the repeating unit. Gillham (14) suggests that geometrical interlocking of the syndiotactic molecules contributes to the T<sub>g</sub>-variation of PMMA samples with their stereoregularity, disruption of such interlocking by the glass braids inherent in the TBA samples possibly being responsible for the low T<sub>g</sub> value indicated by this technique; whereas this geometrical interaction is not expected to occur between PDMI molecules, it has already been concluded from the TBA results in Chapter 3 that "on the molecular level, the effective glass transition for PDMI is not a simple amorphous glass to rubber transition." It is interesting to note from

Table 4 that the median temperature of maximum (1/n) for PDMI 80/25 occurs at about  $105^{\circ} \pm 10^{\circ}\text{C}$  which is the  $T_g$  evaluated by volume-temperature measurements on conventional PMMA and given in Table 2, whereas the analogous TBA temperature for PMMA, of  $86^{\circ}\text{C}$ , is effectively coincident with the temperature of the PDMI 37/100 endothermic peak as quoted in Table 12. As for PMMA, median shift temperatures for second PDMI 37/100 DSC runs differed with the temperature limits of the scans: in the first thermogram obtained over the above-ambient temperature range the endothermic peak occurred at the same temperature, within experimental error, of  $87^{\circ}\text{C}$  as in analogous sub-ambient thermograms and was also approximately 1 degree lower than the median temperature of the net endothermic shift, but exceptionally the simple endothermic shift of the re-run thermogram was centred on  $87.5^{\circ}\text{C}$ , whereas sub-ambient data revealed depression of the median shift temperature by about 8 degrees with the absence of the endothermic peak. The peak was only absent and the persistent, enlarged endothermic shift only depressed in temperature, in records of sub-ambient runs which followed rapid cooling of the PDMI 37/100 sample; the thermogram obtained after slow cooling contained a shallow endothermic peak at  $87^{\circ}\text{C}$ , the median temperature of the overall shift also being coincident with the first run value. An explanation of these PDMI results and of observations made by Velickovic was suggested in the letter (34) accompanying the poly(di-n-alkylitaconate) samples: "... because of its (i.e. PDMI) high density, brittleness, very slow

dissolution, and solubility in a much smaller number of solvents than the first next and higher members of the series, ... I suppose that some kind of internal crystallization occurs in this polymer, probably rendered possible by either internal hydrogen bonding or dipole-dipole interaction, not being hindered by the small methyl substituents of the ester groups (at least critically smaller than the two ethyl groups on the next member of the series)."

It is evident from the PDEI, PDPI and PDBI data in Table 5 that their median temperatures for maximum damping decrease with increase in ester group size, as was apparent in Table 9 for the analogous acylated polysaccharides. However, for interpretation and discussion of Tg's for higher poly(di-n-alkylitaconates), it was necessary to consider their entire thermograms.

The median temperatures for the (1/n) peak occurring in region (4) of Table 8 have been corrected for the temperature differential across the Torsional Braid Analyser sample chamber and are given in Table 18; it is suggested that this transition is due to the onset of rotational motion of the alkyl group within the side-chain, this motion being independent of the oxycarbonyl group and of the main chain (32). Reference 32 contains mechanical loss data, obtained at about  $10^2$  Hz, which indicate peaks at approximately  $-170^{\circ}\text{C}$  for poly(n-propylmethacrylate), at about  $-165^{\circ}\text{C}$  for poly(n-butylmethacrylate) and at about  $-120^{\circ}$  for poly(n-stearyl methacrylate); an alkyl loss peak was reported for poly(ethylmethacrylate) at  $-232^{\circ}\text{C}$  and about 9 Hz and it was inferred that "in PMMA the hindered

rotation of the ester methyl group should lead to a mechanical relaxation below  $-268.8^{\circ}\text{C}$  at about 10 Hz." The authors of reference 32 also considered that motion of the n-propyl group is initiated at similar temperatures in both poly(n-propyl acrylate) and poly(n-propyl methacrylate). In this work, dynamic mechanical evidence of a sub-Tg was not observed within region (4) for poly(di-n-alkylitaconates) or polysaccharide esters (see Table 11) with side groups containing n-alkyl moieties smaller than the n-propyl group; allowing for the difference in measuring frequency, it is evident that the transition temperatures for n-alkyl group motion given in Table 18 are in general agreement with those reported in reference 32.

It has been observed by Boyer (6) that the sub-Tg associated with side group motion of poly(n-alkyl methacrylates) (and of polyolefins and polyvinyl alkyl ethers) increases concomitantly with the number of side-chain carbon atoms and levels out around  $-110^{\circ}$  to  $-125^{\circ}\text{C}$  for samples containing more than about six carbon atoms within the side group. The unusually large increment between the transition temperatures within region (4) of PDPI and of PDBI (containing on average 5.5 carbon atoms per side group) and the gradual increase in this transition temperature with increasing side-chain length, which becomes significant for higher series members, suggest the existence of some constraint on the associated molecular motion. Assuming that six covalently-bonded methylene units are required before the alkyl side-chain in poly(di-n-alkylitaconates) will

crystallize and using the general relationship for symmetrical polymers in  $^{\circ}\text{K}$ :  $T_m = 2T_g$  (6), it is seen from Table 18 that the transition within region (4) and transition B may be identified respectively with  $T_g$  and the melting temperature,  $T_m$ , of the n-alkyl side-chain. Jordan et al (54) showed that for poly(n-alkylacrylates), which are assumed to be atactic, the side-chain length required to maintain a stable side-chain crystal nucleus, composed of the outer methylene groups, was in excess of nine paraffinic methylene groups for the bulk polymer and in excess of eight methylene groups for samples "in the presence of methanol, when main-chain restraints are freed, thus permitting more methylene groups to enter the crystal lattice." With respect to the geometrical interlocking mechanism (14), a poly(di-n-alkylitaconate) structurally resembles the analogous isotactic poly(n-alkylmethacrylate) whose main chain is known to be considerably more mobile than that of the corresponding syndiotactic and atactic samples (32); with reference to the effect of methanol on the side-chain crystallinity (54), it is thought that the greater main-chain mobility of these samples, compared with atactic poly(n-alkyl acrylates), increases the number of side chain methylene groups that can crystallize, thereby decreasing the required side-chain length. An additional factor which may contribute towards the increased proportion of crystallizing methylene units in the poly(di-n-alkylitaconates) is the increased density of alkyl side-chains in these samples as compared with the corresponding poly(n-alkylacrylates).

Boyer (8) states that "there is generally a secondary transition, commonly designated as the  $\beta$  process, lying just

below  $T_g$  such that  $T_\beta = 0.75 T_g$ , in  $^\circ K$  and that this relationship is most applicable to carbon-carbon backbone polymers, such as the poly(di-n-alkylitaconates). The  $\beta$  transition is thought to be "a precursor for the glass transition, involving the same kinds of motion" (8) and in PMMA this transition is generally assigned to motion of the ester side-group; Gillham (55) reports that "recent dielectric studies on copolymers of methacrylates indicate that the moving unit in the side-chain relaxation involves, in addition to the side chain, a segment of the backbone chain" and that "this could be achieved by local relaxations of the main chain." Results for alkyl methacrylate polymers, reported in reference 32, indicate that the glass-rubber and  $\beta$  transitions merge for samples with long n-alkyl groups and that if these two transitions are resolved, as for lower methacrylates at about 1 Hz, the  $\beta$  loss peak is observed in the  $10^\circ$  to  $25^\circ C$  region with the activation energy apparently independent of the side-chain alkyl group. It is suggested that fewer side chains can begin to move at the  $\beta$  transition for isotactic methacrylates, which occurs at lower temperatures than for analogous atactic and conventional (i.e. highly syndiotactic) polymers (32). It is considered that steric hindrance to rotation of the ester side group in poly(methylmethacrylate), PMMA, is largely provided by the main-chain methyl substituents of adjacent repeat units; the main-chain methyl group is absent in poly(methylacrylate) and the  $\beta$  transition for this polymer has a smaller magnitude and occurs at much lower temperatures (at a given frequency) than the  $\beta$  transition for PMMA, a more limited movement of the ester side group possibly being involved in the former sample (32).

With reference to the literature extracts given above, it is suggested that for poly(di-n-hexylitaconate) and subsequent series members transition B may also be interpreted as the  $\beta$  transition, motion of the pendant side groups and localised motion of the backbone being possible on melting of the ordered side-chain phases in the vicinity of the oxycarbonyl groups. The general increase in temperature of transition B with enlargement of the side groups that is evident in Table 8 can be explained by reference to the analogous  $T_m$  increase of homologous paraffins. A similar increase in the magnitude of transition B from PDHI to PDUI inclusive reflects the increasing proportion of each molecule that becomes mobile at  $T_\beta$ : a reason for the exceptional dynamic mechanical behaviour of PDDoI was suggested by its DSC thermogram, shown in Figure 10, the reproducible endothermic peak providing evidence of both a melting and a glass-rubber transition; it is thought that melting of the more perfect crystalline phase of the second critical six-methylene length at the ends of the side groups may only occur with the onset of large-scale backbone motion at  $T_g$ .

The large endothermic peak (illustrated in Figure 9) that characteristically occurs at identical temperatures during first PDMI DSC scans and the re-run following slow cooling (see Table 12) has been tentatively attributed to internal crystallisation: however, the resemblance of this re-run endothermic peak to the one outlined during the effective first run of PDPI (illustrated in Figure 10) raises some doubt about the interpretation of these peaks. Several thermograms illustrated in reference 56 display endothermic

peaks in the glass transition region; Brennan states that "the observed endothermic effect may be due to bulk stress relaxation in the system ..., usually only observed on the first heating through the glass transition, ... or to a free volume effect on the molecular level" (56). More DSC data is required to ascertain whether the PDEI and PDPI peaks persist on re-runs following either fast or slow sample-cooling rates and to enable their significance to be assessed. The absence of such peaks in PDHI and PDNI first run thermograms provides additional confirmation for the supposition that the molecular cause of the PDEI and PDPI peaks differs from that of the reproducible PDDoI endotherm.

TBA data for PDHI and higher series members, together with the observation made by Velickovic of "permanent tack and flow at room temperature" for these poly(di-n-alkylitaconates) (34), imply that  $T_g$  is located between the onset of transition A and room temperature; reference to their  $(1/P^2)$  results, as illustrated in Figures 2 and 3, which show little change with temperature increase above ambient temperatures confirms the choice of this upper limit to  $T_g$ . It is thought that subsequent high  $(1/n)$ , which frequently extends over a considerable temperature region, is associated with the second mechanism by which molecular mobility is enhanced in the region of highest  $(1/n)$ ; with unravelling of the physical cross-links formed by entanglements of the long side-groups, viscous flow can occur. The decrease in the relative magnitude of transition B for PDDI with increase in sample  $\bar{M}_w$ , and therefore in the restriction imposed on molecular motions by these physical cross-links, provides

support for this interpretation.

Reference to Figures 10, 3 and 2 and to Tables 12 and 8 reveals an approximate correspondence between the median temperatures of the largest endothermic shift and the beginning of high  $(1/n)$  that is spanned by the steepest  $(1/P^2)$  decrease for PDHI, PDNI and PDDoI, the minimum value for the relevant temperature being indicated by PDNI. It is evident that these changes in heat capacity and relative shear modulus identify the temperature region of the largest increase in molecular mobility: however, because of the above interpretation of the causes for transition B, it is doubted whether the defined temperature regions are actually the glass transition regions of these samples. By analogy, the interpretation of cellulose triester transition data by Klarman, Galanti and Sperling (16) is also questioned: in reference 16 "Tg" is identified with the temperature of the large modulus change and another transition occurring above "Tg" for triesters with large substituent groups is attributed to secondary side-chain motion in a crystalline phase. When the transitions which occur at the higher, varying temperatures are attributed to Tg, for triesters with four or more methylene groups in each side chain, a decrease in Tg with increase in alkyl-group length is apparent in Figure 4 of reference 16, a Tg minimum being absent in agreement with the poly(alkylmethacrylate) data reported by Nielsen, who considers that "each methylene unit in a polymer makes a fairly constant contribution to lowering the glass transition" (9).

Tg estimates for PDHI and higher poly(di-n-alkyl-itaconates), evaluated as  $1.33 T_g$ , in  $^{\circ}\text{K}$  (8), are given in

column 5 of Table 18. In general these extrapolated  $T_g$ 's occur within the high ( $1/n$ ) region which begins at transition A; it is thought that failure of the relationship, particularly evident in PDUI and PDDoI data, may be related to merging of the glass and  $\beta$  transitions or to side-chain crystallinity. It is interesting to note that, in general, the values given in column 5 undergo a minimum in going from PDMI to PDDoI, reflecting the effect of side-chain crystallinity on  $T_g$  via  $T_\beta$ ; a reasonable explanation for the exhibition of a  $T_g$  minimum by similar polymer systems was provided by Klarman, Galanti and Sperling: "the onset of crystallization will act to restrain the movement of the polymer chain segments via interchain forces ... such a change in structure should effectively raise the  $T_g$ , in that higher temperatures are required to overcome these forces and induce chain mobility" (16). For PDMI to PDBI inclusive, column 4 of Table 18 contains an estimate of the temperature of transition B, obtained with the relationship between  $T_g$  and  $T_\beta$  in  $^{\circ}K$ ; there is no obvious correlation between these temperatures and the transition temperatures given in Table 8. A relative decrease in the magnitude of the  $\beta$  loss peak, also occurring at lower temperatures, for isotactic methacrylates was thought to be due to the onset of motion of fewer ester side groups than in the analogous conventional or atactic samples; the increased density of ester side groups in PDMI compared with PMMA may therefore cause the  $\beta$  transition to be less obvious for the lower poly(di-n-alkylitaconates) than for PMMA. For PMMA, application of this correlation between  $T_g$  and  $T_\beta$  to

the median temperature of maximum (1/n) given in Table 4 indicates that  $T_{\beta}$  occurs at  $-4^{\circ}\text{C}$ , the median temperature, for the (1/n) shoulder that occurs within transition region (2) of Table 8. It was suggested above that disruption of geometrical interlocking of the largely syndiotactic PMMA sample may have contributed to the 20 degree difference between PMMA  $T_g$ 's in Tables 2 and 4, this explanation possibly being applicable to the implied discrepancy between the above  $T_{\beta}$  for PMMA and the location of the  $\beta$  transition between  $10^{\circ}$  and  $25^{\circ}\text{C}$  reported in reference 32. Referring to the interpretation of PMMA sub- $T_g$ 's derived from the literature (32) and given in Chapter 1, it is possible that the small (1/n) shoulder at about  $-157^{\circ}\text{C}$  in the PMMA thermogram traced in Figure 1 is due to rotation of the  $\alpha$ -methyl groups and that the maximum at  $-109^{\circ}\text{C}$  (corrected temperature being about  $-102^{\circ}\text{C}$ ) is due to absorbed water. Gillham (14) observed a small (1/n) peak and concurrent (1/P<sup>2</sup>) minimum, at about  $-10^{\circ}\text{C}$  in the TBA thermogram of xylan, which he attributed to plasticization of the polymer by atmospheric water. From the description of the PMMA thermogram given in Section A(ii) of Chapter 3 it is evident that regions (1) and (2) of Table 8 contain the  $\beta$  transition of PMMA and damping due to the plasticizing effect of water condensation below  $0^{\circ}\text{C}$ , and that (1/n) at  $-4^{\circ}\text{C}$  is not necessarily caused by ester group motion.

(iii) The sub-glass transition temperatures of polysaccharide derivatives

The broad endothermic peak, whose defining temperatures are given in Table 14, was outlined during the first DSC scans of polysaccharide derivatives (and of PMMA)

and is absent from re-run thermograms obtained by immediately re-scanning the samples. The endotherm was outlined during the re-run which followed overnight annealing of the GTC sample at ambient temperatures, the re-run peak being smaller in area and with a lower peak temperature, as illustrated in Figure 16. The area of the peak occurring between  $48^{\circ}$  and  $137^{\circ}\text{C}$  in the ATr(1.0) thermogram (see Figure 14) was estimated and hence the energy absorbed by the sample over this temperature range. The percentage weight lost by ATr(1.0), before the possible onset of degradation at  $330^{\circ}\text{C}$ , is given in Table 17 and hence, assuming that the same relative weight loss occurred in the DSC as in the thermobalance, the equivalent weight lost by the DSC sample was calculated; assuming also that the vapourization of water alone is responsible for this weight loss, as suggested by the reported correlation of weight loss with molecular polarity and age, this weight was divided by 18 in order to evaluate the weight loss in terms of the equivalent number of moles of water. The ratio of the energy absorbed during the broad peak of Table 14 to the number of moles of water lost by  $330^{\circ}\text{C}$ ,  $244^{\circ}\text{C}$  and  $250^{\circ}\text{C}$  respectively was evaluated as 5.2 kcal per mole for ATr(1.0), 5.8 kcal per mole for ATT and 3.3 kcal per mole for GTA. It is known that the dissociation energy for hydrogen bonds is usually about 5 kcal per mole (18). The results of this calculation therefore imply that on average one hydrogen bond is broken for each molecule of water lost and that the disruption of hydrogen bonds is responsible for the broad endothermic peak of Table 14. The peak of this endotherm occurs between  $29^{\circ}$  and  $77^{\circ}\text{C}$  in sub-ambient thermograms, the peak being recorded at the

temperature of maximum absorption by the sample. It is reasonable to expect that the rupture of hydrogen bonds will affect the molecular mobility within TBA samples, resulting in  $(1/n)$  variation in the general region of the endothermic peak.

Stratton concludes his study of the effect of water on the viscoelastic properties of cellulose (57) with the statement: "a loss peak in the  $-20^{\circ}$  to  $-60^{\circ}\text{C}$  range for cellulose at about 1 Hz has been attributed to molecular motion in the amorphous regions directly involving water molecules hydrogen-bonded to the cellulose chains." The peaks manifest at about  $-20^{\circ}\text{C}$  and  $-90^{\circ}\text{C}$  for the sample with effectively zero water content are both depressed in temperature with increase in the water content of the cellulose samples. It is suggested that the loss peak at lower temperatures is caused by short range motion in the amorphous regions of the sample, which is plasticized by water molecules. The molecular motion involving hydrogen-bonded water molecules may have been responsible for the  $(1/n)$  and  $(1/P^2)$  variations observed by Gillham (14) at about  $-10^{\circ}\text{C}$  in the TBA thermogram for a derivative of a similar polysaccharide called xylan. Gillham et al (58) report that in the TBA thermogram for cellulose "peaks of mechanical damping occurring at  $-110^{\circ}\text{C}$ ,  $-50^{\circ}\text{C}$  and  $100^{\circ}\text{C}$  may be attributed to some modes of local motions which will be of the same types as those of amylose and amylopectin"; a small damping peak occurred at  $-30^{\circ}\text{C}$  for cellulose alone, while amylose and amylopectin revealed a small peak at  $0^{\circ}\text{C}$ . The  $100^{\circ}\text{C}$   $(1/n)$  peak for cellulose may well involve a similar motion to that

observed at 112° to 120°C in the specific volume-temperature data for CTA (that was reported in Chapter 1) and attributed by Klarman, Galanti and Sperling (16) to side-chain motion, these workers detecting this secondary transition at 95° and 85°C for CTP and CTB respectively (i.e. with  $\text{sub-Tg} < \text{Tg}$ ). The dynamic mechanical data obtained for CTA by Russel and Van Kerpel (30) indicate a small (1/n) shoulder at about 100°C in addition to the small peak at -48°C which they attributed to mobility of the acetate group.

It was stated in Chapter 1 that the conformations of cyclic glucose structures are similar to those of cyclohexane, the two chair conformations illustrated in Diagram 1 being energetically more favourable. The work of Heijboer on polymers containing the cyclohexyl unit is reported in Chapter 1 of reference 32. It was observed that "the temperature and frequency of the cyclohexyl loss peak" which occurs at about -90°C at 0.4 Hz "is largely independent of the structure of the polymer containing the group"; this transition was identified with the constant interchange between the two chair forms of the cyclohexyl group. It is reasonable to expect that the analogous transition in polysaccharide derivatives will be affected by the size of the substituent groups which will alternate between the equatorial and axial positions; this transition may have been observed at -90°C (57) and -110°C (58) in cellulose and at -115°C in amylose and amylopectin (58). Klarman, Galanti and Sperling (16) suggested that the composition-invariant transition occurring between 35° and 45°C for cellulose triesters "might involve a boat-chair conformation change in the glucoside ring", which may result in rupture of hydrogen bonds.

Correlation of the transition temperatures already discussed in this sub-section with those summarised in Table 11 suggests these interpretations of the molecular motions which are initiated at the latter sub-Tg's. The transition defined within region I is tentatively associated with the breaking of hydrogen bonds, the bonding largely taking place between water and polymer molecules. Transition IIa may be caused by the increase in mobility of water molecules hydrogen-bonded to adjacent polysaccharides, possibly involving local motion of the bonded polymer segments. Transition II, occurring at similar temperatures as the small loss peak associated with mobility of the acetate group in CTA despite large variations in the substituent groups, is attributed to motion of the ester group, predominantly involving the oxycarbonyl group and/or the C6 oxymethylene group. Within region III, the transition apparently occurring between  $-90^{\circ}$  and  $-140^{\circ}\text{C}$  is located at temperatures erroneously low by about 5 to 8 degrees respectively; the apparent variation of these transition temperatures with the type of linkages between pyranose rings and to a greater extent with their substituent groups supports the association of this transition with the onset of the chair-chair conformational interchange of main-chain glucose rings. As with the poly(di-n-alkylitaconates), the transition evident at the low temperature limit of TBA for samples containing the n-propyl group is attributed to motion of the n-alkyl side group.

In the absence of the improved correlation of transition data enabled by variable-frequency and hence activation energy data, this association of molecular motions with the observed transitions can only be speculative.

## REFERENCES

- (1) "Polymer Science and Materials", edited by A. V. Tobolsky and H. F. Mark, Wiley-Interscience (1971).
- (2) "Textbook of Polymer Science" by F. W. Billmeyer Jr., Wiley International (1962).
- (3) "Polymers: Structure and Bulk Properties" by P. Meares, D. Van Nostrand Co. Ltd. (1965).
- (4) "Introduction to Polymer Science" by L.R.G. Treloar, Wykeham Publications (London) Ltd. (1970).
- (5) J. A. Sauer and A. E. Woodward in Chapter 3 of "Techniques and Methods of Polymer Evaluation" 2, edited by P. E. Slade Jr. and L. T. Jenkins, Marcel Dekker, Inc. (New York, 1970).
- (6) R. F. Boyer, Rubber Chem. and Tech. 36 (1963) 1303.
- (7) "Mechanical Properties of Solid Polymers" by I. M. Ward, Wiley-Interscience (1971).
- (8) R. F. Boyer, Thermal Analysis 3 (1971) 3.
- (9) "Mechanical Properties of Polymers" by L. E. Nielsen, Reinhold Publishing Corp. (1962).
- (10) R. F. Boyer, Polymer Eng. and Sci. 8(3) (1968) 161.
- (11) J. H. Daane and R. E. Barker, J.Polymer Sci. B2 (1964) 343.
- (12) R. K. Eby, J.Chem.Phys. 37 (1962) 2785.
- (13) J. Heijboer, Polymer 1 (1969) 3.
- (14) J. K. Gillham, Crit.Rev.Macromolecular Sci. 1(1) (1972) 83.
- (15) Yu. V. Zelenev and V. I. Glazkov, Vysokomol. soyed A4(1) (1972) 16.
- (16) A. F. Klarman, A. V. Galanti and L. H. Sperling, J.Polymer Sci. 7(A-2) (1969) 1513.
- (17) "Natural High Polymers" by C. T. Greenwood and E. A. Milne, Oliver and Boyd (1968).
- (18) "Organic Chemistry", by R. T. Morrison and R. N. Boyd, Allyn and Bacon, Inc. (1966).
- (19) "Comprehensive Biochemistry" 5, edited by M. Florin and E. H. Stotz, Elsevier Publishing Co. (1963).
- (20) J.M.G. Cowie, P. M. Toporowski and F. Costaschuk, Die Makromol Chemie 121 (1969) 51.

- (21) W. Burchard in "Solution Properties of Natural Polymers", Chem.Soc.Special Publ.No. 23 (1968) 135.
- (22) W. Burchard, I. Kratz and B. Pfannemüller, IUPAC Macromoleculare Symposium, Paper V-3 (Helsinki, 1972).
- (23) H. Bittiger and E. Husemann in "Solution Properties of Natural Polymers", Chem.Soc.Special Publ.No. 23 (1968) 159.
- (24) J.M.G. Cowie, Personal Communication.
- (25) J. Velickovic and J. Filipovic, Die Angewandte Makromol. Chemie 13 (1970) 79.
- (26) J. Velickovic, V. Juranicova and J. Filipovic, IUPAC Macromoleculare Symposium, Book of Abstracts 1 (Leiden, 1970) 289.
- (27) J. Velickovic and S. Vasovic, IUPAC Macromoleculare Symposium, Book of Abstracts 1 (Leiden, 1970) 293.
- (28) J.M.G. Cowie and R. J. Ranson, Die Makromol.Chemie 143 (1971) 105.
- (29) J. K. Gillham and R. F. Schwenker Jr., J.Appl.Polymer Sci. Applied Polymer Symposia 2 (1966) 59.
- (30) J. Russel and R. G. Van Kerpel, J.Polymer Sci. 25 (1957) 77.
- (31) A. Sharples and F. L. Swinton, J.Polymer Sci. 50 (1961) 53.
- (32) "Anelastic and Dielectric Effects in Polymeric Solids" by N. G. McCrum, B. E. Read and G. Williams, J. Wiley and Sons (1967).
- (33) J. Heijboer in "Physics of Non-Crystalline Solids", edited by J. A. Prins, North Holland, Amsterdam (1965) 231.
- (34) J. Velickovic, Personal Communication.
- (35) J.M.G. Cowie, Ph.D. Thesis, University of Edinburgh (1958) 75.
- (36) J. W. Mullen and E. Pascu, Ind.Eng.Chem. 34 (1942) 1209.
- (37) A. L. Potter and W. Z. Hassid, J.Amer.Chem.Soc. 70 (1948) 3774.
- (38) A. Maconnachie, Personal Communication.
- (39) J. B. Henshall, Personal Communication.
- (40) I. J. McEwen, Personal Communication.

- (41) "I.R. Spectra of Complex Molecules" by L. J. Bellamy, Methuen and Co. Ltd. (1958).
- (42) N. Bauer and S. Z. Lewin in "Techniques of Organic Chemistry" 1, edited by A. Weissberger, 3rd edition, Interscience (1960) 132.
- (43) "Experiments in Fibre Physics" by R. E. Beevers, Butterworths (1970).
- (44) G. Oster and M. Yamamoto, Chem.Reviews 63 (1963) 257.
- (45) R. J. Ranson and J.M.G. Cowie, Unpublished work.
- (46) M. Gordon and I. A. Macnab, Trans.Faraday Soc. 49 (1953) 31.
- (47) J. K. Gillham, Crit.Reviews in Macromol.Sci. 1 (1972) 83.
- (48) Chemical Instruments Corporation, Personal Communication.
- (49) J. K. Gillham, J.Appl.Polymer Sci. Applied Polymer Symposia, 2 (1966) 45.
- (50) Instruction and Maintenance Manual; Torsional Braid Analyzer Model 100-B1, Chemical Instruments Corporation (New York).
- (51) R. Tranter, Personal Communication.
- (52) E. S. Watson, M. J. O'Neil, J. Justin and N. Brenner, Analytical Chemistry 36(7) (1964) 1233.
- (53) W. Brown, E. Alfthan and A. de Ruvo, Polymer 14 (1973) 329.
- (54) E. F. Jordan, Jr., D. W. Feldeisen and A. N. Wrigley, J.Polymer Sci. 9(A-1) (1971) 1835.
- (55) J. K. Gillham, First Symposium on Torsional Braid Analysis, Society of Plastics Engineers Annual Technical Meeting, Preprints 17 (1971) 89.
- (56) W. P. Brennan, Perkin-Elmer Thermal Analysis Application Study 7 (1973).
- (57) R. A. Stratton, J.Polymer Sci. 11 (1973) 535.
- (58) S. Nakamura, J. K. Gillham and A. V. Tobolsky, Repts.Prog.Polymer Phys.Japan 13 (1970) 89.

Attention is drawn to the fact that the copyright of this thesis rests with its author.

This copy of the thesis has been supplied on condition that anyone who consults it is understood to recognise that its copyright rests with its author and that no quotation from the thesis and no information derived from it may be published without the author's prior written consent.